Interdisciplinary Materials

WILEY

Interdisciplinary Materials Open Access

REVIEW OPEN ACCESS

Beyond the Limits of Lithium Iron Phosphate: Cutting-Edge Innovations Toward High Performance and Sustainability for Next-Generation Batteries

Ashok Kumar Kakarla[1] | Zarmeena Akhtar[1] | Jongsoon Kim[2,3] | Moonsu Yoon[1] | Dongsoo Lee[1] | Junghyun Choi[1]

[1]School of Chemical, Biological & Battery Engineering, Gachon University, Seongnam-Si, Gyeonggi-do, Republic of Korea | [2]Department of Energy Science, Sungkyunkwan University, Suwon-si, Gyeonggi-do, Republic of Korea | [3]Institute of Energy Science and Technology (SIEST), Sungkyunkwan University, Suwon-si, Gyeonggi-do, Republic of Korea

Correspondence: Moonsu Yoon (msyoon23@gachon.ac.kr) | Dongsoo Lee (dslee9117@gachon.ac.kr) | Junghyun Choi (junghchoi@gachon.ac.kr)

Received: 30 May 2025 | **Revised:** 28 September 2025 | **Accepted:** 17 October 2025

Keywords: advanced electrode technology | battery pack architecture | energy density enhancement | $LiFePO_4$ cathodes | lithium-ion batteries | morphology engineering

ABSTRACT

The rapid electrification of transportation and grid systems has placed lithium-ion batteries (LIBs) at the forefront of energy storage innovation. Lithium iron phosphate ($LiFePO_4$, LFP), with its superior safety, long cycle life, and cost advantages, has become a cornerstone cathode material. However, the limited energy density (ED), attributed to its relatively low nominal voltage (~3.2 V) and moderate specific capacity (~170 mAh g^{-1}), hinders its competitiveness in high-energy applications. Furthermore, electrochemical characteristics related to poor charge transfer kinetics and material circularity also limit its overall value. This review highlights recent advances in material design, electrode engineering, and system-level optimization aimed at overcoming these challenges. Key strategies include precision doping, multifunctional coating, and nanostructuring to enhance conductivity and rate performance, development of high-tap-density powders and ultra-thick electrodes for improved ED, and hierarchical electrode architectures and advanced conductive networks for efficient ion/electron transport. Additional focus is given to low-temperature performance, scalable and sustainable synthesis routes, and recycling pathways that ensure long-term environmental viability. Emerging directions such as dry electrode processing, solid-state integration, and artificial intelligence/machine learning-driven optimization are also discussed as transformative tools for accelerating LFP innovation. By integrating these multidisciplinary strategies, LFP can evolve from a safe and stable cathode into a high-performance, sustainable solution for electric vehicles, grid storage, and next-generation energy systems.

1 | Introduction

The rapid advancement of electric vehicles (EVs) has underscored the crucial role of lithium-ion batteries (LIBs) as the primary energy storage solution for sustainable and efficient transportation. As the automotive industry increasingly shifts toward electrification, LIBs have become integral to EVs' success, offering advantages such as high energy density (ED), extended cycle life, and comparatively low self-discharge rates [1–3]. The surging global demand for EVs has amplified the urgency for innovations in battery technologies that achieve superior performance and adhere to sustainability, cost-effectiveness, and operational safety. A critical milestone in this progression is addressing the dual challenge of achieving cost parity with internal combustion

Ashok Kumar Kakarla and Zarmeena Akhtar contributed equally to this study.

engine (ICE) vehicles and delivering driving range parity to meet consumer expectations [4]. Achieving price parity, which refers to reaching economic competitiveness with ICE vehicles without subsidies, is essential for mass-market adoption. Since batteries constitute up to 40% of an EVs' total cost, they represent the most significant cost component in EVs production [5]. Simultaneously, concerns about insufficient driving range and the risk of depleting battery charge remain significant barriers to widespread consumer acceptance. Addressing these intertwined challenges is essential to accelerating EVs adoption and advancing the decarbonization of the transportation sector [6].

The cathode has been the primary driver of battery chemistry evolution among LIB components due to its significant influence on energy capacity and cost. Advances in cathode chemistries, such as ternary layered nickel manganese cobalt oxide ($Li_{1.0}Ni_xMn_yCo_{1-x-y}O_2$, NMC), have continually pushed the boundaries of LIB capabilities. High-Ni NMC cathodes enable extended driving ranges and reduced material costs compared to those of lithium cobalt oxide ($LiCoO_2$, LCO), positioning them as the preferred choice for premium EVs and high-performance applications [7, 8]. However, the notable trade-offs accompany the benefits of high-Ni NMC cathodes. Typically, due to the geographically limited distribution of critical elements, specifically Co and Ni, the production cost has been elevated with intensifying the concerns surrounding supply chain security and ethical sourcing practices [8]. Furthermore, the safety issues related to low thermal durability and the formation of resistive cathode–electrolyte interphases (CEIs) in high-Ni NMC cathodes pose significant challenges, potentially hindering the widespread adoption of EVs [7].

Olivine-structured $LiFePO_4$ (LFP) cathode has emerged as a promising alternative cathode material for EV batteries, particularly in the mass-market sector. First, LFP cathodes utilize earth-abundant elements and low-cost elements, such as Fe and phosphate ($-PO_4$), thus lowering manufacturing costs and enhancing supply chain sustainability [9]. This makes LFP an attractive option for large-scale EV deployment. Furthermore, LFP batteries can offer more stable and longer cycle life than any NMC cathodes, which is an optimal choice for long-term EV ownership. Lastly, their superior thermal stability also minimizes the risk of thermal runaway and associated safety failure, such as fires or explosions, offering a safer option for passenger EVs [10]. Nevertheless, the primary limitation of LFP batteries is their lower ED, resulting in diminished driving ranges that may dissuade consumers from seeking long-range EVs or those requiring high-performance vehicles for specialized applications, such as heavy-duty transport or long-distance travel [11]. The low electronic conductivity and limited Li-ion diffusivity of LFP significantly hinder its performance in fast charge/discharge cycles, limiting its suitability for large-scale energy storage systems [12, 13]. These limitations also hinder its ability to support high-power operations, making it less competitive in applications where rapid electron transfer is crucial for quick acceleration and deceleration, directly impacting efficiency and performance. LFP batteries show sensitivity to temperature fluctuations, and their performance can deteriorate in colder climates [14, 15].

Despite these drawbacks, LFP cathodes are emerging as a pivotal technology in the global LIB market, which is projected to surpass 2500 GWh in annual capacity by 2030, with EVs leading demand due to a global EV fleet exceeding 142 million units [16]. LFP batteries are revolutionizing sustainable energy with their exceptional safety, affordability, and environmental benefits, making them particularly suitable for EVs and grid-scale storage applications where reliability and cost-efficiency are paramount [17]. At the material level, LFP offers excellent thermal and chemical stability, lower toxicity, and cost advantages due to the abundance of iron (Fe), along with a long cycle life that enhances battery longevity [18]. In the EV sector, LFP dominates, especially in China, powering over 60% of new energy vehicles and effectively cutting battery costs by 30%–40% in comparison to traditional Li-ion options, while also reducing dependence on scarce, expensive materials like Co [19, 20]. Beyond transportation, LFPs play a crucial role in enhancing renewable energy integration by storing surplus solar and wind power, thus reinforcing grid stability and minimizing curtailment [21]. Innovations such as silicon (Si)-doped anodes and advanced recycling methods that recover up to 95% of raw materials further augment their sustainability [22, 23].

Driven by favorable regulatory frameworks such as the U.S. Inflation Reduction Act and stringent EU battery directives, global LFP battery production is rapidly transitioning toward localized, low-carbon supply chains [24]. This strategic shift not only mitigates supply chain vulnerabilities and geopolitical risks but also fosters energy independence and resilience. With global LFP demand exhibiting a compound annual growth rate exceeding 25%, LFP technology has become integral to the attainment of net-zero emissions targets and the deployment of decentralized energy systems, owing to its intrinsically long cycle life and diminished rate of electrochemical degradation at electrode, cell, and module levels [25]. The expiration of key patents, notably those of Dr. Goodenough, has further propelled market expansion and cost reductions, contributing to the price parity of LFP batteries compared with competing chemistries [26]. Recent advances in LFP technology, spanning the development of porous electrode architectures, dry electrode manufacturing, and electrolyte optimization, have delivered improvements in energy density, rate capability, and process scalability. These technical breakthroughs, combined with policy incentives, position LFP batteries as competitive candidates for EV and grid-scale storage applications. However, the accelerating penetration of LFP batteries within the clean energy ecosystem necessitates a critical examination of their end-of-life management, particularly recycling and reuse strategies.

Unlike NCM cathodes, LFP batteries present unique recycling challenges due to the robust olivine structure characterized by strong P─O covalent bonding and the relatively low economic value of recovered Fe and P. The absence of high-value transition metals in LFP cathodes renders traditional pyrometallurgical and hydrometallurgical recycling methods economically unattractive and environmentally burdensome [23, 27, 28]. As a consequence, direct regeneration, wet processing, and chemical relithiation strategies have gained prominence in recent research, aiming to restore spent LFP cathodes to functional states with minimal resource input and lower emissions [29, 30]. Pilot-scale demonstrations of direct chemical relithiation have achieved promising results, yielding regenerated cathodes with specific capacities of 152–167 mAh g^{-1} and cycle retention comparable to commercial-grade materials [28, 31]. Nevertheless, the scalability and

industrial applicability of these processes remain constrained by reagent costs, separation complexity, and the quality of the recycled product. Life-cycle assessments further underscore the urgent need for the development and implementation of sustainable, closed-loop recycling methodologies for LFP cells, as mandated by emerging EU regulations requiring recycling efficiencies as high as 70% for lithium-based batteries by 2030. The advancement of LFP recycling science is, therefore, not only an environmental and economic imperative but also a prerequisite for the realization of a fully circular, low-carbon battery industry.

This review builds upon the preceding discussion by emphasizing the need for a circular approach to LFP cathode development. While LFP's intrinsic advantages, safety, cost-effectiveness, abundance, and long cycle life, support its rapid adoption, their lower ED and recycling complexity necessitate integrated strategies that span the entire value chain. To address these challenges, this review explores strategies to boost the ED of LFP cathodes across three critical levels (material, electrode, and cell/module/pack). At the material level, approaches such as elemental doping, surface modification, and nanostructuring aim to overcome limitations in conductivity and Li-ion diffusivity. At the electrode level, innovations in porous architectures, conductive networks, and scalable manufacturing methods enhance rate capability and performance uniformity. Finally, at the cell, module, and pack levels, optimized designs, thermal management, and system integration enable LFP batteries to meet driving range and power requirements while preserving safety and sustainability. Together, these perspectives offer a concise yet comprehensive framework for identifying targeted improvements that align technological advancement with circular economy principles, paving the way toward cost-effective, high-performance, and recyclable LFP batteries for EVs and grid-scale applications.

2 | Fundamentals of LFP Cathode Materials and Limitations

2.1 | Crystal Structure and Morphology of LFP

Since the commercialization of LIBs in 1991, researches have focused on improving energy density, cycle life, safety, and cost efficiency. These goals have driven the development of various intercalation-type cathode materials, mainly based on transition metal oxides [32, 33]. LCO possesses a layered structure that facilitates high Li mobility and energy density but is susceptible to structural collapse and oxygen release at elevated voltages, compromising safety (Figure 1A) [34]. $LiMn_2O_4$ (LMO) adopts a three-dimensional (3D) spinel framework, enabling rapid Li diffusion and good rate capability, however, it suffers from capacity fading due to manganese dissolution and structural instability (Figure 1B) [35]. In contrast, the olivine-type LFP cathode features a hexagonally close-packed oxygen framework with Li^+ and Fe^{2+} ions occupying half the octahedral sites and phosphorus in one-eighth of the tetrahedral sites, forming a robust structure that supports one-dimensional (1D) Li^+ diffusion along the *b*-axis ([010] direction, Figure 1C) [34, 36]. The FeO_6 and LiO_6 octahedra share edges, while PO_4 tetrahedra share corners with FeO_6, enhancing structural stability, thermal resistance, and safety. FeO_6 octahedra are distorted due to strong electrostatic interactions with oxygen, affecting Li^+ mobility and redox dynamics. During delithiation, the framework retains structural integrity due to strong P─O covalent bonds and compensatory $Fe^{2+} \rightarrow Fe^{3+}$ oxidation, ensuring long-term cycling stability [37]. Native point defect calculations (Figure 1D–F) show that Fe_{Li}^{+} and V_{Li}^{-} dominate under Li-deficient conditions, pinning the Fermi level and rendering LFP resistant to conventional doping strategies [38].

These defects also explain its inherently low electronic conductivity (~10^{-9} to 10^{-10} S cm^{-1}) and wide band gap (~3.5 eV), limiting its rate performance without conductive additives. Despite its apparent poor bulk Li^+ diffusivity, atomistic simulations and localized measurement techniques reveal a different picture. First-principles calculations by Morgan et al. [40] and empirical potential studies by Islam et al. [41] showed rapid Li^+ diffusion (~10^{-8} cm^2 s^{-1}) strictly along the [010] direction, with negligible transport in other crystallographic axes (Figure 1G–I) [39]. These findings were experimentally validated by neutron diffraction [42] and muon-spin rotation [43], which estimated Li^+ diffusion values consistent with simulation results. This localized 1D diffusion explains how LFP achieves high-rate performance in practice, resolving the discrepancy between earlier bulk transport measurements and real-world behavior.

The morphology of LFP significantly influences its electrochemical performance, including rate capability, cycling stability, and ED, as illustrated in Figure 2A. Various morphologies, nanoparticles, nanorods, nanoplates, microspheres, porous structures, hollow/core–shell designs, and hierarchical/flower-like forms, each offer distinct advantages [44–48]. Spherical or irregular nanoparticles provide high surface area, shortening Li-ion diffusion paths for enhanced rate performance, though agglomeration can be an issue [49]. 1D nanorods and nanowires promote efficient Li-ion transport along their length, boosting conductivity and electrochemical kinetics [50]. Two-dimensional (2D) nanoplates and nanosheets lower charge transfer resistance and improve electrolyte contact, enhancing performance. Microspheres, formed from aggregated nanoparticles, increase tap density, ideal for high ED applications. Porous structures enhance electrolyte penetration and Li-ion diffusion, supporting fast charging. Hollow and core–shell structures shorten diffusion paths and improve stability, often incorporating carbon or conductive polymers for better electronic conductivity. Hierarchical and flower-like morphologies offer multidimensional diffusion pathways and high surface area, ensuring superior ion/electron transport and structural stability. These tailored morphologies optimize LFP for applications like EVs and long-cycle-life energy storage systems.

2.2 | Electrochemical Performances and Advantages of LFP

LCO cathodes have long been a benchmark for LIBs due to their relatively high ED, typically around 150–200 mAh g^{-1}, and a stable voltage plateau near 3.7 V versus Li/Li^+ (Figure 2B). This

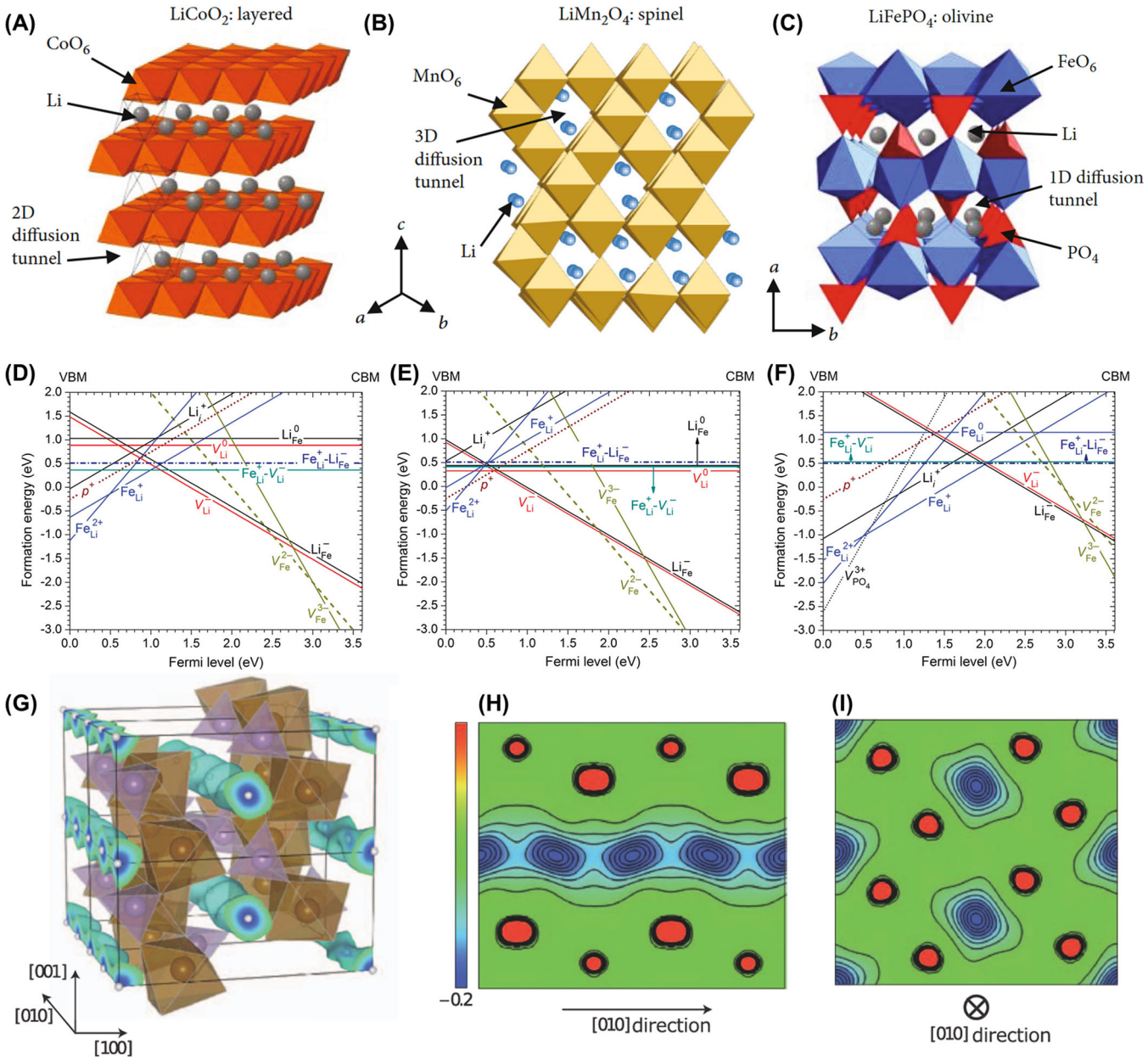

FIGURE 1 | Crystal structures of (A) LCO, (B) LMO, and (C) LFP. Reproduced with permission [35]. Copyright 2021, Energy Material Advances. (D–F) Calculated formation energies of native defects and complexes in $LiFePO_4$ versus Fermi level (relative to VBM) under different oxygen chemical potentials. Reproduced with permission [38]. Copyright 2011, American Chemical Society. (G–I) 1D Li diffusion along [010] shown via Li nuclear density (blue contours). Reproduced with permission [39]. Copyright 2013, IOP Publishing, Ltd.

layered oxide structure allows for efficient Li intercalation and deintercalation, resulting in good initial capacity and power output. However, LCO's structural stability under prolonged cycling is limited, it usually retains only 800 to 1200 cycles before significant capacity fading occurs. Additionally, LCO suffers from thermal instability, beginning to decompose and release oxygen at approximately 180°C, which poses safety risks such as thermal runaway and combustion during abuse conditions. These issues restrict its use, especially in large-format cells where safety and longevity are critical. NMC, a layered ternary oxide, was developed to address some of LCO's shortcomings by tuning the metal ratios to improve capacity, cycle life, and cost (Figure 2C). NMC cathodes offer higher ED, often exceeding 200 mAh g^{-1}, and longer cycle life ranging from 2000 to 3500 cycles, alongside improved electronic conductivity that enhances rate capability. The voltage plateau of NMC cathodes slightly surpasses 3.7 V, contributing to higher cell voltages and ED. However, NMC materials still face limitations in thermal stability, with decomposition temperatures around 220°C. The presence of nickel and cobalt, while boosting capacity and electronic conductivity, also increases the risk of oxygen release and thermal runaway under abuse, raising safety concerns in high-power or high-temperature applications [51]. Furthermore, the reliance on cobalt and nickel raises issues of cost, resource scarcity, and environmental impact. In comparison, LFP cathodes offer a fundamentally different structural and electrochemical profile that addresses many of these challenges (Figure 2D).

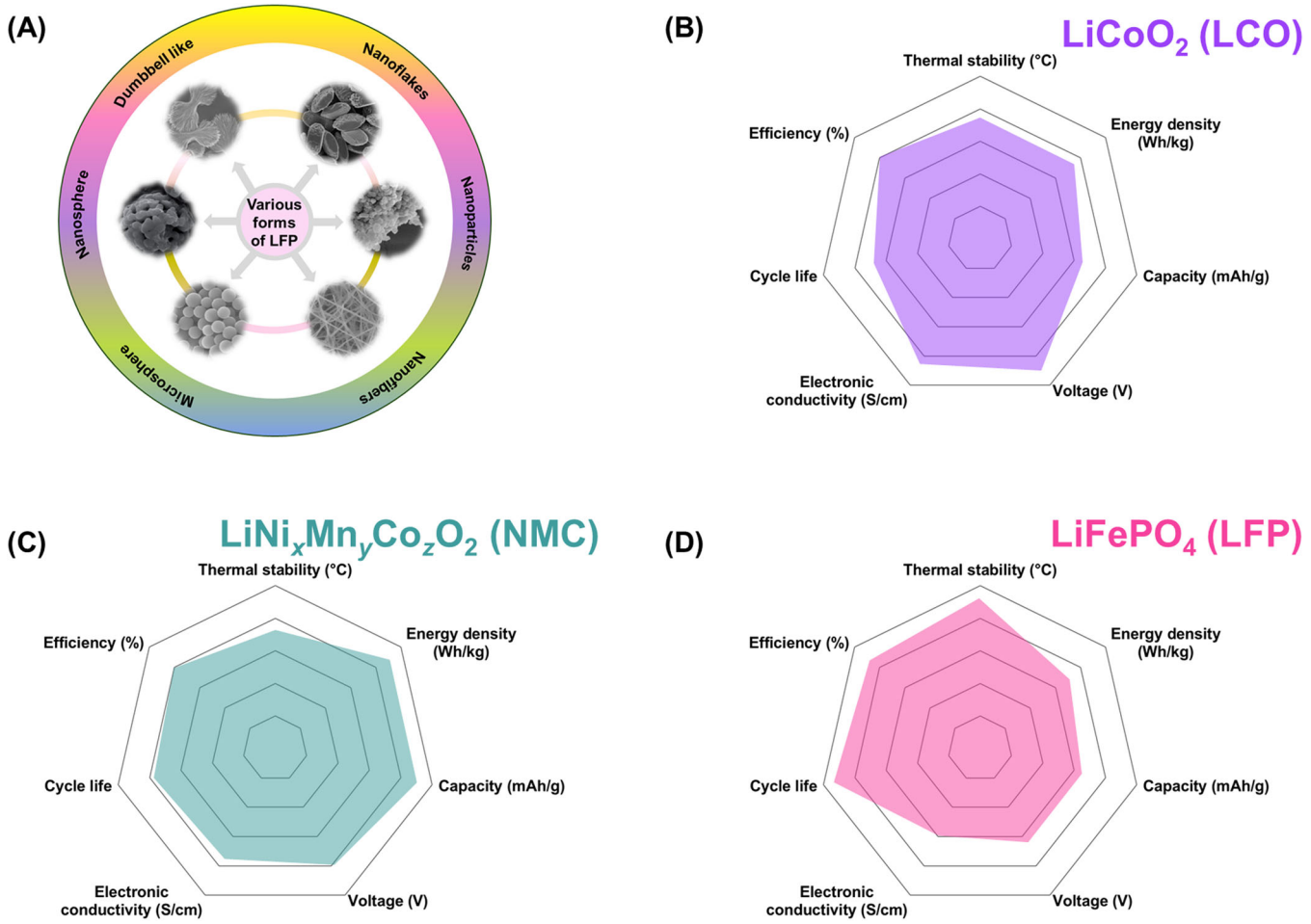

FIGURE 2 | (A) Morphological diversity of LFP cathode particles. Radar plots of (B) LCO, (C) NMC, and (D) LFP cathode materials.

LFP crystallizes in a robust olivine structure characterized by a hexagonally close-packed oxygen framework, within which Li and Fe ions occupy half the octahedral sites, and phosphorus resides in tetrahedral coordination. This stable olivine architecture resists phase collapse and oxygen release, even above 250°C, significantly reducing combustion risk and enhancing safety. LFP also offers outstanding cyclic performance, retaining over 80% of its capacity after more than 4000 cycles, and achieves high Coulombic efficiency (> 99.5%) with a low self-discharge rate (< 3% per month). However, its relatively low ED and modest voltage plateau (~3.4 V vs. Li^+/Li) restricts its competitiveness in high-energy applications. Furthermore, its intrinsic electronic conductivity is low (~10^{-9} to 10^{-10} S cm^{-1}), though this limitation is typically mitigated by the use of conductive additives and surface coatings to improve rate capability. Li-ion transport in LFP is highly directional, occurring primarily along 1D [010] channels, which, while limiting multidirectional ion diffusion, still supports fast kinetics within those pathways. Unlike LCO and NMC, LFP is free of cobalt and nickel, making it more sustainable, environmentally benign, and cost-effective. These comprehensive performance distinctions across thermal stability, energy density, voltage, cycle life, electronic conductivity, and Coulombic efficiency are systematically compared in Table 1, which highlights LFP's advantages in safety and longevity, establishing it as an ideal cathode material for EVs, stationary storage, and high-temperature applications where operational reliability is essential [55].

The electrochemical performance of LFP cathodes is strongly influenced by mass loading and electrolyte formulation, underscoring the importance of these parameters in reliable performance evaluation. High mass loading electrodes (> 10–20 mg cm^{-2}) facilitate increased areal capacity, a key metric for commercial viability. However, challenges such as ion diffusion limitations and increased polarization arise, which require optimized electrode architecture and processing routes to ensure uniform electron/ion transport and mechanical integrity [56–58]. Advanced electrode architectures incorporating carbon nanotubes (CNTs) or additive-free thick films have demonstrated improved rate capabilities and capacity retention, highlighting the importance of structural engineering in mitigating mass loading constraints. The electrolyte plays a critical role in LIBs, impacting their cycling performance, power, safety, and capacity. An ideal electrolyte must exhibit exceptional electrochemical and thermodynamic stability. The commonly used electrolyte salt $LiPF_6$ in commercial LIBs is sensitive to moisture and is thermally unstable, resulting in the generation of hydrogen fluoride (HF) and phosphorus oxyfluoride (POF_3) through reactions ($LiPF_6 + H_2O/2HF + LiF + POF_3$) and accelerated thermal decomposition ($LiPF_6/LiF + PF_5$) at elevated temperatures [59]. Both PF_5 and POF_3 act as strong Lewis acids, initiating the decomposition and polymerization of cyclic carbonate solvents such as ethylene carbonate (EC) [60]. HF, an unavoidable by-product in LIBs, corrodes SEI layers on anode and cathode materials, particularly Li transition metal oxides,

TABLE 1 | Performance metrics of LCO, NMC, and LFP batteries [52–54].

Characteristics	LCO ($LiCoO_2$)	NMC ($LiNi_xMn_yCo_zO_2$)	LFP ($LiFePO_4$)
Crystal structure	Layered	Layered	Olivine
Thermal stability	Poor (decomposes ~180°C–200°C)	Moderate to good (~230°C–250°C)	Excellent (stable > 250°C)
Energy density (Wh kg^{-1})	Cathode: 540–600	Cathode: 600–750	Cathode: 350–580
	Cell: 150–200	Cell: 150–250	Cell: 90–160
Theoretical/experimental capacity (mAh g^{-1})	274/165	~278/200	170/160
Voltage plateau (V vs. Li/Li^+)	3.8–3.9	3.6–3.7	3.3–3.5
Low temperature performance	Poor	Moderate	Moderate to poor
Electronic conductivity (S cm^{-1})	Moderate (~10^{-3})	Moderate (~10^{-6} to 10^{-9})	Very low (~10^{-9} to 10^{-10})
Cycle life	Moderate (~500–1000)	Good (~1000–2000)	Excellent (> 2000)
Coulombic efficiency (%)	Initial: ~98–99	Initial: ~90–96	Initial: ~98–99
	Average: ~90–95	Average: ~85–95	Average: ~98–99
Safety	Low (O_2 release, thermal runaway)	Good (composition-dependent)	Very high (no O_2 release)

resulting in transition metal dissolution, capacity fading, and reduced cycle life [61, 62]. While additives in the electrolyte provide partial solutions to these issues related to $LiPF_6$, the search for alternative lithium salts with high-temperature and water stability continues. LiTFSI, due to its excellent stability in heat and water, is a promising electrolyte salt for Li-ion batteries. However, its strong corrosion behavior on aluminum current collectors (Al oxidative potential around 3.7 V vs. Li/Li^+) limits its application, likely linked to the mechanism of Al oxidative dissolution [63].

2.3 | Challenges and Limitations of LFP Cathodes

At the material level, the olivine-type LFP structure exhibits inherently low ionic (~10^{-14} to 10^{-7} $cm^2 s^{-1}$) and electronic conductivity (~10^{-9} to 10^{-10} S cm^{-1}) due to the insulating nature of the phosphate framework and limited Li^+ transport pathways along the 1D [010] channel. This severely restricts Li^+ diffusion kinetics and charge transfer during high-rate operation. Additionally, the wide band gap (~3.5 eV) and tightly bonded Fe─O network hinder electron mobility, necessitating conductive carbon additives and nanoscale strategies to improve performance, which in turn increases the complexity of synthesis and electrode fabrication. At the electrode level, the low intrinsic conductivity and 1D Li-ion transport impose further challenges. Achieving thick-film electrodes (≥ 100 μm) is difficult without sacrificing rate performance, as ionic pathways and electron percolation are limited across the bulk. This results in poor areal capacities and necessitates high surface area designs or advanced architecture (e.g., carbon-coated nanostructures or hierarchical morphologies). Moreover, sluggish ionic transport within thick LFP films increases polarization and heat generation during fast charging or discharging, negatively affecting power output, and thermal management. These characteristics limit LFP's compatibility with current collector designs optimized for layered oxides and impose engineering trade-offs in electrode formulations.

At the cell level, the overall ED of LFP cells is modest, typically 120–160 Wh kg^{-1}, constrained by both the lower discharge voltage (~3.2 V vs. Li/Li^+) and theoretical capacity (~170 mAh g^{-1}) of the LFP chemistry. In contrast, Ni-rich cathodes like NMC and NCA achieve 180–250 Wh kg^{-1}. This shortfall contributes to "mileage anxiety" in EV applications, where extended driving ranges are essential. Additionally, low-temperature performance is a critical drawback: LFP cells can suffer a 30%–50% capacity loss at −20°C, driven by increased charge-transfer resistance and severely reduced ion mobility. Cold climates also accentuate internal resistance, reducing efficiency and limiting fast-charging capability. Fast-charging is further hindered by the limited number of Li^+ diffusion channels, phase boundary movement resistance, and poor electronic conductivity. Full charging typically requires over 4 h, far exceeding industry benchmarks targeting sub-15-min recharge time. Additionally, while LFP's robust framework is generally stable, repetitive cycling can trigger minor phase transitions or mechanical strain at grain boundaries, promoting microcrack formation, delamination, and eventual capacity fade. From a sustainability standpoint, LFP recycling remains inefficient, with current processes yielding less than 1% Li recovery. The lack of high-value transition metals reduces economic incentives for recycling, posing a long-term environmental challenge as global deployment expands. In sum, while LFP cathodes offer unmatched thermal and cycling stability, widespread adoption in high-energy, cold-climate, and fast-charging applications hinges on overcoming intrinsic transport limitations, architectural constraints, and energy density trade-offs through material engineering, electrode optimization, and improved system integration.

3 | Enhancing LFP: Materials and Methods

LFP is a promising cathode material for LIBs, recognized for its thermal stability, safety, low cost, and high theoretical capacity (~170 mAh g^{-1}). However, it faces challenges such as poor electronic conductivity and limited Li-ion diffusion, both of which restrict its overall performance. The disrupted FeO_6 octahedral sites in LFP hinder Li-ion diffusion, leading to increased impedance [64]. In the past few years, the researcher has addressed these limitations through a variety of advanced materials and processing strategies. Notably, multi-element doping, incorporating elements like Mg, N, S, Co, or Mn, has been shown to create beneficial impurity states, reduce the activation barrier for Li-ion movement, and significantly enhance conductivity [55, 65]. In tandem, nanostructuring approaches, including controlled particle downsizing, optimize electrode surface area and pathways for Li-ion transport, which has been demonstrated to improve rate performance and cycling stability [66, 67]. Another widely adopted enhancement involves carbon encapsulation, applying ultra-thin, uniform carbon coatings on LFP particles has recently resulted in marked reductions in charge transfer resistance and increased long-term cyclability, supporting high-capacity retention even at elevated rates [68–70]. The formation of LFP/carbon composites using advanced conductive frameworks, such as carbon black, graphene, or CNTs, creates continuous conductive networks that further boost capacity, cyclability, and power performance for demanding applications in hybrid EVs (HEVs) and stationary grid storage (Figure 3) [70, 71]. Advances in electrode formulation, including refinement of composite ratios and processing, have also led to greater electrode density, improved interface contact, and superior utilization of active material, with some recent studies achieving discharge capacities above 140 mAh g^{-1} over prolonged cycling [66]. Additionally, the field is moving toward sustainable production methods, incorporating environmentally friendly synthesis techniques and recycled materials to further enable LFP's scalability for large-scale applications [72–74]. Therefore, recent research emphasizes a dynamic and rapidly evolving landscape, firmly establishing LFP as a leading and sustainable cathode material for the next generation of LIBs [75, 76].

3.1 | Tailoring Interfaces via Coating and Doping

3.1.1 | Carbon Coating Strategies

Carbon-coated electrode materials play a crucial role in enhancing the performance of LFP by modifying surface properties. Carbon nanomaterials, such as graphene and CNTs, effectively boost electrical conductivity and prevent particle agglomeration [77, 78]. The efficacy of carbon coatings critically affects electrochemical performance of LFP, with optimal thickness ensuring efficient Li-ion diffusion. Both in situ and ex situ coating methods are used, with specific conditions determining coating uniformity and quality [79].

Cai et al. [80] demonstrated high-performance LFP/C cathodes using a synergistic carbon coating that enhanced electron mobility. Guo et al. [81] synthesized LFP/C composites from coke through low-temperature carbonization, significantly improving conductivity and cycling stability, making them suitable for high-performance LIBs. Wang et al. [82] reported LFP/C composites with a density of 2.73 g cm^{-3}, achieving superior discharge ED. Anjan Sil et al. [83] found that an LFP/C (1:1) composite with a 4.2 nm carbon coating delivered excellent electrochemical performance. Overall, carbon coatings are essential for stabilizing and optimizing LFP in LIBs. Hybrid carbon systems combining carbon black and graphene significantly enhance the conductivity and stability of LFP batteries. Dual carbon coatings leverage graphene's high conductivity and carbon black's connectivity, achieving over 160 mAh g^{-1} at 1 C and retaining > 95% capacity after 500 cycles, optimizing electron pathways and electrolyte infiltration for high-energy applications like EVs [84]. Self-catalyzed carbon architectures offer a simple route to enhance cathode design. In particular, in situ growth of CNTs and amorphous carbon shells on LFP microclews improves electronic/ionic conductivity (0.68 S cm^{-1}/2.1 × 10^{-12} cm^2 s^{-1}) and structural stability, leading to high capacity and long cycle life, as shown in Figure 4A [85]. Carbon coatings on current collectors enhance adhesion and electrical contact, while CNTs boost conductivity between binder particles, improving rate performance and cycling stability. Figure 4B illustrates that electrodes on coated current collectors retain 89% of initial discharge capacity at 5 C in a half-cell configuration, far surpassing uncoated foils [86].

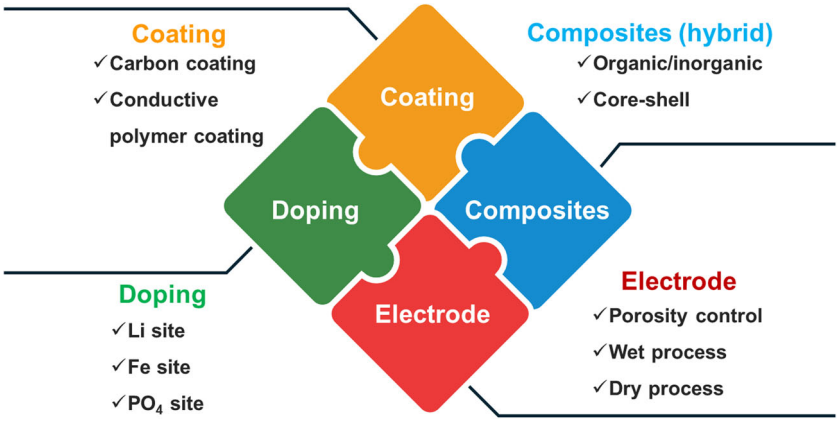

FIGURE 3 | Techniques to improve electrochemical properties.

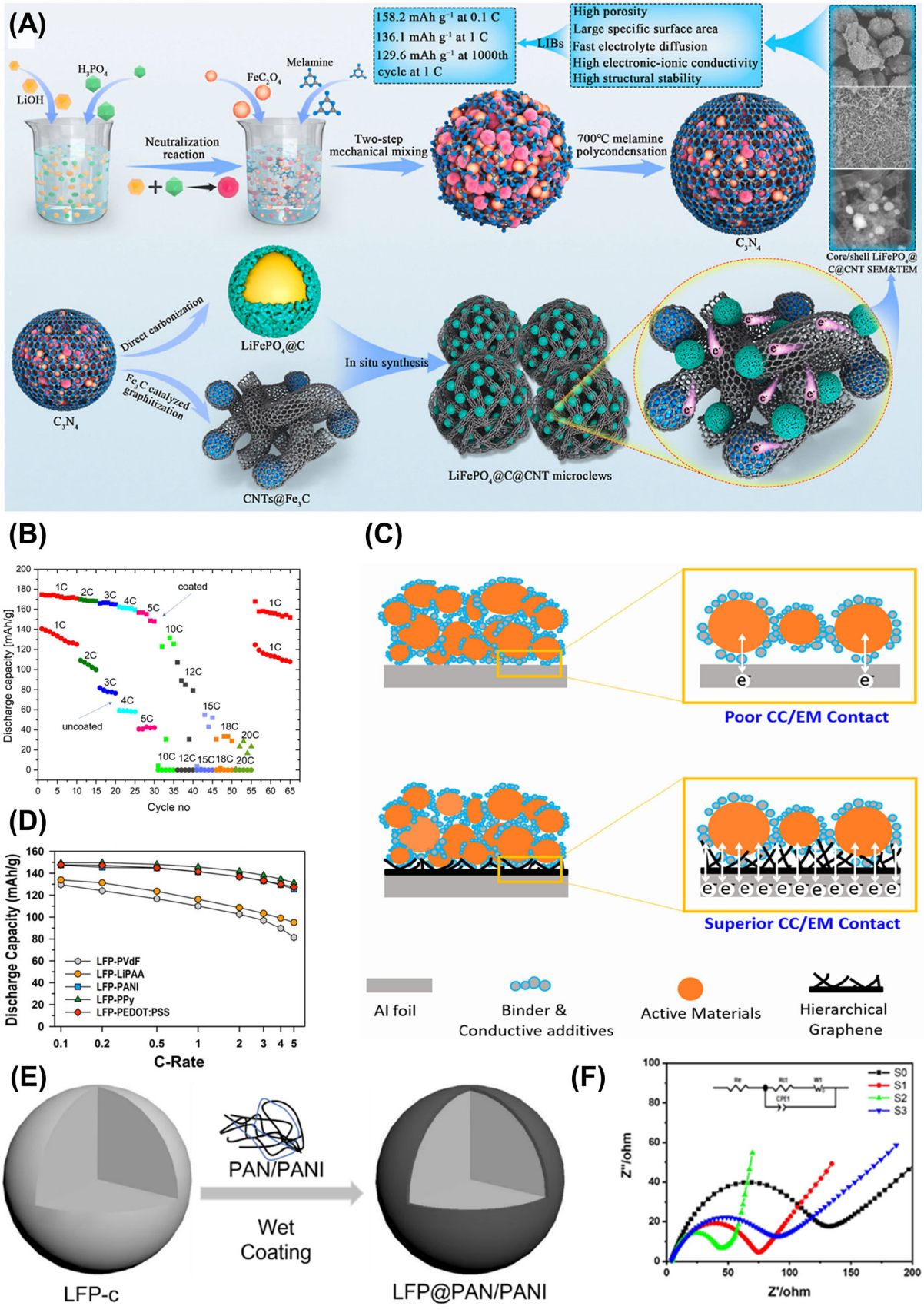

FIGURE 4 | Legend on next page.

Notably, LFP cathodes on coated collectors deliver ~80 mAh g^{-1} at 12 C, while uncoated foils fail at 10 C and above. Figure 4C reveals poor interfacial contact between micrometer-sized active materials and bare aluminum foil, causing weak adhesion and high resistance. In contrast, a hierarchical graphene layer on the foil markedly improves adhesion and electrical connectivity, effectively addressing these limitations [87].

In parallel, surface engineering strategies yield significant improvements. Yang et al. [90] developed a composite cathode using LFP/C, featuring a hybrid-layer coating of $Li_{1.4}Al_{0.4}Ti_{1.6}(PO_4)_3$ (LATP) and graphene nanosheets (GNS). The LATP layer boosts ionic conductivity, while the GNS layer enhances electronic conductivity. This LFP/C@LATP@GNS configuration exhibited excellent electrochemical performance and stability over a broad temperature range (−20°C to 50°C). Jiang et al. [91] developed an LFP@Carbon/reduced graphene oxide composite, achieving 148.3 mAh g^{-1} at 1 C and excellent cycling stability, outperforming LFP modified with carbon or graphene while demonstrating superior rate capability and minimal capacity fading after 500 cycles. Wu et al. [92] reported that LFP-2 with graphitized carbon retained 87.7% capacity after 500 cycles at 1 C, ~8% higher than LFP-1, and showed 21.3% better retention at 2 C after 235 cycles. Furthermore, the incorporation of multiple elements into the carbon layers optimized electronic conductivity and reduced Li-ion migration activation energy. Zhang et al. [93] reported MXene-decorated carbon-coated LFP with 139 mAh g^{-1} at 20 C and 94.8% retention after 500 cycles, ideal for high-power LIBs. Sulfur modification, as reported by Kwak et al. [94] using cellulose-derived carbon coatings, boosted LFP cathode performance, achieving ~152 mAh g^{-1} at 0.05 C, enhanced rate capability, and better stability at 60°C due to improved graphitization and reduced impedance. Phosphorus-doped carbon layers further reduce charge transfer resistance and enhance graphitization, improving conductivity and electrochemical performance, making these strategies critical for optimizing LFP in high-performance LIBs.

3.1.2 | Conductive Polymer Coating Strategies

Conductive polymer coatings on LFP serve as an effective alternative to carbon coatings, simplifying processing and enhancing ionic and electronic conductivity. These electroactive polymers, with conjugated backbones, achieve electrical conductivities up to 10^6 S cm^{-1} and support fast kinetics and additional capacity through Li^+ storage in their anionic structures, improving active material utilization during rapid charge/discharge cycles [95, 96]. They also provide mechanical strength, enhancing particle contact and electrode stability. The selection of polymers, such as polyaniline (PANI), polypyrrole (PPy), or poly(3,4-ethylenedioxythiophene)-poly(styrene sulfonate) (PEDOT:PSS), depends on factors including voltage stability, electronic conductivity, redox capacity, charge-discharge rates, and chemical stability in processing solvents [97, 98]. Rao et al. [88] investigated conductive polymer coatings (PANI, PPy, PEDOT:PSS) on LFP cathodes with a lithium polyacrylate (LiPAA) binder to enhance fast-charging performance in LIBs (Figure 4D). The polymers form a network around LFP particles, improving charge transport and reducing Ohmic overpotential. Using only constant current charging at 5 C-rate, which represents true fast-charging without using constant voltage charging mode, LFP cathodes with conductive polymers and LiPAA binder successfully achieved 85%–88% of their initial capacities at 25°C, outperforming 63% of a conventional LFP cathode with poly(vinylidene fluoride) (PVDF) binder. LFP–PEDOT:PSS showed the highest conductivity (0.219 S cm^{-1}), suppressing Ohmic overpotential by 71%. After 100 cycles at C/3, LFP–PPy and LFP–PEDOT:PSS retained 145 and 142 mAh g^{-1}, respectively, versus 117 mAh g^{-1} for LFP–PVDF. These findings suggest conductive polymers enable fast charging and improved stability for EV applications.

Liu et al. [89] explored improving the low-temperature rate performance of LFP cathodes by surface modification with polyacrylonitrile/polyaniline (PAN/PANI) polymers (Figure 4E). LFP@PAN/PANI exhibits superior electrochemical performance compared to bare LFP, with a discharge capacity of 3088.97 mAh at low temperature and high rate conditions (−20°C, 26650-type cylindrical battery, 5 C rate), and a relatively high low-temperature discharge plateau (2.68 V). Electrochemical impedance spectroscopy (EIS) revealed that the PAN/PANI coating increased the Li^+ diffusion coefficient by an order of magnitude, reducing charge transfer resistance and enhancing capacity retention (Figure 4F). The polar cyano groups in PAN improved Li^+ interaction, while PANI boosted electronic conductivity, with their synergistic effect enhancing both electronic conductivity and Li^+ transport via dipole-dipole interactions with the electrolyte [99, 100]. These PAN/PANI coatings significantly enhance LFP's low-temperature and high-rate performance, making them ideal for EV applications in cold climates. Boyano et al. [101] developed a C-LFP/PPy composite cathode using potential step electrodeposition, optimizing parameters like oxidation time and step count. The PPy coating improved conductivity, adhesion, and charge-storage capacity, achieving 154 mAh g^{-1}, a 20% improvement over conventional cathodes. The PPy-LFP composite reduced charge-transfer resistance to 75.14 Ω cm^{-2}, compared to 840 Ω cm^{-2} for bare LFP, enhancing electrochemical performance.

3.2 | Lattice and Interface Doping Strategies

When dopants of different elements are introduced into the crystal structure of LFP, they influence the material's properties

FIGURE 4 | (A) Schematic illustration of C_3N_4 formation from melamine and its in situ use for synthesizing CNT-wrapped, carbon-coated LFP via Fe_3C-catalyzed carbonization at 700°C. Reproduced with permission [85]. Copyright 2022, Elsevier. (B) Discharge capacities of LFP cathodes with/without carbon-coated current collectors at various C-rates (2.5–4 V). Reproduced with permission [86]. Copyright 2022, Springer Nature. (C) Electrode interface schematics: bare versus graphene-coated aluminum foil. Reproduced with permission [87]. Copyright 2020, American Chemical Society. (D) Specific discharge capacity variation. Reproduced with permission [88]. Copyright 2024, American Chemical Society. (E) Schematic of LFP@PAN/PANI synthesis and (F) EIS plots (25°C, −20°C) and corresponding equivalent circuits. Reproduced with permission [89]. Copyright 2023, Springer Nature.

through their intrinsic characteristics such as atomic radius, charge density, and electronic configuration. The variation in atomic radius can alter lattice parameters and introduce strain, potentially improving structural stability or causing distortions that affect material performance [102]. Charge density plays a key role in modifying electronic and ionic conductivity, with higher charge density generally enhancing electronic conductivity but potentially altering charge distribution and local electrostatic interactions. The electronic configuration of the dopants directly impacts the redox behavior and charge transfer kinetics, influencing overall electrochemical performance [103, 104]. Balancing these factors is crucial for optimizing capacity, rate capability, and cycle life while avoiding negative interactions that could compromise the material's stability and efficiency. Research on multi-element doping explores the effects of doping on different crystal sites, with a focus on doping at single or multiple sites like Li, Fe, and PO_4. Notably, studies report co-doping on Fe/Li and Fe/PO_4 sites. The doping strategy is typically guided by factors such as ionic radii and charge density, with density functional theory (DFT) calculations used to evaluate the formation energy of the dopants before structural analysis through various characterization techniques [102].

3.2.1 | Li-Site Doping Strategies in LFP

The main dopants for the Li-site in LFP are alkaline metal ions that have the same valence state as Li^+ and hence, do not alter the charge state. Both Na^+ and K^+ have been studied as single dopants on the Li-site, and it was proven by first-principle calculations that they enhance the electronic conductivity enormously [105, 106]. Na^+ and K^+ doping at the Li site in LFP increases charge density around the Li site, promoting electron transfer and enhancing conductivity. First-principle calculations suggest that higher dopant concentrations improve conductivity; however, experimental data shows that only low doping levels ($x < 0.25$ in $Li_{1-x}Na_xFePO_4$ and $x = 0.005$ in $Li_{1-x}K_xFePO_4$) improve performance, as the larger ionic radii compared to Li^+ (0.76 Å) cause structural distortion and reduced capacity at higher concentrations [55, 105, 107, 108]. Sovizi et al. [108] studied Na^+ and K^+ co-doping in $Li_{1-x-y}Na_xK_yFePO_4$/C using a sol–gel method. X-ray diffraction (XRD) confirmed a single-phase olivine structure with improved crystallinity in co-doped samples. The optimal composition, $Li_{0.97}Na_{0.02}K_{0.01}FePO_4$/C, increased lattice parameters *a*, *c*, and unit cell volume while reducing *b*, enhancing Li^+ diffusion along the *b*-axis. This composition achieved the highest discharge capacity of 163.9 mAh g^{-1} at 0.1 C with excellent high-rate performance (94.3 mAh g^{-1} at 5 C). Cyclic voltammetry (CV) indicated minimal polarization, and EIS showed the lowest charge transfer resistance and highest Li^+ diffusion coefficient, confirming superior electrochemical kinetics.

In contrast, Ti^{4+} doping (ionic radius 0.61 Å) provides a distinct approach, achieving excellent cycling stability with a discharge capacity of 133 mAh g^{-1} at 1C after 100 cycles, and 102.3% retention of initial capacity, driven by improved electronic conductivity, reduced particle agglomeration, and enhanced rate capability at high C-rates [109]. Figure 5A illustrates improved charge transfer kinetics with increasing Ti^{4+} content, confirming enhanced Li^+ diffusion and reduced charge transfer resistance, mitigating kinetic limitations [110]. Similarly, niobium (Nb) doping, as in $Li_{0.98}Nb_{0.02}FePO_4$/C, expands lattice volume and reduces charge transfer resistance, enhancing both electronic and ionic conductivity, making it a promising approach for high-performance LIBs [117]. Beyond alkali metal doping, multivalent cations like aluminum (Al^{3+}, ionic radius 0.54 Å), zirconium (Zr^{4+}, 0.72 Å), and tungsten (W^{6+}, 0.60 Å) introduce Li vacancies to balance charge, lowering the energy barrier for Li^+ diffusion [118]. Al^{3+} doping in the Li sublattice of LFP improves Li^+ diffusion and electrochemical performance, offering better capacity retention at high rates compared to undoped LFP, though its capacity is lower than nanostructured LFP. This highlights the critical role of Li vacancies in enhancing ionic conductivity [119]. Figure 5B shows that Al-doped LFP (LAFP01) delivers the highest specific capacity at 5 C, while all samples, including undoped LFP, maintain similar capacity retention over 100 cycles, indicating stable cycling with Al^{3+} doping [111]. The potential of doping at the Li-site, combining alkali and multivalent cations, remains underexplored due to uncertain synergistic interactions, but it holds promise for further optimizing LFP's electrochemical performance for EV and HEV applications.

3.2.2 | Fe-Site Doping Strategies in LFP

Iron (Fe) site doping in LFP outperforms Li site doping, attracting greater research interest due to its promising results [120]. It weakens the Li–O bond, expanding lattice volume and enhancing ion mobility and diffusion coefficients. Additionally, it reduces lattice distortion and crystal surface energy, leading to smaller particle sizes and improved electrochemical performance. Multi-element doping at the Fe site further optimizes LFP as a cathode material for LIBs. This approach significantly boosts electronic conductivity, specific capacity, and cycling stability, making LFP ideal for high-performance applications such as EVs, portable electronics, and renewable energy storage systems.

First-principles DFT studies show that substituting the Fe site in LFP with metals of slightly different ionic radius, such as V, Co, Nb, Mn, or Mo, does not disrupt the overall crystal structure but leads to changes in lattice parameters and an expansion of the cell volume [102, 103, 121]. This structural change, seen experimentally via Rietveld refinement, facilitates Li-ion diffusion in the 1D channels and can restrain volume fluctuations during cycling, as shown by Cao et al. [104] report of Co- and Nb-doped LFP (Figure 5C). Additionally, dopant d-orbitals near the Fermi level narrow the band gap, enhancing electronic conductivity by promoting electron hopping, with density of states (DOS) analyses confirming the key role of dopant-derived states (Figure 5F). Therefore, Fe-site substitution has proven to be a practical and effective strategy for improving the electrochemical behavior and structural resilience of LFP cathodes, particularly under challenging conditions. Doping with transition metals, such as Zn and Ru, introduces a "pillar effect" within the olivine lattice, stabilizing the crystal framework during repeated lithiation and delithiation cycles. This effect not only prevents lattice shrinkage but also expands the

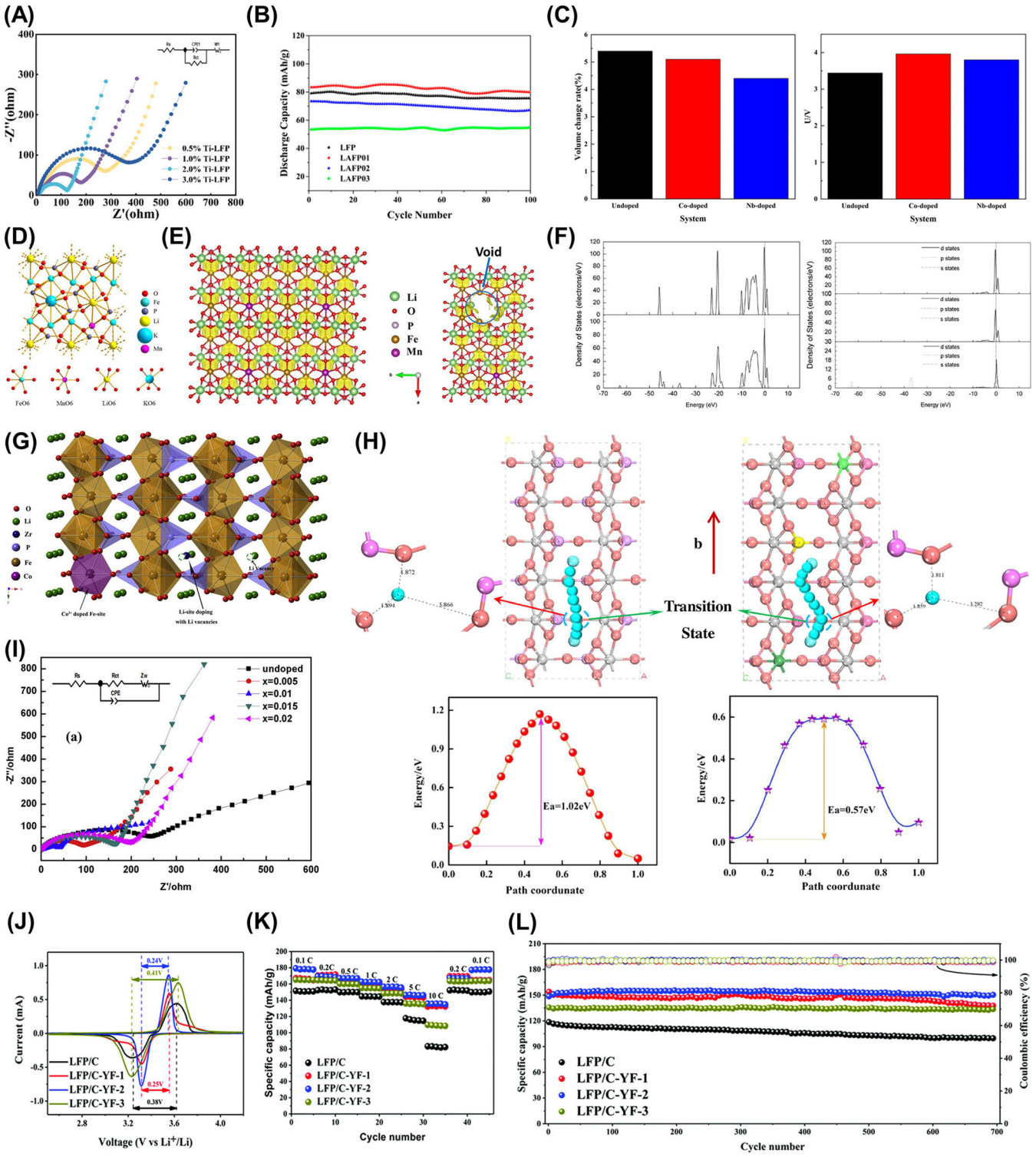

FIGURE 5 | (A) EIS and corresponding circuit model. Reproduced with permission [110]. Copyright 2025, Springer Nature. (B) Cycling performance at 5 C. Reproduced with permission [111]. Copyright 2025, American Chemical Society. (C) LFP volume change rate and average Li extraction voltage. Reproduced with permission [104]. Copyright 2024, Springer Nature. (D) Crystal structure and elemental composition, and (E) Li^+ diffusion paths and proposed Mn dissolution mechanism. Reproduced with permission [113]. Copyright 2023, Elsevier. (F) Calculated TDOS of LFP and $LiFe_{1-3/12}Mo_{1/12}PO_4$; Fe and Fe/Mo DOS, with Fermi level at 0 eV. Reproduced with permission [112]. Copyright 2012, Elsevier. (G) Crystal structure of Zr, Co co-doped LFP and (I) Nyquist plots for LFP and $Li_{0.99}Zr_{0.0025}Fe_{1-x}Co_xPO_4$ (x = 0.005–0.02). Reproduced with permission [114]. Copyright 2017, Elsevier. (H) Li^+ migration in $LiFe_{10/12}Co_{1/12}Mn_{1/12}P_{11/12}S_{1/12}$ along b-channel. Reproduced with permission [115]. Copyright 2021, Elsevier. (J) CV curves at 0.1 mV s^{-1}, (K) rate performance, and (L) cycling performance at 5 C of LFP/C, LFP/C-YF-1, LFP/C-YF-2, and LFP/C-YF-3 electrodes. Reproduced with permission [116]. Copyright 2021, Royal Society of Chemistry.

diffusion pathways for Li^+ ions, resulting in higher conductivity and improved Li-ion diffusion, which ultimately enhances rate capability and discharge capacity [122, 123]. Additionally, the substitution of Co has been shown to reinforce the PO_4 tetrahedron while weakening the Li—O bonds, contributing to better cycling stability and improved overall performance in $LiFe_{0.99}Co_{0.01}PO_4$/C composites [124].

Doping LFP with optimal levels of vanadium enhances performance by inducing precise lattice distortion and refining particle structures. This transformation lowers the energy barrier for Li ion migration through the 1D diffusion channels in both LFP and $FePO_4$ phases, boosting overall material efficiency [125]. The reduction in diffusion resistance is directly linked to the expansion of ion channels. Vanadium doping weakens Li—O interactions and boosts conductivity, leading to improved electrochemical response in LFP/C systems [126]. Similarly, Cu^{2+} substitution increases interplanar spacing in the [010] direction, enabling faster Li-ion movement. Consequently, Cu-doped LFP/C shows superior Li^+ storage kinetics and enhanced electrochemical activity compared to LFP/C [127]. Optimizing Mo doping at the Fe site effectively maintains the olivine structure of LFP while significantly boosting Li^+ diffusion compared to undoped materials [128]. The $LiTi_{0.08}Fe_{0.92}PO_4$ cathode showcases impressive specific capacities, superior capacity retention, and excellent rate capabilities [129]. This remarkable performance is likely attributed to the enhanced ionic migration pathways created by the strategically positioned NASICON particles nestled between the olivine particles. The introduction of doped Ni leads to a reduction in electrode polarization and electrochemical impedance when compared to pure LFP. This results in a specific capacity of 175 mAh g^{-1} at 0.2 C following adequate activation, exceeding the theoretical limit of 170 mAh g^{-1} [130].

Furthermore, targeted Mn^{2+} doping has been shown to enhance both electronic and ionic transport, markedly improving the performance of LFP/C composites even under demanding conditions [131, 132]. The substitution of Fe by Mn in LFP ($LiMn_xFe_{1-x}PO_4$, $0 \leq x \leq 1$, LMFP) introduces a dual effect due to the relatively large ionic radius of Mn and its intrinsically sluggish electrochemical kinetics. Partial Mn incorporation expands the unit cell, which facilitates lithium-ion migration and improves electronic conductivity, thereby enhancing the overall electrochemical response of the cathode [133]. Gupta et al. [134] reported that conductivity improved steadily up to 15 at% Mn substitution but declined sharply at 20 at% due to structural instabilities associated with excessive doping. This nonlinear trend reflects the balance between lattice expansion, which eases Li^+ migration, and the emergence of high-spin Mn^{3+}, which induces Jahn–Teller (J–T) distortions that hinder ion diffusion and slow charge transfer [135, 136]. In addition to these structural issues, dissolution of Mn^{2+} during cycling progressively disrupts the cathode framework, contributing to capacity fading. Beyond conductivity, Mn doping also impacts the electrochemical profile by introducing the Mn^{2+}/Mn^{3+} redox couple, which operates at ≈ 4.1 V, substantially higher than the ≈ 3.45 V of the Fe^{2+}/Fe^{2+} redox pair, thereby increasing the cell voltage and theoretical energy density [137, 138]. However, this voltage gain is offset by sluggish Mn redox kinetics, aggravated J–T distortions, and reduced structural stability, which together limit rate capability and cycle life [139, 140]. To overcome these challenges, recent studies have proposed strategies including co-doping with Mg, Ni, Nb, or V to suppress J–T activity and improve redox kinetics [140, 141], carbon coatings to enhance conductivity and mitigate Mn dissolution [138], and engineered microstructures such as core–shell or heterostructured LMFP to decouple Mn-rich regions from strain-sensitive domains [137]. Collectively, these findings demonstrate that while Mn substitution raises the voltage and ED of olivine cathodes, excessive doping introduces severe structural and kinetic limitations, making LMFP a high-energy but design-sensitive material system.

Rare-earth metal-doping strategies have further extended the performance enhancements of LFP cathodes. Specifically, cerium (Ce) doping optimizes crystal microstructure and particle size, decreases charge transfer resistance, and improves electrical conductivity and Li^+ diffusion rate in LFP/C [142]. The $LiCe_{0.1}Fe_{0.9}PO_4$/C has good cycle performance, that is, the capacity retention ratio is 99.6% after 100 cycles of 1 C. Moreover, rhodium (Rh) substitution enhances the rate capability of LFP/C, with the $LiFe_{0.975}Rh_{0.025}PO_4$/C sample demonstrating a high-rate performance and a longer cycling life than LFP/C at high temperatures [143]. Additionally, appropriate samarium (Sm) doping at the Fe sites enhances electronic conductivity and Li^+ diffusion, while concurrently decreasing charge transfer resistance [144]. In conclusion, the substitution of Fe ions stands out as an effective strategy for significantly enhancing the structural stability and electrochemical properties of LFP cathode materials, even under extreme conditions. To further amplify these electrochemical benefits through synergistic effects, innovative approaches like co-doping, introducing elements such as Ni and Mn or Ti and V at the Fe site, have been explored [145, 146]. However, similar to the Li site substitution, the amount of element doping is too much; it could hinder the Li^+ diffusion during the cycle, which would harm the electrochemical performance. Therefore, meticulous adjustment of the substitution levels during the synthesis process is essential for optimizing the properties and ensuring superior functionality.

3.2.3 | PO_4 Site Doping Strategies in LFP

Anionic site (PO_4) doping in LFP, targeting oxygen (O) and phosphorus (P) sites with elements, such as fluorine (F), chlorine (Cl), sulfur (S), nitrogen (N), boron (B), and silicon (Si), offers a transformative approach to enhancing its electrochemical performance for advanced LIB cathodes [147]. Substitutions at O-sites (e.g., F, Cl, S, N) and P-sites (e.g., B, Si) modulate the electronic and ionic properties, addressing LFP's intrinsic limitations like low conductivity and sluggish Li-ion diffusion [148–151]. *Ab initio* calculations demonstrate that N–S co-doping strengthens Fe—N bonds, minimizing the band gap (e.g., $Li_8Fe_8P_8O_{29}NS_2$ exhibits the smallest band gap) and reducing Li-ion migration barriers to 0.31 eV ($Li_8Fe_8P_8O_{29}S_3$) and 0.36 eV ($Li_8Fe_8P_8O_{28}NS_3$), enabling faster diffusion pathways critical for high-rate applications [152]. These findings highlight the potential of co-doping to optimize LFP for energy storage applications. Similarly, B–Mg co-doping in $LiFeMg_xP_{1-x}B_xO_4$ optimizes oxygen vacancy distribution, enhances electronic conductivity, and lowers charge-transfer resistance, resulting in superior cycling stability and rate capability [153].

F doping, as in $LiFePO_{4-x}F_x/C$ ($x = 0.15$), achieves a remarkable capacity of 115.7 mAh g^{-1} at 30 C, recovering to 164 mAh g^{-1} at 0.1 C [151]. The introduction of F doping leads to a beneficial rearrangement of the electron cloud in the PO_4^{3-}, enhancing the intrinsic conductivity and addressing the inherent limitations of LFP materials.

This advancement contributes significantly to improved structural stability. DFT calculations indicate that co-doping LFP with Si at the P site and F at the O site alters the characteristics of the conduction band edge [70]. Specifically, this modification transitions the conduction band from being dominated by localized Fe 3d states to featuring more delocalized states derived from F s and cation s orbitals. Consequently, this transition changes the carrier transport mechanism from a polaron-like process to a band-like mechanism, resulting in a substantial enhancement of the electrical conductivity of LFP [154]. Cl doping enhances the microstructure, conductivity, and Li^+ diffusion in LFP/C, leading to 164.1 mAh g^{-1} at 0.1 C (96.5% of theoretical) [155]. It retains 68.9 mAh g^{-1} at 20 C and shows full recovery, indicating excellent structural integrity. The use of acid-washed iron oxide red offers a cost-effective synthesis route. These advancements position anionic doping as a key strategy for tailoring LFP's lattice dynamics and electrochemical kinetics, promising high-performance, durable cathodes for EVs, grid storage, and portable electronics, though optimizing dopant ratios and long-term stability remains critical for commercial adoption.

3.2.4 | Multiple Sites Doping Strategies in LFP: Li and Fe Sites

Synergistic co-doping of Li and Fe sites in LFP significantly enhances its electrochemical performance by mitigating challenges like charge imbalance and microstructural instability, as the secondary dopant compensates for issues introduced by the primary ion. For instance, Geng et al. [113] demonstrated that doping Li sites with alkali metals and Fe sites with transition metals stabilizes the lattice and boosts performance. The energetic favorability of Li–Fe anti-site defects, driven by the similar ionic radii of Li^+ (0.76 Å) and Fe^{2+} (0.77 Å), promotes mutual substitution, reducing lattice strain and facilitating Li^+ diffusion. Additionally, high-valence dopants further amplify performance by introducing holes into the lattice, which boosts electronic conductivity and accelerates Li-ion transport through enhanced charge carrier mobility. These modifications collectively improve LFP's ionic and electronic kinetics, critical for achieving high-rate performance in LIB cathodes.

The strategic use of dopants with varying valence states also minimizes defect-related energy barriers, promoting structural resilience during repeated charge-discharge cycles. Yang et al. [156] investigated Na/V co-doping in LFP/C, finding that $Li_{0.97}Na_{0.03}Fe_{0.97}V_{0.03}PO_4/C$ delivered 156.5 mAh g^{-1} at 0.1 C and 111.8 mAh g^{-1} at 5 C, with 90% retention after 30 cycles. Co-doping reduced particle size and enhanced Li^+ diffusion, improving ionic transport. At −20°C, it outperformed pristine LFP, delivering 76.7 mAh g^{-1} at 1 C versus 52.5 mAh g^{-1}, due to reduced charge-transfer resistance and improved conductivity. Na^+/Ti^{4+} co-doping in $Li_{1-x}Na_xFe_{1-x}Ti_xPO_4/C$ ($x = 0.00$–0.05) expands the lattice and reduces particle size, with $Li_{0.97}Na_{0.03}Fe_{0.97}Ti_{0.03}PO_4/C$ achieving 151 mAh g^{-1} at 0.1 C, 99.3% capacity retention after 100 cycles, and superior rate capability up to 20 C, driven by enhanced Li^+ diffusion and lowered charge-transfer resistance. Tian et al. [157] investigated Nb^{5+}/Ti^{4+} co-doping combined with graphene coating in $Li_{0.99}Nb_{0.01}Fe_{0.97}Ti_{0.03}PO_4/G$ yields 163 mAh g^{-1} at 0.1 C (near theoretical capacity), 99.1% retention after 30 cycles, and 140 mAh g^{-1} at 5 C, attributed to improved ionic conductivity and a 3D graphene network facilitating rapid Li^+ and electron transport. Geng et al. [113] studied K^+/Mn^{2+} co-doping in LFP (KLMFP) by replacing 3% Li and 5% Fe with K and Mn, respectively, using a solvothermal method. KLMFP exhibited lattice expansion due to larger ionic radii and a narrower band gap from Fe–Mn orbital hybridization, improving Li-ion diffusion, structural stability, and electronic conductivity (Figure 5D,E).

Gao et al. [114] synthesized $Li_{1-x}Zr_{x/4}Fe_{0.99}Co_{0.01}PO_4$ composites by incorporating Zr^{4+} and Co^{2+} into the Li and Fe sites, respectively. Among $Li_{0.99}Zr_{0.0025}Fe_{1-x}Co_xPO_4$ ($x = 0.005$, 0.01, 0.015, 0.02) composites, $Li_{0.99}Zr_{0.0025}Fe_{0.99}Co_{0.01}PO_4$ delivered the best performance, achieving an initial discharge capacity of 139.9 mAh g^{-1} at 0.1 C with 85% retention after 50 cycles. The optimized crystal structure (Figure 5G) revealed that Zr^{4+} substitution creates Li^+ vacancies and Co doping weakens Li–O interaction, lowering the band gap from 0.549 to 0.514 eV. EIS results (Figure 5I) further confirmed that the $x = 0.01$ sample had the lowest charge-transfer resistance and highest Li-ion diffusion coefficient. These approaches underscore the potential of tailored co-doping to overcome LFP's intrinsic conductivity limitations, paving the way for advanced cathode materials, with ongoing research needed to refine dopant combinations and assess their impact on long-term electrochemical stability.

3.2.5 | Multiple Sites Doping Strategies in LFP: Fe and PO_4 Site

Simultaneous co-doping of Fe and PO_4 sites in LFP leverages synergistic effects to significantly enhance its electrochemical performance, with transition, alkaline, or alkaline-earth metals substituting at Fe sites and non-metals doping the PO_4 anionic sites. Cui et al. [115] performed a DFT study using the CASTEP program on Co/Mn (Fe-site) and S (P-site) co-doped LFP ($LiFe_{10/12}Co_{1/12}Mn_{1/12}P_{11/12}S_{1/12}$). Doping expanded the unit cell and showed good stability with a formation energy of 2.01 eV and binding energy of −54.298 eV. The migration pathway, as well as activation energies for undoped and co-doped LFP (Figure 5H), reveals that the activation energy was almost twice smaller for the co-doped sample, hence the diffusion values were calculated to be 2×10^{-22} and 3×10^{-12} $cm^2 s^{-1}$ for undoped and doped LFP, respectively. In other studies, modified cathode, La–F–LFP, demonstrates superior discharge capacities of 139.3 mAh g^{-1} at a high rate of 5 C and 127.2 mAh g^{-1} at −20°C, along with excellent capacity retention of 97.1% after 100 cycles at 45°C [158]. These improvements are attributed to the expanded lattice parameters and enhanced Li^+ diffusion pathways due to La^{3+} doping, as well as the weakening of Li–O bonds and stabilization of the crystal structure by F doping. The (LF(CM)P(S)O) system demonstrates enhanced stability and conductivity, achieving an operating voltage of 4.76 V due to co-doping strategies. This improvement is attributed to a significant reduction in

activation energy, a diminished band gap, and the widening of Li-ion diffusion pathways, collectively promoting superior Li-ion transport characteristics [115].

Lv et al. [159] reported that co-doping of Fe and PO_4 sites in LFP/C with V^{3+}/F^- and Mg^{2+}/F^- significantly enhances its electrochemical performance, particularly for high-rate and low-temperature LIB applications, by optimizing ionic and electronic conductivity. V^{3+}/F^- co-doping, achieved via high-temperature ball milling, yields a capacity of 165.7 mAh g^{-1} at 0.1 C with 98.5% retention after 100 cycles and 133.6 mAh g^{-1} at 10 C under low temperatures, driven by reduced polarization, enhanced Li-ion diffusion, and a stable carbon-coated porous morphology that lowers charge transfer resistance (R_{ct}). Similarly, Mg^{2+}/F^- co-doping, prepared by a solid-state method, delivers a superior discharge capacity of 164 mAh g^{-1} at 0.1 C and 98 mAh g^{-1} at 10 C, with excellent cycling stability across low and high temperatures, attributed to improved ionic/electronic conductivity and minimized R_{ct}. These enhancements result from synergistic effects: V^{3+} and Mg^{2+} at Fe sites modify the electronic structure to boost conductivity, while F^- substitution at PO_4 sites restructures the lattice to facilitate Li-ion diffusion by reducing diffusion barriers and stabilizing the carbon coating. Wang et al. [116] developed a dual-site co-doping strategy for LFP, substituting Fe with Y and P with F to optimize Li^+ diffusion and electronic conductivity. The LFP/C-YF-2 composite, synthesized via carbothermal reduction using Span80 to control particle size, exhibited superior electrochemical performance (Figure 5J–L). It delivered a high initial discharge capacity of 179.3 mAh g^{-1} at 0.1 C and maintained 135.8 mAh g^{-1} at 10 C, far outperforming pristine LFP. The co-doped sample showed a minimal voltage gap in CV profiles, indicating enhanced redox kinetics, and achieved remarkable cycling stability with negligible capacity loss after 700 cycles at 5 C. Y doping introduced Li^+ vacancies, reducing spatial diffusion resistance, while F doping improved electronic conductivity by modulating the PO_4^{3-} electron cloud. Additionally, the LFP/C-YF-2 composite exhibited surface/interface Li storage, contributing to capacities exceeding the theoretical value. These results highlight the strong potential of Y/F co-doping in advancing fast-charging, long-life LIB cathodes (Tables 2 and 3).

3.3 | Hybridization and Composite Engineering Strategies

The primary objective of LFP composite with metallic elements, metal oxides, or binders is to enhance interparticle conductivity while maintaining the structural integrity of the material. Figure 6A is a schematic diagram of LFP and zwitterionic polymer (ZIP), due to which ZIPs exhibit excellent structural stability in liquid electrolytes and strong adhesion [176]. Moreover, the ethylene oxide (EO) units and zwitterionic groups in the binder enhance Li^+ transport, as evidenced by improved ionic conductivity. The synthesis of LFP cathode materials coated with reduced graphene oxide (rGO) for advanced LIBs formed through a high-temperature reduction strategy, features LFP nanoparticles uniformly embedded within an rGO matrix, creating a core–shell structure [172]. This design enhances electronic conductivity and structural stability, addressing LFP's inherent limitations. The composite exhibits a high reversible capacity of 165 mAh g^{-1} at 0.2 C, excellent rate capability (up to 10 C), and remarkable cycling stability (98% capacity retention after 1000 cycles at 5 C).

Liu et al. [181] compare the electrochemical performance of LFP with different conductive additives. Another study reveals that rGO enhances electrical conductivity by enabling efficient electron transport. Carbon nanofibers (CNFs) prevent rGO stacking and LFP nanoparticle agglomeration during pyrolysis. The resulting LFP@rGO/CNF composite exhibits excellent rate performance and high ion mobility. This simple synthesis method shows great promise for LFP-based LIBs in EVs and beyond. GCD measurements reveal that LFP with 10 wt% rGO-5 offers optimal electrochemical performance, achieving an initial discharge capacity of 160.95 mAh g^{-1} at 0.1 C and excellent cycling stability with 92% retention after 100 cycles at 1 C. This performance surpasses standard carbon black (SP) and other rGO variants (Figure 6B,C) [177, 181]. Additionally, incorporating small amounts of carbon additives, such as CNTs, into PEDOT:PSS binders can further enhance LIB performance [182].

Zhu et al. [178] explore the use of liquid metal (GaIn) nanoparticles as a conductive agent in LFP cathodes to improve volumetric ED and electrochemical performance. Unlike carbon black, GaIn reduces electrode porosity and minimizes side reactions, especially at high temperatures. The LFP@nGaIn electrodes achieve a 20.7% increase in volumetric ED, with porosity reduced to 19.1% compared to 36.6% in carbon black-based electrodes (Figure 6D). Zhou et al. [183] introduce a novel synthesis method for LFP/polyacene (PAS) nanocomposites. This results in nanosized LFP particles (20–60 nm) uniformly coated with a thin PAS layer, enhancing electronic conductivity and Li^+ diffusion. The LFP/PAS nanocomposite delivers high discharge capacities of 142, 135, 124, 110, and 80 mAh g^{-1} at 1, 2, 5, 10, and 20 C, respectively, and exhibits stable performance across a wide temperature range (−20°C to 60°C). Liu et al. [179] investigated the modification of LFP/C composites with tantalum carbide (TaC) to address the limitations of low electronic conductivity and poor Li-ion diffusivity in LFP, a promising cathode material for LIBs. By co-coating LFP particles with TaC and amorphous carbon, the authors demonstrate enhanced electron and Li-ion transfer, leading to improved electrochemical kinetics (Figure 6E).

The synthesis of LFP/very-few-layer-graphene (VFLG) composites significantly enhances LIB performance, increasing specific discharge capacity by 58.3% at a 1 C rate [180]. The discharge curve is flatter, indicating better electrochemical kinetics and efficiency, while polarization is reduced to 0.747 V. Lower charge-transfer resistance and a higher Li-ion diffusion coefficient (2.29×10^{-13} cm^2 s^{-1}) further highlight the improvements due to a conductive VFLG network (Figure 6F,G). Overall, LFP/VFLG composites show superior performance, making them promising for high-performance batteries. Mahmud et al. [184] found that 0.01 mol NiO doping into LFP/C forms a solid solution, boosting Li-ion diffusion and achieving 158.8 mAh g^{-1} capacity. León reported ZnO doping slightly improved capacity but reduced cycle stability [185]. Hu et al. [186] developed ZnO-doped nano-LFP, achieving remarkable cycling stability with only 1.8% capacity loss after 100 cycles, attributed to nanoscale ZnO particles enhancing electronic conductivity and stabilizing the lattice against

TABLE 2 | Summary of electrochemical performances of multi-doped LFP cathodes.

#	Doping elements	Specific capacity (mAh g^{-1})	Energy density (Wh kg^{-1})	Undoped LFP (mAh g^{-1})	Charge-transfer resistance (Ω)	Li-ion diffusion coefficient (cm^2 s^{-1})	Reference
	Li-Site Doping						
1	Na, K	163.9	557.3	153	47.6	1.27×10^{-11}	[108]
2	Co, Zr	139	472.6	99	31	3.80×10^{-12}	[114]
3	Na	156	530.4	158	—	—	[160]
	Fe-Site Doping						
4	V, Ni	134.2	456.3	132	48	8.08×10^{-16}	[161]
5	Mg, Ti	164	557.6	161	—	1.5×10^{-10}	[162]
6	Nb	169	574.6	137	51	5.29×10^{-15}	[163, 164]
	Ti	143	486.2	138	40	—	
7	Mg	127	431.8	—	—	—	[165]
8	Ni, Mn	164	557.6	152	104.2	3.01×10^{-13}	[145]
	PO_4-Site Doping						
9	S, N	157	533.8	126	80	1.38×10^{-13}	[166]
10	F	165.7	563.4	140	—	40	[167]
11	B, Mg	147	499.8	137	167	1.9×10^{-14}	[153]
12	La, F	139.3	473.6	110	111	2.82×10^{-16}	[158]
	Other Co-Doping (Li, Fe, PO_4 Sites)						
13	Na, V	156.5	531.7	134	—	—	[156, 157]
	Nb, Ti (Li, Fe-site)	163	554.2	131	90	—	
14	La, Y (Fe, PO_4 site)	160	544.0	150	45	3.68×10^{-13}	[168]
15	Y, F (Fe, PO_4-site)	179.3	609.6	151	—	2.257×10^{-9}	[116]

TABLE 3 | Summary of electrochemical performances of other optimized LFP cathodes.

#	Doping/ coating strategy	Specific capacity (mAh g^{-1})	Energy density (Wh kg^{-1})	Undoped LFP (mAh g^{-1})	Charge transfer resistance (Ω)	Li-ion diffusion coefficient (cm^2 s^{-1})	Reference
1	Ru	162	550	154	59	2.12×10^{-13}	[169]
2	La, Ce	92	300	—	—	—	[170]
3	Ni	152	516	—	—	—	[171]
4	rGO	165	561	—	—	—	[172]
5	Nb	164	557	—	73	2.47×10^{-14}	[173]
6	Mn	156	530	—	110	—	[174]
7	MXene	156	530	—	17	1.53×10^{-13}	[93]
8	F	113	384	—	3.38	1.15×10^{-11}	[175]
9	Ti	133	452	—	126	—	[109]
10	Al	158	537	—	—	—	[119]

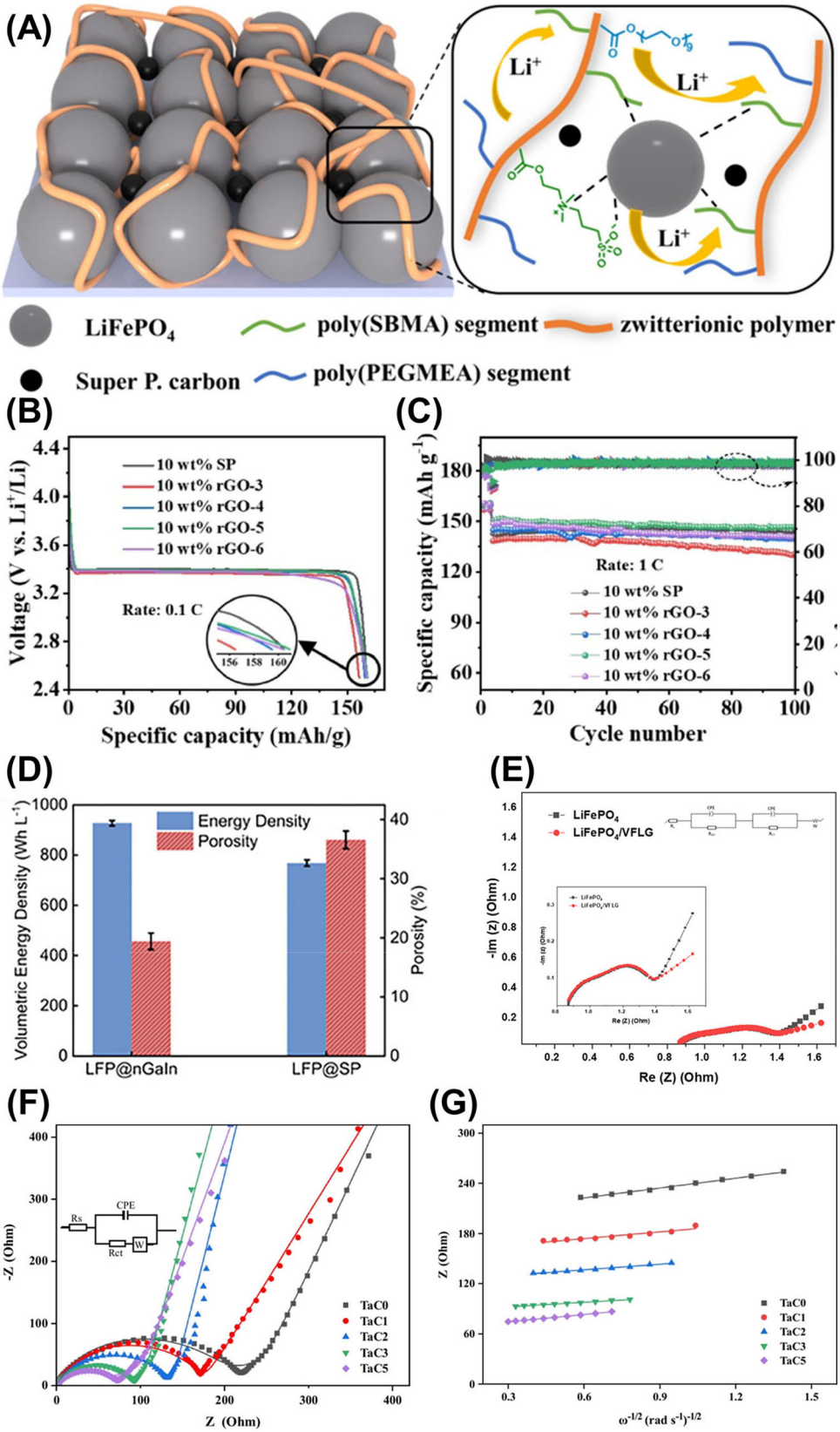

FIGURE 6 | (A) Zwitterionic polymer-coated LFP. Reproduced with permission [176]. Copyright 2025, Elsevier. (B) Discharge curves at 0.1 C and (C) cycling performance at 1 C of LFP electrodes with 10 wt% Super P and rGO-x (x = 3, 4, 5, and 6). Reproduced with permission [177]. Copyright 2024, Elsevier. (D) Volumetric ED and porosity of LFP@nGaIn vs. LFP@SP electrodes. Reproduced with permission [178]. Copyright 2024, Wiley-VCH GmbH. (E) EIS of LFP and LFP/VFLG after three cycles. Reproduced with permission [180]. Copyright 2024, Elsevier. (F) EIS in the frequency range between 0.01 Hz and 100 kHz, (G) the relationship between Z' versus $\omega^{-1/2}$ in low frequency regions for TaC-LFP/C. Reproduced with permission [179]. Copyright 2023, Springer Nature.

degradation during cycling. Croce et al. [187] utilized nanosized Cu/Ag doping to increase capacity to 145 mAh g^{-1}, leveraging the high conductivity of Cu/Ag nanoparticles to reduce charge transfer resistance and improve electrochemical kinetics. Bae et al. [188] introduced a bio-assisted nanostructuring approach using deoxyribonucleic acid (DNA) to fabricate LFP–CNT–DNA micro-rose cathodes, where DNA disperses CNTs and templates LFP nanoparticle growth, yielding 110 mAh g^{-1} at 5 C and 88% capacity retention after 2000 cycles due to optimized Li^+ diffusion pathways and a robust CNT conductive network.

3.4 | Strategies for Enhancing Low-Temperature Performance of LFP Cathodes

LFP batteries suffer from considerable performance degradation at low temperatures, marked by reduced energy and power output, shortened cycle life, and increased capacity loss, especially under high charge rates and elevated states of charge (SOC) [189, 190]. While LFP cathodes are structurally stable during prolonged cycling, their intrinsic low electronic and ionic conductivities become critical bottlenecks under cold conditions. Li-ion diffusion within the bulk slows down significantly, and charge transfer resistance at the cathode–electrolyte interface increases, suppressing reaction kinetics and causing significant electrochemical polarization [191]. During discharge, Li^+ transport proceeds through multistep processes, from migration in the electrolyte to solid-state diffusion within the cathode lattice, with the bulk diffusion most severely hindered at low temperatures. This kinetic limitation disrupts the phase transformation between LFP and $FePO_4$, reducing overall efficiency. Furthermore, elevated SOC and fast charging can induce mechanical stress, leading to particle cracking and iron dissolution. The dissolved iron migrates to the anode and alters the SEI, compounding degradation. In addition, kinetic hysteresis during low-temperature cycling intensifies mechanical strain within the electrode, as observed by Choi et al. [192], resulting in poor structural stability during prolonged cycles (Figure 7A). These internal and interfacial limitations highlight the LFP cathode as a central focus for low-temperature optimization. Consequently, various strategies such as coating to electrode materials, doping to increase conductivity, and controlling the particle size have been extensively investigated to enhance conductivity, reduce resistance, and facilitate Li transport under cold conditions [159, 193, 198–202].

Surface modification is a critical strategy for enhancing the low-temperature performance of LFP cathodes by addressing their intrinsic limitations in electronic and ionic conductivity. Among various approaches, carbon coatings are the most widely adopted, substantially improving electron transport and reducing resistance during charge/discharge. This conductive layer also suppresses particle agglomeration and facilitates controlled crystal growth. Ren et al. [193] reported that co-doping carbon coatings with heteroatoms such as nitrogen, sulfur, or phosphorus introduces structural defects and active sites, boosting Li-ion transport and lowering charge transfer resistance. Notably, N/S co-doped carbon coatings achieved 100.3 mAh g^{-1} at 1 C and −20°C with ~100% retention over 500 cycles (Figure 7D). Similarly, Liang et al. [203] demonstrated that applying an ultrathin carbon layer derived from a carbon aerogel improved low-temperature performance, enabling LFP to retain 80.23% of its room-temperature capacity at −20°C. In addition, various carbon sources such as polystyrene, polyol, and fructose have also been explored for surface coatings to boost conductivity, control particle size, and maintain LFP's electrochemical stability in harsh temperature conditions [204–207].

In addition to carbon coatings, other materials such as conductive polymers, modified carbon, and metals/metal oxides have been applied to enhance the low-temperature performance of LFP [89, 208–210]. Zhu et al. [194] coated LFP with PPy, and the optimized LFP/PPy composite with 2.95% PPy showed excellent capacity, rate capability, and low-temperature performance, delivering 128, 106.5, and 85.7 mAh g^{-1} at −20°C under 0.1, 0.5, and 1 C, respectively (Figure 7B). Li et al. [198] reported that P-doped carbon-coated LFP (LFP/C-P) improved Li-ion diffusion by widening the interlayer distance, reducing diffusion resistance, and enhancing low-temperature performance, with an initial discharge capacity of 82.7 mAh g^{-1} at 0.1 C and −40°C. Wu et al. [211] used CeO_2 coating via a sol–gel method, which preserved the crystal structure but reduced polarization, improved particle–current collector connectivity, and facilitated charge transfer, achieving 99.7 mAh g^{-1} at 0.1C and −20°C, with 98.6% capacity retention after 30 cycles. Guo et al. [200] coated LFP with Ti_3SiC_2, achieving 116.0 mAh g^{-1} at 0.1C and −20°C, and 97.0% capacity retention after 100 cycles at −10°C and 1C, significantly higher than the 81.2% for LFP/C, while increasing the Li-ion diffusion coefficient from 1.06×10^{-12} to 2.91×10^{-11} cm^2 s^{-1} by forming a highly conductive plane-to-point network that lowered charge transfer resistance. These performance gains are primarily attributed to four critical effects of surface coatings: (i) formation of a conductive network that enhances electron flow, (ii) reduction of electrode polarization and improved contact with the current collector, (iii) promotion of interfacial charge transfer through heteroatom incorporation and defect engineering, and (iv) improved Li-ion diffusion enabled by fast ion-conducting coating layers. Collectively, these mechanisms mitigate kinetic limitations and significantly improve the electrochemical behavior of LFP cathodes under cold conditions.

LFP's inherent 1D Li-ion diffusion pathway restricts ion mobility, which becomes more pronounced at low temperatures, severely limiting its electrochemical performance. Doping has emerged as a key strategy to overcome these limitations. Incorporating metal ions (e.g., Mn^{2+}, Nb^{5+}, Ti^{4+}) into the Li or Fe sites expands the lattice parameters, increases atomic spacing, and reduces charge transfer resistance, thereby enhancing Li-ion diffusion and electrochemical kinetics. For instance, Liao et al. [195] incorporated a small amount of Mn into LFP/C to form $LiFe_{0.98}Mn_{0.02}PO_4$/C, achieving discharge capacities of 124.4, 99.8, 80.7, and 70 mAh g^{-1} at 0.1, 1, 2, and 5 C, respectively, at −20°C, with lower polarization resistance (R_p) and charge transfer resistance (R_{ct}) values than undoped LFP/C due to reduced interfacial charge-transfer resistance and improved Li^+ diffusion aided by Mn^{2+} alongside Fe^{2+}/Fe^{3+} (Figure 7G,J). Lu et al. [212] synthesized Nb-doped $Li_xNb_{0.005}Fe_yPO_4$/C, which delivered 82.2 mAh g^{-1} at −20°C. During sintering, Nb_2O_5 acted as a nucleating agent, refining grains into smaller, more uniform particles, thereby increasing surface area and shortening Li^+ diffusion paths, though excessive doping could harm performance.

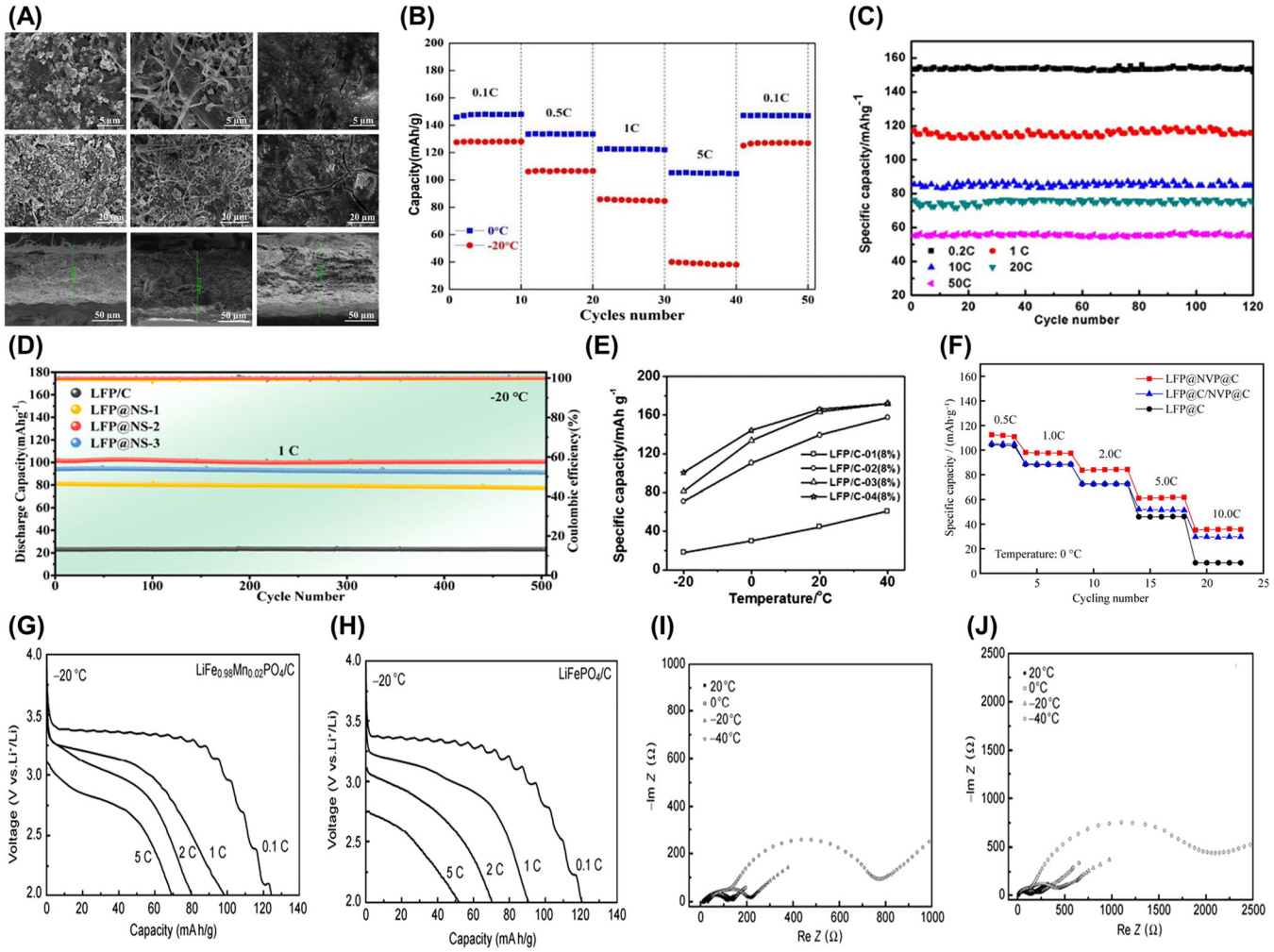

FIGURE 7 | (A) SEM and cross-sectional images of pristine LFP, cycled at room temperature, and cycled at different temperatures from 20 to −30°C. Reproduced with permission [192]. Copyright 2023, Springer Nature. (B) Cycling performance of LFP/Ppy at 0 and −20°C. Reproduced with permission [194]. Copyright 2019, Elsevier. (C) Cycling stability of doped LFP/CA at −20°C. Reproduced with permission [196]. Copyright 2012, Elsevier (D) Cycling performance at 1 C in −20°C. Reproduced with permission [193]. Copyright 2024, Elsevier. (E) Specific capacities of LFP/C with various particle sizes at different temperatures. Reproduced with permission [190]. Copyright 2014, Elsevier. (F) Rate performance of LFP@NVP@C, LFP@C, and LFP@C/NVP@C at 0°C. Reproduced with permission [197]. Copyright 2021, Springer Nature. Rate performance of (G) $LiFe_{0.98}Mn_{0.02}PO_4/C$ and (H) LFP/C at −20°C. Impedance spectra of (I) $LiFe_{0.98}Mn_{0.02}PO_4/C$ and (J) LFP/C at different temperatures. Reproduced with permission [195]. Copyright 2011, Springer Nature.

Liang et al. [201] reported that Ti doping in LFP/C must be carefully controlled, as high Ti content can deform Li^+ channels, lower diffusion coefficients, and degrade low-temperature electrochemical performance. In addition to single-element doping, co-doping two elements can create synergistic effects that enhance the electrochemical properties of LFP. Xu et al. [196] developed La- and Mg-co-doped $Li_{0.99}La_{0.01}Fe_{0.9}Mg_{0.1}PO_4$/carbon aerogel composites, where the dopants generated cationic defects that improved Li^+ diffusion and increased electronic conductivity, resulting in 85 mAh g^{-1} at −20°C at 10 C, more than double the undoped material's capacity, along with excellent cycling stability at multiple rates after 120 cycles (Figure 7C). Wen et al. [159] synthesized V^{3+}- and F^--co-doped LFP/C via a wet milling-spray drying-carbothermal reduction (WSC) process, where co-doping lowered charge-transfer resistance, enhanced conductivity, and formed a porous surface that provided extra ion transport channels, yielding 86 mAh g^{-1} at 0°C and 10 C, 20 mAh g^{-1} higher than the undoped sample, making it highly suitable for high-rate, low-temperature applications.

Beyond compositional modification, tailoring particle size and morphology provides an effective pathway to mitigate the kinetic limitations of LFP at low temperatures. By controlling synthesis conditions to produce submicron or nanoscale particles or specific morphologies, the Li^+ diffusion distance is shortened, material–electrolyte contact is increased, and more active sites are exposed, all of which enhance reaction kinetics under cold conditions. Chen et al. [190] reported that particle size strongly affects low-temperature performance, with capacity at −20°C rising from 18.0 mAh g^{-1} for 7.4 μm particles to 100.5 mAh g^{-1} for 0.1 μm particles (Figure 7E). However, Yu et al. [213] showed that while 200 nm particles give superior low-temperature capacity, 400 nm particles cycle more stably due to lower surface energy and reduced agglomeration. Various engineered morphologies, such as nanoplates [214],

nanoporous particles [215], coral-like [216], capsule-like [202], grape-like [217], and 3D network structures [218, 219], have been developed to enhance the low-temperature electrochemical performance of LFP. Yao et al. [214] synthesized rectangular nanosheet LFP via a solvothermal method with optimized raw material ratios and feeding sequences, producing a dominant (010) crystal plane that shortened Li^+ transport distances and delivered discharge capacities of 116.7 mAh g^{-1} at 0°C and 61.4 mAh g^{-1} at −20°C at 5 C. Dong et al. [215] prepared nanoporous LFP@C composites, achieving 117 mAh g^{-1} at −20°C at 5 C. The porous architecture increased electrode–electrolyte contact, which is especially advantageous at low temperatures where electrolyte viscosity is higher, thereby facilitating faster ion transport and improving performance.

In addition to the strategies discussed above, several alternative approaches have been explored to enhance the low-temperature performance of LFP. These include designing composite architectures to optimize conductivity and ion transport, applying magnetization treatments to influence ion diffusion and reactivity, and controlling defects within the crystal lattice to improve Li^+ mobility [197, 220, 221]. Liu et al. [197] demonstrated that a multicore–shell LFP@$Na_3V_2(PO_4)_3$@C structure, in which a $Na_3V_2(PO_4)_3$ (NVP) layer was combined with an external carbon coating, boosted both ionic and electronic conductivities. At 0°C, this composite delivered 111.8, 97.6, 84.4, and 61.8 mAh g^{-1} at 0.5, 1, 2, and 5 C, representing capacity gains of up to 33.7% compared with LFP@C (Figure 7F). The 3D NVP framework provided interstitial windows for rapid Li^+ transport, significantly improving low-temperature behavior. Zhang et al. [221] found that 72 h of magnetization treatment on LFP@C yielded 114.6 mAh g^{-1} at −10°C, 74% of its room-temperature capacity, by enhancing charge-transfer kinetics. While Fe–Li antisite defects are usually seen as blocking Li^+ pathways [222], Ren et al. [220] showed that introducing a controlled 3.77% defect concentration reduced diffusion anisotropy, enabling partial 2D Li^+ transport and achieving 126.0 mAh g^{-1} at −20°C, or 80.1% of room-temperature capacity. This improvement stemmed from the formation of additional Li^+ migration channels, making defect engineering a promising tool for low-temperature optimization.

3.5 | AI/ML Approaches to LFP Cathode Optimization

LFP is a widely used cathode material noted for its safety and thermal stability, but its low electronic/ionic conductivity motivates doping and nanostructuring to improve rate capability. Recent work has begun to leverage data-driven machine learning (ML) to accelerate LFP materials design by predicting how dopants and process parameters affect performance metrics (conductivity, capacity, stability, etc.). For example, Elbarbary et al. [223] compiled a data set from literature on singly doped LFP/C materials, extracting features such as dopant atomic number, valence, ionic radii difference, electronegativity, doping fraction, and C-rate. They trained ensemble ML models (Random Forest and Gaussian Process Regression) on this data and found that the optimal model could predict specific discharge capacity from composition. This model was then used to assess co-doping synergy: predicted capacities for Y/Nd co-doped $LiY_xNd_yFe_{1-x-y}PO_4$/C were compared to values from the superposition of single-dopant models. The ML-guided prediction was validated by experimentally synthesizing several $LiY_xNd_yFe_{1-x-y}PO_4$/C samples and testing them (SEM/TEM images, CV, electrochemical impedance, charge/discharge), confirming that the best combinations indeed enhanced capacity.

Key ML methodologies and techniques

1. **Random forests (RF)/Gaussian process regression (GPR):** this method is used for regression of electrochemical performance versus compositional features. Elbarbary et al. [223] trained RF and GPR models on atomic/molecular descriptors of doped LFP and used them to predict capacity.
2. **Neural-network interatomic potentials:** ML models (often neural network or Gaussian Approximation Potentials) trained on first-principles data to predict material properties. Li et al. [224] developed an ML potential for LFP and applied the phonon Boltzmann transport equation to show that Li-deintercalation significantly reduces LFP's thermal conductivity (due to shortened phonon lifetimes). Similarly, Xie et al. [225] trained an ML potential to study Na-for-Li substitution; they found that partial Na doping ($Li_{0.75}Na_{0.25}FePO_4$) markedly increases thermal conductivity by boosting phonon group velocity and reducing anharmonic scattering. These ML-driven simulations reveal how compositional changes (dopants or Li content) affect heat transport, guiding design for better thermal management.
3. **Optimization frameworks (Bayesian and active learning):** though not yet widely published for LFP doping specifically, Bayesian optimization and active-learning loops are conceptually powerful for navigating high-dimensional dopant/process spaces. In principle, a predictive ML model can be coupled with an acquisition function to iteratively suggest the next best experiment (e.g., dopant ratio or synthesis temperature) to try. Similar approaches have been used in battery materials discovery to optimize electrolytes and cathodes, and a proof-of-concept has been shown for LFP using classical design-of-experiments (e.g., response-surface optimization of Ti/V co-doping) [226]. A Bayesian scheme would generalize this by automatically balancing exploration versus exploitation across many dopant variables.
4. **Neural Networks and Deep Learning:** beyond interatomic potentials, deep neural networks (including graph neural networks) are broadly applicable for structure–property prediction, though specific reports on LFP doping are still emerging. In related battery studies, artificial neural networks (ANNs) have been used to predict capacity and lifetime from composition and operational data [227]. As more LFP data become available, deep architectures may learn complex correlations between crystal structure, microstructure, and performance.

In all these approaches, feature engineering and data sets are critical. The co-doping ML study used physicochemical descriptors (atomic radii, electronegativities, dopant amount, etc.) from published experiments [223]. ML potentials rely on DFT or high-fidelity simulation data for training (e.g., forces and energies for various atomic configurations). Public

databases (Materials Project, literature compilations) can seed models, but LFP-specific data sets remain small, so integrating data from experiments and first-principles calculations is common. Model validation is done both statistically and experimentally. ML models are typically cross-validated on held-out data to ensure predictive accuracy. Crucially, predictions are tested in the lab. ML potential studies validate their models by comparing predicted phonon spectra and conductivities with independent calculations or experiments. Such validation builds confidence that the ML models capture relevant physics. These ML-driven approaches can dramatically speed up LFP materials design. Instead of exhaustively testing many dopant combinations or process recipes, ML models can prioritize candidates with high predicted performance. ML-informed simulations also suggest novel strategies to improve thermal transport. In aggregate, ML integration transforms LFP development into a closed-loop of modeling and experiment: models trained on existing data propose new formulations, experiments test them, and new data refine the models. This accelerates the discovery of dopants and processing conditions that maximize conductivity, stability, and capacity. As data volume grows, advanced techniques (deep learning, active learning) will further enhance predictive power, pushing toward rational, rapid design of high-performance LFP cathodes.

4 | Recycling and Reuse Strategies for LFP Cathodes

As LFP batteries gain widespread use in EVs and stationary energy storage due to their safety, long cycle life, and low cost, efficient recycling has become essential for sustainability and resource recovery [30]. Unlike NCM batteries, LFP contains low-value metals like Fe and P, reducing traditional economic incentives for recycling [228]. However, the stable olivine structure of LFP helps preserve material integrity at end-of-life, making regeneration a viable alternative to complete decomposition [229]. Recycling approaches typically fall into three categories: hydrometallurgical recycling, direct recycling, and pyrometallurgical recycling. Hydrometallurgical recycling, which employs chemical leaching to selectively recover metals, has become more applicable to LFP thanks to inexpensive Li leaching oxidants and improved cathode regeneration, though its economic appeal is constrained by low Fe and P prices and chemical consumption [230]. Direct recycling targets material restoration by removing contaminants, replenishing Li, and recovering the crystal and electrochemical structure without extensive decomposition, making it particularly promising for LFP due to its structural and thermal resilience [229, 231]. Pyrometallurgical recycling uses high-temperature processes to recover metals from LIBs and is effective for NCM batteries, but it is less suitable for LFP due to its thermal and chemical stability, low-value metals, and poor cost-effectiveness, yielding mainly Fe-rich alloy and slag while losing Li and P [30, 228].

4.1 | Hydrometallurgical Method

The hydrometallurgical method can treat various types of spent LFP material, including spent LFP materials with differences in production, failure reasons, and impurity composition. It mainly includes pretreatment, leaching, and material regeneration processes [232].

Pretreatment for hydrometallurgical recovery of spent LFP batteries generally includes discharging, crushing, and sorting, and also separation of active materials. Hydrometallurgy has less stringent raw material requirements, so the pretreatment process is simpler. Discharging is commonly achieved through short-circuiting, using conductive media such as solid powders (e.g., metal powder or graphite) and salt solutions (e.g., NaCl, $NaSO_4$, $FeSO_4$, or $ZnSO_4$) to safely discharge residual energy [233, 234]. Solid media can effectively discharge batteries but may cause heat buildup, whereas salt solutions are easier to handle and more suitable for industrial scale. However, salt solutions can corrode battery casings, leading to electrolyte leakage that requires additional treatment. Following discharge, the spent battery is crushed, and the resulting material is sorted based on size, density, or magnetic properties. Crushing separates materials into fine particles (< 0.25 mm) containing active anode and cathode materials, intermediate particles (0.25–2 mm) containing fragments of copper and aluminum foils, and coarse particles (> 2 mm) including metallic shells and separators [235]. Size-based sieving allows rough separation of anode and cathode materials. More precise separation uses pneumatic methods to isolate low-density separators and magnetic separation to recover iron shells due to their magnetic properties. These combined pretreatment steps prepare the materials effectively for subsequent hydrometallurgical recovery processes [236, 237].

Crushing and sorting effectively separate the cathode, anode, organic separator, and battery shell. The separator and shell can be directly recycled, while the spent electrolyte is collected for safe disposal. However, active materials and metal foils remain bonded by polymer binders like PVDF or polytetrafluoroethylene (PTFE), requiring further separation [238]. Common strategies to remove these binders include organic solvent dissolution, alkali decomposition, ultrasound-assisted separation, and thermal treatment. Organic solvent dissolution employs solvents such as dimethyl carbonate (DMC), 1-methyl-2-pyrrolidinone (NMP), acetone, or ethanol to dissolve binders efficiently [239]. However, repeated use increases solvent viscosity, complicating recycling. Alkali decomposition uses hydroxide solutions to hydrolyze binders cheaply without the need for solvent recovery, but aluminum foils react to form meta-aluminate, causing aluminum loss. Ultrasound-assisted separation leverages cavitation to weaken the adhesion between active materials and current collectors, enhancing exfoliation. For example, combining 0.5 M NaOH with ultrasound fully separates the cathode material from the aluminum foil, whereas only partial separation occurs without ultrasound. Thermal treatment exploits differences in pyrolysis temperatures of binders (~400°C) and the melting point of aluminum (~650°C) [240, 241]. Heating between 400°C and 500°C decomposes binders into gaseous byproducts, effectively freeing active materials from metal foils. This method is widely adopted in industrial practice due to its efficiency and simplicity, yielding clean copper and aluminum foils along with active material powders [235]. Additionally, thermal treatment decomposes residual electrolyte, preventing contamination of recycled materials and enhancing overall recovery quality.

As LFP batteries reach the end of their life, recovering valuable elements, particularly lithium, is essential for both sustainability and economic viability. After initial pretreatment, including controlled discharge, dismantling, and separation of components, valuable metals are extracted from the spent cathode. Among the available methods, acid leaching remains the most widely employed, and it can be broadly divided into inorganic acid leaching and organic acid leaching [242–253]. In selective oxidative acid leaching, lithium ions are recovered by converting LFP into $FePO_4$ using an oxidizing agent. This approach allows Li^+ to dissolve efficiently into the solution while minimizing the co-dissolution of Fe, Al, and P, which are less economically valuable. Common oxidizing agents include H_2O_2, O_2, $(NH_4)_2S_2O_8$, and $Na_2S_2O_8$, which have demonstrated lithium recovery efficiencies above 96% [243–247]. Mechanical activation or electrolysis can further improve recovery while reducing reagent consumption, making the process more environmentally and economically attractive [248–250]. Building on these findings, a new process has been developed to recycle soft-package LFP batteries. As shown in Figure 8A, the cathode, anode, and separator can be recovered directly from a spent battery after discharging and dismantling [246]. The cathode pieces, which include LFP and Al foil, are then treated with $Na_2S_2O_8$ for oxidation leaching, selectively extracting Li with over 99% efficiency, while Al, Fe, and P remain largely unaffected (< 0.6%) due to the passivation of Al in the strong oxidizing environment. The resulting Li-rich solution (~13.9 g L^{-1}) can be directly converted to high-purity Li_2CO_3 by adding Na_2CO_3, and the leftover solution can be reused for further batches. During leaching, some $FePO_4$ detaches from the Al foil (photograph in Figure 8A), making separation easier, so $FePO_4$ can be reused for LFP cathodes and Al foil recovered. Thermodynamic analysis using the *E*–pH diagram (Figure 8B) shows that $Na_2S_2O_8$ oxidizes LFP to $FePO_4$ at pH 2–6 without additional acids or bases. The amount of oxidant is critical: as shown in Figure 8C, 1.05 times the theoretical $Na_2S_2O_8$ achieves ~97% Li recovery with minimal Fe loss, while higher amounts slightly increase Fe dissolution due to weak acidification. This approach offers a simple, selective, and cost-effective method to recover lithium from spent LFP batteries.

Organic acids provide a simpler alternative to conventional inorganic acids. They are classified based on their chemical behavior: neutral acids, such as citric and acetic acids, can achieve selective lithium leaching with the addition of an oxidant; reducing acids, like ascorbic acid, prevent Fe oxidation, enabling efficient multi-element recovery, and precipitation-capable acids, such as oxalic acid, can selectively remove Fe while leaving lithium in solution [256–260]. These organic acid strategies allow flexible, environmentally friendly lithium recovery, often with minimal generation of harmful waste. Enhancing recovery efficiency can also involve physical treatments. Mechanical activation, such as ball milling or grinding, disrupts the crystal structure of spent LFP, exposing more lithium sites and improving leaching rates. Combining chemical selectivity with physical treatment ensures maximum recovery of Li and Fe while minimizing reagent use and energy consumption [260]. Therefore, selective leaching of Li from LFP batteries combines high efficiency, environmental friendliness, and economic feasibility. This method not only recovers the most valuable element efficiently but also simplifies downstream processes by generating high-purity Li_2CO_3, reusable $FePO_4$, and recyclable Al. By integrating chemical, mechanical, and process optimization strategies, the recycling of spent LFP batteries can become both sustainable and cost-effective, supporting a circular economy in LIB technologies.

4.2 | Direct Recycling

Direct recycling, as an effective strategy, can restore the components and structure of spent cathode material to its original state. The spent cathode material is first obtained via a refined pretreatment process, and then the appropriate recycle method is selected based on the specific failure of the spent cathode material to restore its electrochemical performance [254]. Pretreatment for recycling spent LFP materials begins with a controlled discharge process, typically using discharge cabinets to avoid electrolyte leakage and ensure safety, though it is time-intensive due to manual battery connections [231, 261]. To improve efficiency, safer and faster discharge methods are needed. After discharging, the batteries are dismantled to separate the components. Manual dismantling is precise but slow, prompting the development of automated techniques. In these, cells are opened, and internal parts are immersed in DMC solution to dissolve the electrolyte, allowing separators to float and electrodes to sink for easy separation [231]. Further sorting is achieved using visual intelligent systems, and the electrodes are crushed to remove metals like Cu and Al through sieving and pneumatic methods [262].

Direct recycling refers to the recycling of components and defects of spent LFP material and to restoring its electrochemical performances without destroying the original lattice structure of the material. Currently, the recycling of LFP material can be generally divided into three categories: direct calcination, replenishment of elements, and modification. Direct calcination is a straightforward method used to enhance the electrochemical performance of spent LFP materials by thermally decomposing surface binders and residual electrolytes [262, 263]. The process requires precise temperature control to prevent damage to the LFP's crystal structure. At temperatures below 350°C, binder removal is incomplete, leading to particle agglomeration, while temperatures above 800°C can degrade the host structure, causing reduced performance [264]. Hu et al. [265] reported a two-step calcination process, initially at 300°C for 2 h followed by 750°C for 7 h, which has been shown to improve discharge capacity from 134.67 to 147.29 mAh g^{-1} with 95.08% retention over 100 cycles at 0.2 C.

Element replenishment is a strategy aimed at restoring the performance of spent LFP materials, especially those from waste batteries that suffer from elemental loss [266]. This process involves correcting the stoichiometric imbalance of Li, Fe, or P by introducing appropriate metal salts. A subsequent heat treatment facilitates the incorporation of these elements back into the crystal lattice, recycling structural defects. Depending on which elements are depleted, the process may focus solely on Li or include all three key elements, Li, Fe, and P. To replenish Li alone, both hydrothermal and solid-state methods are commonly employed. In the hydrothermal method, Li ions are inserted into the lattice through a reaction in an alkaline solution, followed by a thermal step to solidify the structure [267]. Chen et al. [268] regenerated spent LFP materials by

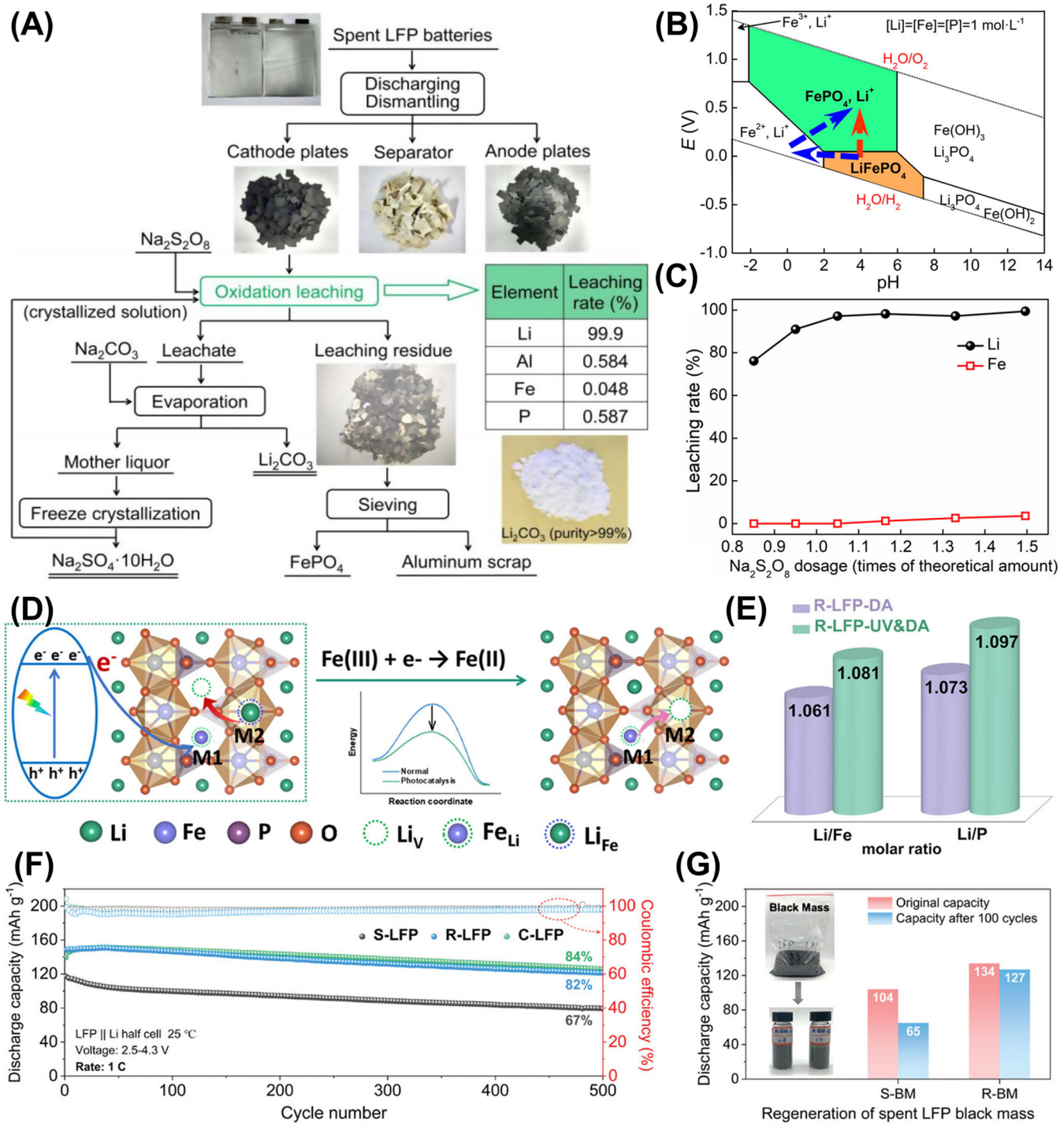

FIGURE 8 | (A) Flowsheet of the proposed method for treating spent LFP batteries. (B) Pourbaix diagram of Li-Fe-P-H_2O at 298.15 K. (C) Effect of $Na_2S_2O_8$ dosage on the selective leaching of Li from LFP scrap. Reproduced with permission [246]. Copyright 2019, ACS Publications. (D) The specific pathway of FeLi anti-site defects reordering in photocatalysis regeneration. (E) Li/Fe and Li/P molar ratio of S-LFP and C-LFP based on ICP-OES. Reproduced with permission [254]. Copyright 2025, Wiley-VCH GmbH. (F) Cycling performance of S-LFP, R-LFP, and C-LFP at 1 C. (G) Discharge capacity of S-BM and R-BM. Reproduced with permission [255]. Copyright 2023, Wiley-VCH GmbH.

immersing them in a LiOH solution at 80°C for 5 h, followed by hydrothermal treatment at 600°C for 2 h to recycle damaged crystal lattices. The restored material exhibited a discharge capacity of 159 mAh g^{-1} with less than 1% capacity loss after 100 cycles at 0.5 C. Alternatively, Zhang et al. [269] employed a solid-phase calcination method by ball-milling spent LFP with Li_2CO_3, then calcining the mixture under Ar/H_2 atmosphere at 650°C for 1 h, achieving a capacity of 140.4 mAh g^{-1} and 95.3% retention after 100 cycles at 0.2 C. Since some spent LFP also loses Fe and P during cycling, simultaneous replenishment of Li, Fe, and P is essential.

In addition to replenishing elemental deficiencies, recent studies have shown that anti-site defects, such as FeLi formation, can

significantly influence the performance of recycled LFP [254]. FeLi anti-site defects arise from lithium loss, generating local lattice instability and charge imbalance, where Fe ions occupy Li sites and vice versa, as seen in Figure 8D. The correction of these defects generally requires overcoming a high activation energy barrier, which can be substantially lowered using electron donors like DA polymer or via photocatalytic UV irradiation (alone or together). This promotes Fe migration back to the proper sites and restores structural order. ICP-OES further confirms that spent LFP (S-LFP) commonly exhibits lithium deficiency, with a measured Li/Fe ratio of 0.669 (Figure 8E). Yu et al. [270] mixed spent LFP with Li_2CO_3, $Fe(NO_3)_3$, and $NH_4H_2PO_4$, followed by calcination at ~700°C for 10 h, resulting in an initial capacity of 103.1 mAh g^{-1} at 1 C and 97.2% retention over 300 cycles. Similarly, Hou et al. [271] restored elemental composition and crystal structure by ball-milling spent LFP with Li, Fe, and P salts, spray drying at 220°C (inlet) and 120°C (outlet), then calcining at 650°C for 10 h, yielding 139 mAh g^{-1} at 0.2 C with 95% retention after 100 cycles.

Modification is a key strategy to improve the structural stability and electrochemical performance of spent LFP materials, mainly through carbon coating or ion doping [272, 273]. Due to LFP's low electrical conductivity (10^{-9} to 10^{-10} cm^2 s^{-1}), commercial LFP is often coated with carbon to enhance conductivity. However, the carbon layer can degrade during cycling, causing performance loss. Recycle processes that restore this carbon coating, typically by adding a carbon source alongside element supplementation, effectively recover battery performance. For example, Zhang et al. [274] combined spent LFP with Li_2CO_3 and sucrose, followed by heat treatment at 350°C and 650°C, achieving a discharge capacity of 146 mAh g^{-1} at 0.2 C. Similarly, Qi et al. [273] added glucose and Li_2CO_3 to spent LFP, with subsequent milling and calcination, yielding 147.7 mAh g^{-1} at 0.2 C. Ion doping also enhances material stability; doping with 1% V^{5+}, which has a smaller ionic radius than Fe^{2+}, reduces particle size, and improves structure. This resulted in 140 mAh g^{-1} capacity at 1 C with nearly full retention after 100 cycles, compared to 85 mAh g^{-1} without doping. In addition to carbon coating and ion doping, recent work demonstrates that structural modification through regeneration substantially restores performance. Long-term cycling tests show that regenerated LFP retains 82% of its capacity after 500 cycles at 1 C (Figure 8F), similar to commercial LFP (84%), and maintains 86% retention after 500 cycles even at 5 C, signifying competitive electrical performance [255]. Restoration approaches are also effective for cathodes with varying Li deficiencies, as demonstrated by using a saturated Li concentration to return a degraded S-LFP from 92 to 137 mAh g^{-1} at 1 C, with 71% retention after 700 cycles. Practical application feasibility is supported by industrial black mass regeneration: R-BM achieved 134 mAh g^{-1} at 1 C (Figure 8G), compared to the degraded 104 mAh g^{-1}, and retained 95% of its capacity after 100 cycles, far surpassing spent black mass (S-BM, 64%).

Direct recycling methods are attractive due to their shorter processing time, lower chemical consumption, and reduced carbon footprint. However, variability in damage types, such as lattice collapse, elemental loss, and surface defects, and sensitivity to impurities make consistent recycling challenging, especially for mixed or contaminated spent materials. These limitations restrict the broad application of direct recycling techniques in recycling spent LFP batteries.

4.3 | Pyrometallurgy Method

Pyrometallurgical techniques involve the application of high temperatures to extract metals and other valuable substances, offering a simple process with high throughput [275]. This approach is less dependent on the composition of the raw material and generates minimal liquid waste, making it well-suited for large-scale industrial operations [276]. Moreover, the intense heat treatment effectively neutralizes residual carbon, organic matter, and fluorine compounds present in spent LFP materials, simplifying subsequent processing and improving overall material handling [277]. However, pyrometallurgical methods alone often struggle to produce high-purity outputs, and the extreme temperatures involved can lead to the loss of valuable metals, making it difficult to achieve lithium recovery rates above 95% [278]. While pyrometallurgy is generally insufficient for complete LIB recycling, it plays a key role in converting battery components into forms that are more amenable to subsequent hydrometallurgical processing [279]. As a result, combining pyrometallurgy with hydrometallurgy often improves the efficiency of spent LFP recovery. Typical applications of pyrometallurgy include [280–282] (i) thermal decomposition of cathode materials to remove organic residues and conductive carbon, enhancing later chemical recovery; (ii) facilitating the separation of cathode active materials from the aluminum current collector; and (iii) salt-assisted roasting to disrupt the LFP crystal structure, promoting the extraction of valuable elements.

Thermogravimetric analyses (TGA) show that spent LFP cathodes undergo complete decomposition of PVDF binder and carbon above 600°C, allowing efficient separation of active material from the current collector [275, 281]. Dai et al. [283] demonstrated that annealing crushed LFP sheets at 600°C enabled full separation, with sulfuric acid leaching and ammonia precipitation recovering 97% of Li and 98% of Fe. Similarly, Zhou et al. [284] disrupted the olivine structure via high-temperature treatment, enhancing Li accessibility and leaching efficiency. The oxidative activation transformed LFP into a uniform, porous structure, reducing acid consumption and achieving 98.48% Li recovery. He et al. [285] further improved recovery by roasting LFP with Na_2SO_4, converting over 99% of Li into high-purity lithium carbonate, while Fe and P converted to value-added $Fe_2P_2O_7$ and $Na_4P_2O_7$. This pyroprocessing-based strategy not only maximizes metal recovery but also reduces wastewater and residue by over 66% and 93%, respectively, with an estimated profit of 1.44 \$ kg^{-1} of LFP batteries.

5 | Engineering Advanced Electrodes and Battery Pack Architecture

5.1 | Tailoring Electrode Porosity for LFP Performance

The hierarchical porous structure of electrodes, featuring interconnected macropores and mesopores, significantly enhances electrochemical performance in energy storage devices. In studies, LFP@C nanoplates uniformly anchored on MXene nanosheets create a highly porous network with abundant voids, enabling efficient electrolyte penetration and rapid ion

diffusion [93, 286]. This architecture prevents particle aggregation, offers ample active sites for redox reactions, and ensures robust ion/electron transport, collectively contributing to superior rate capability and cycling stability. The synergy of high surface area, structural integrity, and enhanced transport properties makes this porous design highly promising for advanced energy storage applications.

Recent advancements in LFP cathode materials, like the LFP@NS material developed by Liu et al. [193], incorporate N and S co-doped carbon layers within a 3D porous framework, improving electrical conductivity and forming continuous Li-ion migration channels for faster diffusion kinetics and charge transfer (Figure 9A). The LFP@NS-2 sample achieves an impressive discharge capacity of 158.5 mAh g^{-1} at room temperature and 101.3 mAh g^{-1} at −20°C at a 1 C rate, while retaining 92.5% capacity after 2000 cycles at 10 C, demonstrating remarkable cycling stability. When paired with a graphite anode, the LFP@NS-2‖Gr full cell delivers a capacity of 100.1 mAh g^{-1} at −20°C, underscoring the potential of heteroatom-doped carbon coatings and porous designs for high ED, low-temperature energy storage applications. Lotenberg et al. [287] developed porous LFP–PVDF composites for redox targeting flow batteries (RT-RFBs) using a scalable melt-extrusion method, where hierarchical porosity was introduced by selectively leaching poly(ethylene oxide) (PEO) from LFP–PVDF–PEO blends, yielding a uniform sub-micron porous structure. This architecture enabled efficient electrolyte penetration, enhanced ion transport, and increased surface area for redox reactions, significantly improving electrochemical performance; notably, a 65% porous sample achieved complete oxidation of LFP to $FePO_4$ within 5 h under flow conditions using a $Fe(CN)_6^{3-}$ mediator at high mediator/LFP molar ratios (Figure 9B) [287]. While the study demonstrated the benefits of porosity in RT-RFBs, it mainly addressed oxidation, leaving questions about reaction reversibility with the solid booster.

Ongoing work aims to optimize the redox-mediator/solid booster pairing and explore processing parameters, alternative PVDF copolymers, and diverse electroactive particles to further improve ED and system scalability. Lv et al. [290] synthesized bowl-like mesoporous LFP/C composites via a wet milling–spray drying–carbothermal reduction method, achieving a

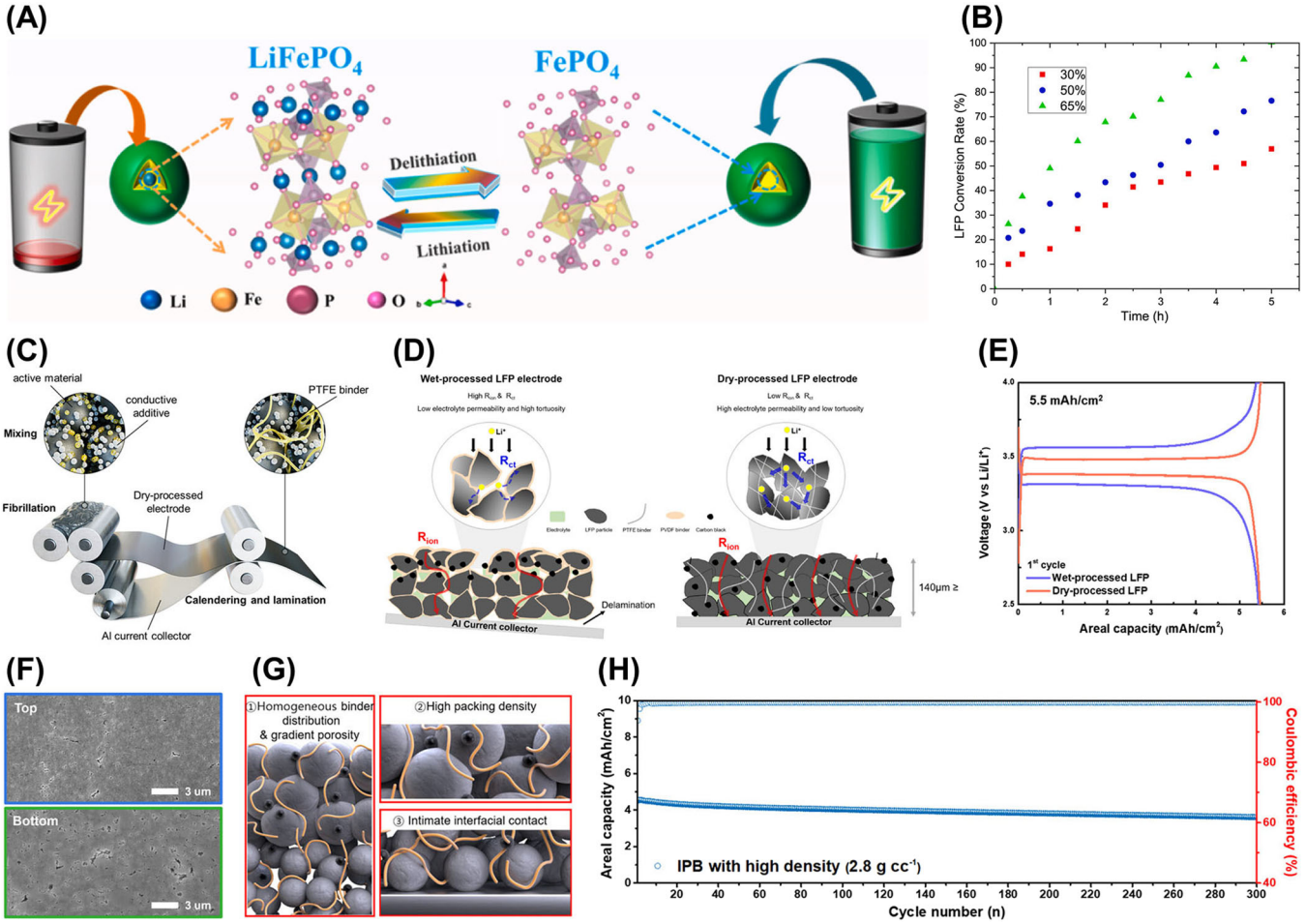

FIGURE 9 | (A) Phase transition schematic of LFP during charge/discharge. Reproduced with permission [193]. Copyright 2024, Elsevier. (B) LFP → $FePO_4$ kinetics for LFP_{50}–$PVDF_{50}$ composites with 30–65% porosity in 0.5 M LiCl + 0.1 M $K_3Fe(CN)_6$ aqueous flow system (R = 5). Reproduced with permission [287]. Copyright 2024, Elsevier. (C) Schematic illustration of the dry electrode processes, (D) the morphology of polymeric binder and distributions of conductive additives and polymeric binders in wet- and dry-processed LFP electrode, and (E) the voltage profiles of the first cycle of LFP-Li cells with wet and dry processed LFP electrodes. Reproduced with permission [288]. Copyright 2024, Wiley-VCH GmbH. (F) Cross-sectional SEM images of IPB electrode (top layer-P_{hd} and bottom layer-P_{sp}), (G) gradient-porosity LFP thick electrode, and (H) long-term cycling stability of a full cell at high electrode density of 2.8 g cc^{-1}. Reproduced with permission [289]. Copyright 2025, Wiley-VCH GmbH.

specific surface area of 29.40 $m^2 g^{-1}$ and an average pore size of 13.30 nm. The unique morphology, featuring interconnected mesopores and carbon-coated nanoparticles, enhanced ionic and electronic conductivity, enabling a high discharge capacity of 123 mAh g^{-1} at 10 C with no capacity loss over 100 cycles. This porous architecture facilitated rapid Li^+ diffusion, improved electrolyte penetration, and increased active surface area, collectively enhancing ED and rate performance. Additionally, PEG-modified porous LFP electrodes demonstrated significantly higher Li^+ intercalation rates (4.45 vs. 2.10 g(Li) $m^{-1} h^{-1}$), owing to improved hydrophilicity, minimized particle agglomeration, and faster reaction kinetics observed in CV tests [291]. These results confirm the critical role of porosity in reducing polarization, boosting reaction kinetics, and ensuring long-term cycling stability, establishing porosity engineering as a powerful strategy to optimize LIB performance, especially for high-rate and durable applications.

In practical applications such as EVs and stationary storage systems, the tap density and Coulombic efficiency of LFP play critical roles in determining the volumetric ED and long-term operational performance. While carbon coating is widely adopted to enhance electronic conductivity, it has been observed to monotonically decrease tap density due to the much lower density of carbon compared to LFP, as well as the potential porosity introduced by carbon deposition [292]. Chang et al. reported that increasing carbon content from 3 to 9 wt% decreased the tap density from ~2.15 to ~1.66 g cm^{-3}, with an optimal balance achieved at 7 wt% (1.80 g cm^{-3}), providing superior electrochemical performance [293]. The tap density of C/LFP is governed not solely by the carbon fraction but also by factors such as particle size, morphology, and size distribution. Spherical C/LFP particles prepared via precipitation methods have demonstrated significantly higher tap densities (≈ 1.75 g cm^{-3}) compared to nonspherical powders of comparable size (≈ 1.0–1.3 g cm^{-3}) [294].

Tailoring particle aggregation is another effective route for improvement. For example, spark plasma sintering (SPS) has been used to produce agglomerated C/LFP composites with a tap density of about 1.1 g cm^{-3} [295]. A two-stage drying process can further enhance packing density, raising values from ~1.37 to ~1.80 g cm^{-3}, by forming a 3D network that promotes controlled agglomeration of colloidal particles [292]. This dense packing facilitates grain growth and crystallization during drying. Additionally, using a blend of Fe^{3+} precursors containing both nano- and microscale particles has been shown to reduce structural vacancies compared to single-precursor routes, leading to a measurable tap density increase (1.19 to 1.40 g cm^{-3}) [296]. These findings highlight that engineering particle shape, aggregation behavior, and precursor selection are equally critical as carbon coating in achieving high-density C/LFP electrodes. The tap density of carbon-coated LFP varies depending on the synthesis route and processing conditions. Among these, calcination temperature in coprecipitation synthesis significantly influences both crystal quality and particle morphology [297]. For example, Oh et al. found that samples calcined at 800°C achieved a tap density of 1.09 g cm^{-3}, noticeably higher than those treated at 650°C–750°C or 850°C, due to better crystallinity [298]. Using self-synthesized $FePO_4$ as the precursor and pitch as the carbon source, later work increased the tap density to 1.5 g cm^{-3}. The product, featuring 200–300 nm particles with 100–200 nm pores, attained a volumetric ED more than twice that of conventional nano-LFP while maintaining similar rate performance. More recent methods aim to balance uniform carbon coating with dense particle packing [299]. A notable example is a two-step coating process where sucrose provides the initial carbon layer, followed by a second treatment with Li_2CO_3 and pitch during calcination. The resulting microscale, nanoporous LFP maintained a tap density of 1.5 g cm^{-3} despite containing only 0.5 wt% carbon, delivering high specific capacity and excellent rate capability. Another study used PVP as a carbon precursor to enhance coating dispersion during precursor preparation. This approach produced smooth carbon shells on micrometer-sized LFP particles, resulting in 6 μm microspheres with a tap density of 1.6 g cm^{-3}. These microspheres exhibited strong rate performance and reached a volumetric capacity of 225 mAh cm^{-3} [300].

Coulombic efficiency is another essential parameter for assessing LFP's practical viability, as high CE (> 99.5%) ensures minimal irreversible capacity loss over extended cycling. Optimized LFP materials with uniform carbon coatings, controlled particle morphology, and minimal defect density have demonstrated initial CE values above 99.8% and retention near 100% over thousands of cycles [292, 298, 300]. High tap density, when combined with high Coulombic efficiency, maximizes both gravimetric and volumetric performance while reducing total inactive mass content, making it indispensable for the development of high ED and long-life commercial LFP electrodes.

5.2 | Innovative Electrode Technologies for High Energy Density LFP

To meet the growing demand for high ED LFP batteries in EVs and grid-scale storage, optimizing electrode manufacturing is critical. Traditional wet-processing methods, based on slurry casting followed by solvent evaporation and drying, have been widely adopted in industry. However, these methods can suffer from performance limitations, especially in thick electrodes, due to binder migration driven by solvent capillarity. LFP electrodes are more susceptible to binder migration, primarily due to their typical slurry composition, which contains low solid content and relatively high concentrations of binder and conductive carbon, conditions that exacerbate binder segregation during drying. This leads to an inhomogeneous distribution of components, increased tortuosity, and weakened electrode-current collector adhesion. As a promising alternative, dry electrode processing eliminates the use of solvents and drying steps, thereby reducing energy consumption by over 46% and manufacturing costs by approximately 11.5% [301]. The process involves mechanically mixing active materials, binders (e.g., PTFE), and conductive additives, followed by calendering into free-standing films and lamination onto current collectors (Figure 9C) [288]. This yields electrodes with improved component uniformity, lower ionic resistance, and stronger mechanical stability.

In a notable demonstration, Kwon et al. [288] developed dry-processed thick-film LFP electrodes using PTFE binder, which forms fibrous networks that bridge particles, facilitating efficient Li-ion and electron transport (Figure 9D,E). Their LFP/graphite

full cells achieved a high areal capacity of 7.8 mAh cm^{-2} with excellent cycle life over 300 cycles. Electrochemical impedance measurements confirmed reduced charge-transfer and ionic resistance, attributed to the uniform microstructure and a more stable cathode–electrolyte interphase (CEI). Similarly, Tao et al. [302] studied the role of dry mixing (DM) time in enhancing PTFE fiberization and found that moderate DM time optimizes binder morphology, leading to robust electrode structures and improved cycling performance. Dry press-coated electrodes (DPCEs), fabricated using multi-walled CNTs (MWNTs) and PVDF binders with etched aluminum foil, achieved higher discharge capacities and EDs (up to 360 Wh kg^{-1} and 701 Wh L^{-1}) than slurry-coated electrodes (SCEs), with 84% capacity retention over 700 cycles compared to 78% for SCEs [303]. In parallel with advances in dry processing, carefully engineered wet-processed architectures also show promise for high-energy LFP electrodes. Choi et al. [289] developed a bilayer gradient-porosity LFP electrode via wet processing, combining a lower layer of small particles to enhance ionic/electronic conductivity and an upper layer of large, high-density particles to maximize mass loading (Figure 9F–H). This gradient design helped mitigate typical wet-process challenges such as binder migration and inhomogeneous porosity. The resulting electrode exhibited an areal capacity of 6.3 mAh cm^{-2}, a density of 2.5 g cm^{-3}, and retained 70.4% capacity at 6 mA cm^{-2}. Full-cell testing with graphite and Si-Gr anodes confirmed strong cycling performance, with up to 90.9% retention after 100 cycles and continued stability beyond 300 cycles at increased electrode density.

In summary, both dry and wet electrode processing routes offer valuable solutions for developing high-energy-density LFP cathodes. Dry processing stands out for its streamlined production workflow, reduced energy and solvent usage, and improved scalability due to fewer processing steps and simplified equipment requirements, making it a promising route for sustainable LFP electrode fabrication. At the same time, innovative wet-processing approaches—such as gradient-porosity architectures—demonstrate that, with intelligent design, conventional slurry-based techniques can still deliver competitive energy densities and robust electrochemical performance. By leveraging the distinct advantages of both dry and wet methods, these complementary strategies establish a strong platform for the continued development of next-generation LFP batteries, optimized for a wide range of applications from environmentally friendly EVs to long-duration grid-scale energy storage.

5.3 | Pack Architecture Technologies for High Energy Density LFP Battery Pack

The development of high ED LFP battery packs for EVs has advanced considerably with innovations in pack architecture that maximize active material volume while ensuring electrical, mechanical, and thermal stability under demanding operating conditions. Traditional EV battery pack designs, especially those employing high-nickel layered oxide cathodes, often rely on a modular approach in which cells are assembled into protective modules before being integrated into the pack. This structure allows for the addition of mechanical reinforcement, thermal barriers, and propagation prevention layers necessary to mitigate the higher thermal reactivity and gas evolution risks associated with high-nickel chemistries. However, the inclusion of these intermediate module components imposes significant penalties on volumetric ED due to increased inactive mass and reduced packing efficiency.

For LFP chemistries, which already exhibit superior thermal stability, chemical robustness, and negligible oxygen release under abuse conditions, these extensive protective layers are less critical. This inherent safety margin has enabled the adoption of high-integration strategies such as cell-to-pack (CTP) and cell-to-chassis (CTC) technologies (Figure 10). In CTP designs, the module layer is eliminated entirely, and cells, typically large-format prismatic LFP, are integrated directly into the pack structure. By removing redundant module housings, interconnect plates, and excess busbar segments, CTP architecture significantly increases packing efficiency and reduces inactive weight. For example, BYD reports that its CTP integration can improve pack-level ED by up to 50% compared to conventional cell–module–pack designs, offsetting LFP's lower gravimetric ED relative to high-Ni cathodes [304, 305]. Similarly, CATL's third-generation CTP ("Qilin") achieves volume utilization improvements from ~52% to ~72%, enabling LFP packs to reach gravimetric EDs of ~160 Wh kg^{-1}, levels competitive with some lower-Ni chemistries [306].

CTC architecture represents a further evolution, in which the battery pack is structurally integrated into the vehicle chassis itself. This design not only eliminates the module layer but also merges the pack casing with structural vehicle components such as the floor pan, longitudinal beams, and cross members. By embedding the battery into the chassis, CTC maximizes available volume for active material, reduces part count, and improves structural rigidity while lowering the overall vehicle mass. This integration can also contribute to crash safety by distributing impact loads through the combined chassis–pack structure. Manufacturers, including CATL, Tesla, and Leapmotor, have reported CTC-based LFP designs that achieve a > 10% improvement in driving range and a > 25% increase in torsional stiffness compared to conventional pack installations [307, 308].

Electrical configuration plays a pivotal role in ensuring high power performance in these dense architectures. LFP's lower electronic conductivity relative to nickel-rich cathodes necessitates highly efficient current collection and distribution systems to minimize resistive losses during high C-rate operation. CTP and CTC designs often employ wide, low-resistance busbars and direct cell-to-busbar connections to reduce electrical path length and eliminate intermediate joints. Optimized series–parallel arrangements balance voltage and current requirements, while careful spatial distribution of current collectors helps avoid localized overcurrent zones that could accelerate heat generation. The combination of these strategies supports stable performance even at charge rates exceeding 3–4 C, a critical requirement for fast- and ultra-fast-charging EV applications [309–311].

Thermal management is a critical enabler for high ED LFP packs, particularly under high magnification conditions (i.e., high C-rate fast charging or high-power discharge), where elevated current flow significantly increases heat generation. One advantage of CTP over traditional modular designs is the improved thermal

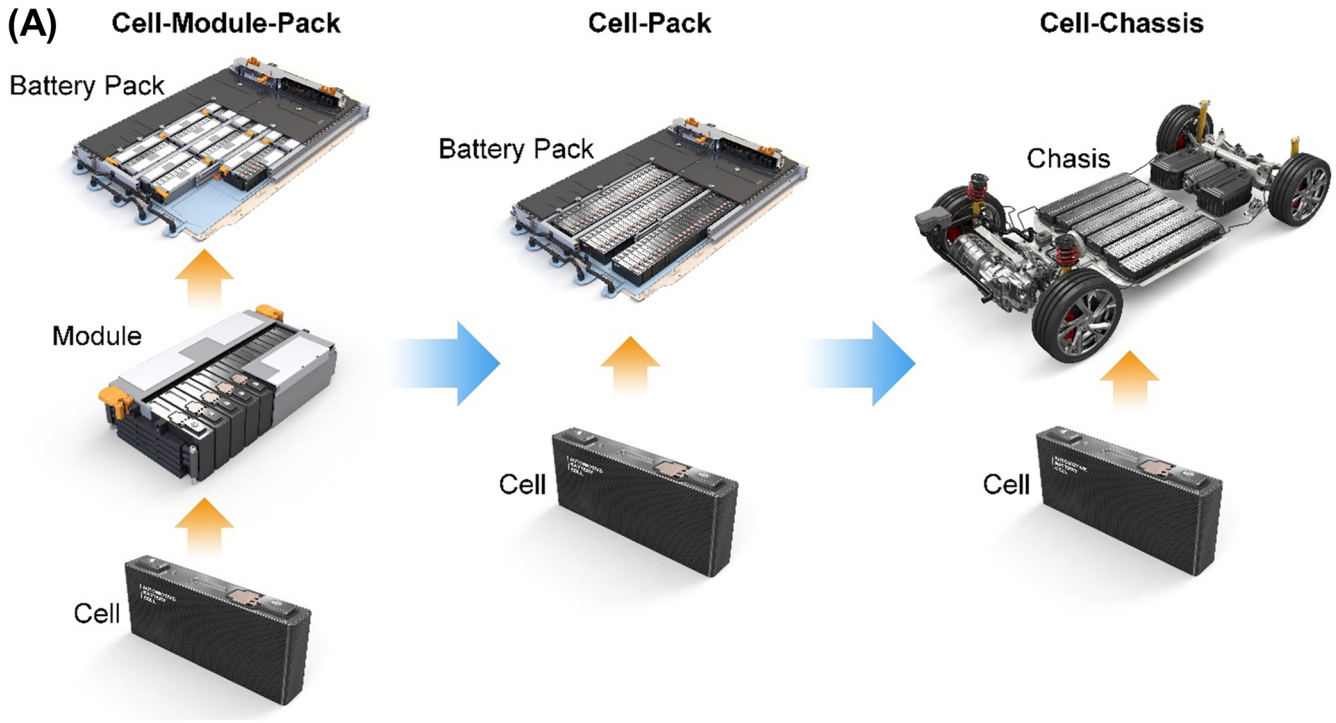

(B)

	Features	Details	Target Performance
Electronic Configuration	Efficient Current Collection	Wide and low-resistance busbars Direct cell-to-busbar connections	Fast Charging High Power
	Optimized Electrical Path	Removal of intermediate joints	
	Balanced Voltage–Current Design	Optimized series–parallel arrangements	
Thermal Management	Improved Thermal Coupling	Direct cell–cooling plate contact	Safety
	Advanced TCIMs	Gap fillers, conductive epoxies, adhesives with alumina/BN fillers	
	Passive Thermal Buffering	Composite PCMs with graphite/copper/aluminum	
	Hybrid Cooling Strategies	Combination of liquid cooling with forced-air flow Heat pump-assisted loops	

FIGURE 10 | (A) Schematic illustration of conventional and next-generation battery pack architectures. (B) Key advantages of electric configuration and thermal management in battery pack systems.

coupling between cells and cooling interfaces. With the elimination of module casings and internal insulation layers, cells can be placed in direct contact with large-area cooling plates, embedded heat spreaders, or chassis-integrated cooling circuits, reducing thermal resistance pathways and improving conductive heat transfer. Advanced thermally conductive interface materials, including gap fillers loaded with alumina or boron nitride, thermally conductive epoxies, and structural adhesives, further enhance this coupling. For transient heat spikes during rapid charge pulses, phase change materials (PCMs) offer passive thermal buffering by absorbing latent heat during melting. Composite PCMs reinforced with graphite sheets, copper mesh, or aluminum foam have been shown to improve both thermal conductivity and heat absorption capacity, reducing intra-pack temperature differentials to within a few degrees Celsius under high load [312, 313].

In CTC designs, thermal management is integrated at the chassis level, leveraging the large surface area of the vehicle underbody to spread and dissipate heat. Liquid cooling channels, embedded heat pipes, and even immersion cooling systems are employed to manage the high heat fluxes generated during rapid charging. For example, XING Mobility's LFP-based CTC battery system uses immersion cooling in dielectric fluids to maintain cell temperatures 20°C–30°C lower than with conventional cold plates, enabling repeated ultra-fast charging without exacerbating degradation. Innovative hybrid thermal strategies, such as combining liquid cooling with forced-air flow or integrating heat pump-assisted liquid loops, further ensure stable temperature regulation under extreme environmental and operational conditions [314–316]. These systems are particularly effective in maintaining LFP cells within the optimal 15°C–40°C range during prolonged operation under high-rate cycling.

The mechanical and thermal integration in CTP and CTC packs also supports safety-critical functions. By preserving uniform temperature distribution across cells, these architectures effectively suppress localized hotspots that could otherwise trigger thermal propagation. In addition, the high stiffness of the integrated pack structures minimizes mechanical deformation caused by aggressive driving stresses or thermal expansion during operation. This ensures consistent cell contact with

cooling elements, preserving stable thermal management. The direct structural bonding of cells to load-bearing chassis members further enhances crash safety while promoting efficient heat conduction away from the electrochemical core. Therefore, pack-architecture technologies such as CTP and CTC have reshaped the design landscape for high-energy-density LFP battery systems. By eliminating module redundancies, optimizing electrical pathways, and embedding advanced thermal management within the structural framework, these designs enable LFP chemistry to reach both the volumetric energy densities and high-power charging capabilities demanded by next-generation electric mobility. Combined with LFP's inherent safety and long cycle life, these architectural innovations strongly support its deployment in long-range and fast-charging EV platforms.

6 | Summary and Perspective

The limited ED of LFP electrodes has been a critical bottleneck in advancing LIBs research, particularly due to its relatively low nominal voltage (~3.2 V vs. Li/Li^+) and moderate specific capacity (~170 mAh g^{-1}). To unlock the full potential of LFP for next-generation energy storage systems, a multifaceted approach including material innovation, electrode design, and system-level optimizations is essential. Nanostructuring LFP, including the development of single-crystalline structures and porous frameworks, offers significant advantages by reducing ionic diffusion barriers while maintaining a high tap density. These designs help enhance high-rate performance by eliminating grain boundary resistance, allowing for better active material utilization in fast-charging conditions. To compensate for the inherently low volumetric energy density of LFP, high-tap-density LFP powders must be developed (> 2.8 g cm^{-3}).

Tap density plays a critical role not only in maximizing volumetric ED but also in improving packing efficiency and mechanical integrity of electrodes. Higher tap density allows for higher mass loading without excessive electrode thickness, which is essential for increasing ED in practical cells. Simultaneously, developing advanced conductive networks, such as dual carbon coatings or hybrid graphene-CNT composites, can enhance electronic conductivity without significantly increasing the overall volume, addressing one of the key challenges of traditional carbon coatings. In addition to material improvements, the design of electrode architectures must be optimized for higher ED and performance. The development of ultra-thick electrodes (> 200 μm) with graded porosity or advanced 3D current collectors (e.g., laser-structured foils) can significantly increase the amount of active material, while maintaining efficient ionic and electronic transport. Dry electrode processing, already explored in commercial LIBs, is a promising method to improve particle packing density and reduce production costs.

Mass loading and electrolyte composition are equally critical for LFP electrochemical performance. High mass loading can increase areal capacity but may lead to poor electrolyte penetration and slow Li^+ transport, especially at high rates or low temperatures. Carefully selecting electrolyte type, viscosity, and Li^+ transference number is essential to balance ionic conductivity with stable SEI formation. Coulombic efficiency is another important metric; high Coulombic efficiency minimizes irreversible capacity loss, enhances cycle life, and boosts overall energy throughput, particularly in long-duration grid storage. At the cell and pack level, coupling LFP with high-voltage electrolytes, Li-metal anodes, or even solid-state architectures could lead to dramatic improvements in ED. Although the implementation of solid-state batteries using LFP faces challenges, such as stability at high voltages and interface compatibility, advances in novel electrolyte materials (e.g., sulfide-based and polymer electrolytes) are paving the way for their future use.

Low-temperature performance remains a major hurdle for LFP, as Li^+ diffusion within the olivine lattice slows significantly with decreasing temperature, leading to reduced capacity and rate capability. Strategies such as particle downsizing, morphology engineering, doping, conductive surface coatings, and advanced electrolyte formulations have been explored, and these approaches can mitigate kinetic limitations and enable stable operation even under subzero conditions. At the same time, it is critical to consider the sustainability of LFP-based batteries. Integrating scalable and eco-friendly synthesis methods, alongside effective recycling strategies, will be essential for ensuring the long-term environmental viability of these technologies. Recycling and reuse of LFP-based LIBs offer an effective pathway to reduce raw material demand, lower production costs, and mitigate environmental impacts. The approaches, such as direct regeneration techniques, hydrometallurgical recovery, and refurbishment of degraded cathodes, can facilitate the material circularity and strengthen the foundation for a sustainable battery economy. Advanced battery pack architectures, when combined with high-density electrodes, have the potential to match or even surpass the energy density of high-Ni layered oxide systems.

Looking ahead, the following research directions hold the potential to overcome existing barriers and push the boundaries of LFP-based cathodes:

- **Precision Engineering of Dopant Architectures:** tailoring dopants at the atomic level (both on the Li-site and Fe-site) to optimize electronic structure and minimize performance degradation due to lattice distortions.
- **Multifunctional Coating Strategies for Performance Enhancement:** developing coatings that enhance both ionic conductivity and structural stability, while simultaneously mitigating side reactions and improving cycle life.
- **Hierarchical Electrode Architectures for Enhanced Ion Transport:** engineering electrodes with a well-defined hierarchical structure that facilitates ion diffusion at multiple length scales, thus improving overall battery performance.
- **Materials and Electrode Technology for High Electrode Density:** development of high-pressure–density LFP powder and optimized processing techniques to achieve uniform and dense electrode structures.
- **Strategies for Achieving High-Rate and Low-Temperature Performance:** investigating the role of advanced electrolytes and the possibility of integrating new cell configurations, as well as optimizing LFP for these high-demand applications.

- **Sustainable and Scalable Approaches for Practical Applications:** focusing on scalable synthesis methods that lower costs and improve recyclability to ensure that advances in LFP technology do not come at the expense of environmental impact.
- **Recycling as a Critical Enabler:** incorporating recycling strategies is vital for sustainability, including the development of direct recycling and hydrometallurgical processes that recover valuable materials while maintaining LFP cathode integrity during reuse.
- **Integration of AI/ML for LFP Optimization:** artificial intelligence and machine learning can be applied to efficiently predict optimal doping strategies, coating parameters, particle morphologies, electrolyte formulations, and electrode architectures. Such data-driven approaches enable the targeted enhancement of key performance metrics, including low-temperature capability, high tap density, and extended cycle life.

The future of LFP-based batteries is bright, but the path forward will require addressing key challenges in performance, manufacturing, and sustainability. By overcoming these challenges, LFP could transition from a well-established but underutilized cathode material to a leading candidate for applications in EVs, grid energy storage, and even emerging fields like electric aviation. With concerted efforts across material science, engineering, and sustainability, LFP-based batteries have the potential to contribute significantly to the next generation of high-performance, long-lifetime, and environmentally friendly energy storage systems.

Acknowledgments

This work was supported by the National R&D Program through the National Research Foundation of Korea (NRF) funded by Ministry of Science and ICT (RS-2024-00408156 and RS-2025-16069043). M. Y. acknowledges the support from the National Research Foundation of Korea (NRF) grant funded by the Korea government (Ministry of Science and ICT, MSIT) (RS-2024-00343847).

Conflicts of Interest

The authors declare no conflicts of interest.

References

1. G. Crabtree, "The Coming Electric Vehicle Transformation," *Science* 366 (2019): 422–424.

2. J. Ruan, S. Luo, S. Wang, et al., "Enhancing the Whole Migration Kinetics of Na^+ in the Anode Side for Advanced Ultralow Temperature Sodium-Ion Hybrid Capacitor," *Advanced Energy Materials* 13 (2023): 2301509.

3. K. W. Leong, W. Pan, X. Yi, et al., "Next-Generation Magnesium-Ion Batteries: The Quasi-Solid-State Approach to Multivalent Metal Ion Storage," *Science Advances* 9 (2023): eadh1181.

4. A. Gharehghani, M. Rabiei, S. Mehranfar, et al., "Progress in Battery Thermal Management Systems Technologies for Electric Vehicles," *Renewable and Sustainable Energy Reviews* 202 (2024): 114654.

5. G. Zhao, X. Wang, and M. Negnevitsky, "Connecting Battery Technologies for Electric Vehicles From Battery Materials to Management," *Iscience* 25 (2022): 103744.

6. Y. Cao, S. Derrible, M. Le Pira, and H. Du, "Advanced Transport Systems: The Future Is Sustainable and Technology-Enabled," *Scientific Reports* 14 (2024): 9429.

7. J. U. Choi, N. Voronina, Y. K. Sun, and S. T. Myung, "Recent Progress and Perspective of Advanced High-Energy Co-Less Ni-Rich Cathodes for Li-Ion Batteries: Yesterday, Today, and Tomorrow," *Advanced Energy Materials* 10 (2020): 2002027.

8. M. M. Thackeray and K. Amine, "Layered Li–Ni–Mn–Co Oxide Cathodes," *Nature Energy* 6 (2021): 933.

9. L. Lu, G. Jiang, C. Gu, and J. Ni, "Revisiting Polyanionic $LiFePO_4$ Battery Material for Electric Vehicles," *Functional Materials Letters* 14 (2021): 2130006.

10. Y. Wang, J. Zhang, J. Xue, X. Ke, and G. Liang, "$LiFePO_4$/C Composites With High Compaction Density as Cathode Materials for Lithium-Ion Batteries With High Volumetric Energy Density," *Ionics* 27 (2021): 4687–4694.

11. Z. Xiao, T. Chen, T. Zhao, et al., "Advances in Performance Degradation Mechanism and Safety Assessment of $LiFePO_4$ for Energy Storage," *Nanotechnology* 35 (2024): 292001.

12. Y. Li, L. Wang, K. Zhang, Y. Yao, and L. Kong, "Optimized Synthesis of $LiFePO_4$ Cathode Material and Its Reaction Mechanism During Solvothermal," *Advanced Powder Technology* 32 (2021): 2097–2105.

13. S.-P. Chen, D. Lv, J. Chen, Y.-H. Zhang, and F.-N. Shi, "Review on Defects and Modification Methods of $LiFePO_4$ Cathode Material for Lithium-Ion Batteries," *Energy & Fuels* 36 (2022): 1232–1251.

14. P. J. Bugryniec, J. N. Davidson, D. J. Cumming, and S. F. Brown, "Pursuing Safer Batteries: Thermal Abuse of $LiFePO_4$ Cells," *Journal of Power Sources* 414 (2019): 557–568.

15. W. Wu, W. Wu, X. Qiu, and S. Wang, "Low-Temperature Reversible Capacity Loss and Aging Mechanism in Lithium-Ion Batteries for Different Discharge Profiles," *International Journal of Energy Research* 43 (2019): 243–253.

16. L. A.-W. Ellingsen, G. Majeau-Bettez, B. Singh, A. K. Srivastava, L. O. Valøen, and A. H. Strømman, "Life Cycle Assessment of a Lithium-Ion Battery Vehicle Pack," *Journal of Industrial Ecology* 18 (2014): 113–124.

17. Y. Hua, S. Zhou, Y. Huang, et al., "Sustainable Value Chain of Retired Lithium-Ion Batteries for Electric Vehicles," *Journal of Power Sources* 478 (2020): 228753.

18. T. Zhao, H. Mahandra, R. Marthi, et al., "An Overview on the Life Cycle of Lithium Iron Phosphate: Synthesis, Modification, Application, and Recycling," *Chemical Engineering Journal* 485 (2024): 149923.

19. T. Feng, W. Guo, Q. Li, Z. Meng, and W. Liang, "Life Cycle Assessment of Lithium Nickel Cobalt Manganese Oxide Batteries and Lithium Iron Phosphate Batteries for Electric Vehicles in China," *Journal of Energy Storage* 52 (2022): 104767.

20. S. S. Rangarajan, S. P. Sunddararaj, A. Sudhakar, et al., "Lithium-Ion Batteries—The Crux of Electric Vehicles With Opportunities and Challenges," *Clean Technologies* 4 (2022): 908–930.

21. C. Qi, T. Yao, W. Zhai, M. Zhang, L. Song, and J. He, "Advances in Degradation Mechanism and Sustainable Recycling of $LiFePO_4$-type Lithium-Ion Batteries," *Energy Storage Materials* 71 (2024): 103623.

22. X. Zhang, D. Wang, X. Qiu, et al., "Stable High-Capacity and High-Rate Silicon-Based Lithium Battery Anodes Upon Two-Dimensional Covalent Encapsulation," *Nature Communications* 11 (2020): 3826.

23. K. Cui, M.-C. Zhao, Y. Li, A. Atrens, and F. Zhang, "Recycling of Spent Lithium Iron Phosphate Batteries: Research Progress Based on Environmental Protection and Sustainable Development Technology," *Separation and Purification Technology* 354 (2025): 128982.

24. B. Jetin, "Electric Batteries and Critical Materials Dependency: A Geopolitical Analysis of the USA and the European Union,"

International Journal of Automotive Technology and Management 23 (2023): 383–407.

25. A. Ravi, A. E. Prasad, N. R. Weston, Z. Liu, and D. N. Mavris, "Life Cycle Assessment and Risk Analysis of Lithium for Battery Systems in Aerospace Applications," AIAA SCITECH 2024 Forum (2024).

26. L.-X. Yuan, Z.-H. Wang, W.-X. Zhang, et al., "Development and Challenges of $LiFePO_4$ Cathode Material for Lithium-Ion Batteries," *Energy & Environmental Science* 4 (2011): 269–284.

27. B. Luo, B. Xu, Q. Yan, et al., "Advances and Challenges in Recycling Spent $LiFePO_4$ Batteries," *Separation and Purification Technology* 362 (2025): 131780.

28. T. Ouaneche, L. Stievano, L. Monconduit, C. Guery, N. Recham, and M. T. Sougrati, "Challenges in Spent LFP Cathodes' Direct Lithiation: The Crucial Role of Reducing Agents," *EES Batteries* 1 (2025): 1068–1082.

29. D.-W. Kim, H.-S. Kim, and H.-L. Choi, "Comprehensive Review on Wet Recycling Methods for $LiFePO_4$ Batteries," *Resources Recycling* 33 (2024): 28–40.

30. C. B. Van Beek, E. Yilmaz, and D. H. A. Boom, "Sustainable Hydrometallurgical LFP Battery Recycling: Electrochemical Approaches," *Chemsuschem* 18 (2025): e202402699.

31. D. F. Barbosa de Mattos, S. Duda, and M. Petranikova, "Recycling of Lithium Iron Phosphate ($LiFePO_4$) Batteries From the End Product Quality Perspective," *Batteries* 11 (2025): 33.

32. Y. Nishi, "Lithium Ion Secondary Batteries; Past 10 Years and the Future," *Journal of Power Sources* 100 (2001): 101–106.

33. F. Schipper, E. M. Erickson, C. Erk, J.-Y. Shin, F. F. Chesneau, and D. Aurbach, "Review—Recent Advances and Remaining Challenges for Lithium Ion Battery Cathodes: I. Nickel-Rich, $LiNi_xCo_yMn_zO_2$," *Journal of the Electrochemical Society* 164 (2016): A6220–A6228.

34. J. Molenda and M. Molenda, *Composite Cathode Material for Li-Ion Batteries Based on $LiFePO_4$ System* (IntechOpen, 2011).

35. X. Shen, X.-Q. Zhang, F. Ding, et al., "Advanced Electrode Materials in Lithium Batteries: Retrospect and Prospect," *Energy Material Advances* 2021 (2021): 1205324.

36. Z. Chen, W. Zhang, and Z. Yang, "A Review on Cathode Materials for Advanced Lithium Ion Batteries: Microstructure Designs and Performance Regulations," *Nanotechnology* 31 (2019): 012001.

37. C. A. J. Fisher, V. M. Hart Prieto, and M. S. Islam, "Lithium Battery Materials $LiMPO_4$ (M = Mn, Fe, Co, and Ni): Insights Into Defect Association, Transport Mechanisms, and Doping Behavior," *Chemistry of Materials* 20 (2008): 5907–5915.

38. K. Hoang and M. Johannes, "Tailoring Native Defects in $LiFePO_4$: Insights From First-Principles Calculations," *Chemistry of Materials* 23 (2011): 3003–3013.

39. R. Malik, A. Abdellahi, and G. Ceder, "A Critical Review of the Li Insertion Mechanisms in $LiFePO_4$ Electrodes," *Journal of the Electrochemical Society* 160 (2013): A3179–A3197.

40. D. Morgan, A. Van der Ven, and G. Ceder, "Li Conductivity in Li_xMPO_4 (M = Mn, Fe, Co, Ni) Olivine Materials," *Electrochemical and Solid-State Letters* 7 (2003): A30.

41. M. S. Islam, D. J. Driscoll, C. A. J. Fisher, and P. R. Slater, "Atomic-Scale Investigation of Defects, Dopants, and Lithium Transport in the $LiFePO_4$ Olivine-Type Battery Material," *Chemistry of Materials* 17 (2005): 5085–5092.

42. S. Nishimura, G. Kobayashi, K. Ohoyama, R. Kanno, M. Yashima, and A. Yamada, "Experimental Visualization of Lithium Diffusion in Li_xFePO_4," *Nature Materials* 7 (2008): 707–711.

43. J. Sugiyama, H. Nozaki, M. Harada, et al., "Magnetic and Diffusive Nature of $LiFePO_4$ Investigated by Muon Spin Rotation and Relaxation," *Physical Review B* 84 (2011): 054430.

44. E. Meng, J. Sun, Y. Huang, and H. Tang, "Morphology Evolution and Improved Electrochemical Properties of $LiFePO_4$ Cathode Materials for Li-Ion Batteries," *International Journal of Electrochemical Science* 17 (2022): 221225.

45. L. Peng, Y. Zhao, Y. Ding, and G. Yu, "Self-Assembled $LiFePO_4$ Nanowires With High Rate Capability for Li-Ion Batteries," *Chemical Communications* 50 (2014): 9569–9572.

46. M. A. M. M. Alsamet and E. Burgaz, "Synthesis and Characterization of Nano-Sized $LiFePO_4$ by Using Consecutive Combination of Sol-Gel and Hydrothermal Methods," *Electrochimica Acta* 367 (2021): 137530.

47. Y. Gao, Z. Pan, J. Sun, Z. Liu, and J. Wang, "High-Energy Batteries: Beyond Lithium-Ion and Their Long Road to Commercialisation," *Nano-Micro Letters* 14 (2022): 94.

48. X. Huang, S. Yan, H. Zhao, et al., "Electrochemical Performance of $LiFePO_4$ Nanorods Obtained From Hydrothermal Process," *Materials Characterization* 61 (2010): 720–725.

49. A. Vu and A. Stein, "Lithium Iron Phosphate Spheres as Cathode Materials for High Power Lithium Ion Batteries," *Journal of Power Sources* 245 (2014): 48–58.

50. J. Y. Cheong, S.-H. Cho, J. Lee, J.-W. Jung, C. Kim, and I.-D. Kim, "Multifunctional 1D Nanostructures Toward Future Batteries: A Comprehensive Review," *Advanced Functional Materials* 32 (2022): 2208374.

51. F. I. Saaid, M. F. Kasim, T. Winie, et al., "Ni-Rich Lithium Nickel Manganese Cobalt Oxide Cathode Materials: A Review on the Synthesis Methods and Their Electrochemical Performances," *Heliyon* 10 (2024): e23968.

52. S. Xu, X. Tan, W. Ding, et al., "Promoting Surface Electric Conductivity for High-Rate $LiCoO_2$," *Angewandte Chemie* 135 (2023): e202218595.

53. W. Yu, G. Ou, L. Qi, and H. Wu, "Textured $LiFePO_4$ Bulk With Enhanced Electrical Conductivity," *Journal of the American Ceramic Society* 99 (2016): 3214–3216.

54. J. Zahnow, T. Bernges, A. Wagner, et al., "Impedance Analysis of NCM Cathode Materials: Electronic and Ionic Partial Conductivities and the Influence of Microstructure," *ACS Applied Energy Materials* 4 (2021): 1335–1345.

55. K. Akhmetova, F. Sultanov, A. Mentbayeva, N. Umirov, Z. Bakenov, and B. Tatykayev, "Advances in Multi-Element Doping of $LiFePO_4$ Cathode Material for Capacity Enhancement in Li-Ion Batteries," *Journal of Power Sources* 624 (2024): 235531.

56. X. Zhang, J. Li, Z. You, Z. Yang, Z. Lv, and Y. Xu, "Ultrahigh-Mass-Loading Flexible $LiFePO_4$ Cathode With the Drop-Shaped Low-Tortuosity Architecture for High-Performance Flexible Lithium-Ion Batteries," *Journal of Colloid and Interface Science* 690 (2025): 137320.

57. D. Y. Han, H. B. Son, S. H. Han, et al., "Hierarchical 3D Electrode Design With High Mass Loading Enabling High-Energy-Density Flexible Lithium-Ion Batteries," *Small* 19 (2023): 2305416.

58. C. de La Torre-Gamarra, M. E. Sotomayor, J.-Y. Sanchez, et al., "High Mass Loading Additive-Free $LiFePO_4$ Cathodes With 500 μm Thickness for High Areal Capacity Li-Ion Batteries," *Journal of Power Sources* 458 (2020): 228033.

59. M. Koltypin, D. Aurbach, L. Nazar, and B. Ellis, "On the Stability of $LiFePO_4$ Olivine Cathodes Under Various Conditions (Electrolyte Solutions, Temperatures)," *Electrochemical and Solid-State Letters* 10 (2007): A40.

60. S. E. Sloop, J. K. Pugh, S. Wang, J. B. Kerr, and K. Kinoshita, "Chemical Reactivity of PF_5 and $LiPF_6$ in Ethylene Carbonate/Dimethyl Carbonate Solutions," *Electrochemical and Solid-State Letters* 4 (2001): A42.

61. H. Yang, G. V. Zhuang, and P. N. Ross, Jr., "Thermal Stability of $LiPF_6$ Salt and Li-Ion Battery Electrolytes Containing $LiPF_6$," *Journal of Power Sources* 161 (2006): 573–579.

62. P. Arora, R. E. White, and M. Doyle, "Capacity Fade Mechanisms and Side Reactions in Lithium-Ion Batteries," *Journal of the Electrochemical Society* 145 (1998): 3647–3667.

63. L. Péter and J. Arai, "Anodic Dissolution of Aluminium in Organic Electrolytes Containing Perfluoroalkylsulfonyl Imides," *Journal of Applied Electrochemistry* 29 (1999): 1053–1061.

64. H. Wu, Q. Liu, and S. Guo, "Composites of Graphene and $LiFePO_4$ as Cathode Materials for Lithium-Ion Battery: A Mini-Review," *Nano-Micro Letters* 6 (2014): 316–326.

65. Z. Qiu, Q. Man, Y. Mu, et al., "Modification Strategies for Enhancing the Performance of Lithium Manganese Iron Phosphate Cathodes in Lithium-Ion Batteries," *Chemistry–Methods* 5 (2025): 2400065.

66. H. Erabhoina and M. Thelakkat, "Tuning of Composition and Morphology of $LiFePO_4$ Cathode for Applications in All Solid-State Lithium Metal Batteries," *Scientific Reports* 12 (2022): 5454.

67. S. S. Sahoo, J. Narayan, R. J. Narayan, X.-G. Sun, and M. P. Paranthaman, "Enhancement of the Electrochemical Performance of $LiFePO_4$ Cathode Material by Nanosecond Laser Annealing," *MRS Communications* 15 (2025): 255–264.

68. H. An and K. Park, "LFP via Nanoscale Surface Reforming With a Tiny Minimal Amount of Conductivity-Enhancing Material," *Langmuir* 41 (2025): 1821–1829.

69. D. E. Kim and Y. J. Park, "Improving the Electrochemical Properties of $LiFePO_4$ by Mixed-Source-Derived Carbon Layer," *Journal of Electrochemical Science and Technology* 16 (2025): 456–467.

70. L. Wang, H. Chen, Y. Zhang, J. Liu, and L. Peng, "Research Progress in Strategies for Enhancing the Conductivity and Conductive Mechanism of $LiFePO_4$ Cathode Materials," *Molecules* 29 (2024): 5250.

71. M. A. M. M. Al-Samet and E. Burgaz, "Improving the Lithium-Ion Diffusion and Electrical Conductivity of $LiFePO_4$ Cathode Material by Doping Magnesium and Multi-Walled Carbon Nanotubes," *Journal of Alloys and Compounds* 947 (2023): 169680.

72. J. Yan, J. Qian, Y. Li, L. Li, F. Wu, and R. Chen, "Toward Sustainable Lithium Iron Phosphate in Lithium-Ion Batteries: Regeneration Strategies and Their Challenges," *Advanced Functional Materials* 34 (2024): 2405055.

73. M. Zhang, L. Wang, S. Wang, T. Ma, F. Jia, and C. Zhan, "A Critical Review on the Recycling Strategy of Lithium Iron Phosphate From Electric Vehicles," *Small Methods* 7 (2023): 2300125.

74. S. Yasa, O. Aydin, M. Al-Bujasim, B. Birol, and M. Gencten, "Recycling Valuable Materials From the Cathodes of Spent Lithium-Ion Batteries: A Comprehensive Review," *Journal of Energy Storage* 73 (2023): 109073.

75. C. Lara, M. Maril, P. Tobosque, J. Núñez, L. Pizarro, and C. Carrasco, "Comprehensive Analysis of Improved $LiFePO_4$ Kinetics: Understanding Barriers to Fast Charging," *Journal of Power Sources* 640 (2025): 236747.

76. L. X. Jiao, Z. Q. Li, Y. Z. Zhu, et al., "Enhanced Electrical Conductivity and Lithium Ion Diffusion Rate of $LiFePO_4$ by Fe Site and P Site Doping," *AIP Advances* 13 (2023): 075306.

77. Y. Guo, S. Wang, K. Ruan, H. Zhang, and J. Gu, "Highly Thermally Conductive Carbon Nanotubes Pillared Exfoliated Graphite/Polyimide Composites," *NPJ Flexible Electronics* 5 (2021): 16.

78. L. Li, D. Zhang, J. Deng, et al., "Carbon-Based Materials for Fast Charging Lithium-Ion Batteries," *Carbon* 183 (2021): 721–734.

79. H.-C. Chuang, J.-W. Teng, and W.-F. Kuan, "Supercritical CO_2-Enhanced Surface Modification on $LiFePO_4$ Cathodes Through Ex-Situ Carbon Coating for Lithium-Ion Batteries," *Colloids and Surfaces, A: Physicochemical and Engineering Aspects* 684 (2024): 133110.

80. Y. Cai, D. Huang, Z. Ma, et al., "Construction of Highly Conductive Network for Improving Electrochemical Performance of Lithium Iron Phosphate," *Electrochimica Acta* 305 (2019): 563–570.

81. F. Guo, X. Huang, Y. Li, et al., "In Situ Low-Temperature Carbonization Capping of $LiFePO_4$ With Coke for Enhanced Lithium Battery Performance," *Molecules* 28 (2023): 6083.

82. Y. Wang, J. Zhang, J. Xue, X. Ke, and G. Liang, "$LiFePO_4$/C Composites With High Compaction Density as Cathode Materials for Lithium-Ion Batteries With High Volumetric Energy Density," *Ionics* 27 (2021): 4687–4694.

83. H. Raj and A. Sil, "Effect of Carbon Coating on Electrochemical Performance of $LiFePO_4$ Cathode Material for Li-Ion Battery," *Ionics* 24 (2018): 2543–2553.

84. K. Dhanabalan, P. T. Thong, M. Prakash, and H. Y. Jung, "Graphitic Carbon Nitride/Carbon Coating on Negative Plate Extends Lead-Acid Batteries Cycle Life," *Journal of Power Sources* 641 (2025): 236861.

85. M. Chen, F.-M. Liu, S.-S. Chen, et al., "In Situ Self-Catalyzed Formation of Carbon Nanotube Wrapped and Amorphous Nanocarbon Shell Coated $LiFePO_4$ Microclew for High-Power Lithium Ion Batteries," *Carbon* 203 (2023): 661–670.

86. M. Onsrud, A. O. Tezel, S. Fotedar, and A. M. Svensson, "Novel Carbon Coating on Aluminum Current Collectors for Lithium-Ion Batteries," *SN Applied Sciences* 4 (2022): 225.

87. M. Wang, H. Yang, K. Wang, et al., "Quantitative Analyses of the Interfacial Properties of Current Collectors at the Mesoscopic Level in Lithium Ion Batteries by Using Hierarchical Graphene," *Nano Letters* 20 (2020): 2175–2182.

88. L. Rao, H. Cho, C. J. Brooks, J. R. Sayre, and J.-H. Kim, "Advancing Extreme Fast-Charging Capabilities of $LiFePO_4$ Using Conductive Polymer Coatings and Lithium Polyacrylate Binder," *ACS Applied Energy Materials* 7 (2024): 7131–7139.

89. R. Liu, H. Guo, H. Gu, et al., "Influence of PAN/PANI Polymer on Low-Temperature Rate Performance of $LiFePO_4$," *Ionics* 29 (2023): 2175–2189.

90. C.-C. Yang, J.-R. Jiang, C. Karuppiah, et al., "LATP Ionic Conductor and In-Situ Graphene Hybrid-Layer Coating on $LiFePO_4$ Cathode Material at Different Temperatures," *Journal of Alloys and Compounds* 765 (2018): 800–811.

91. G. Jiang, Z. Hu, J. Xiong, X. Zhu, and S. Yuan, "Enhanced Performance of $LiFePO_4$ Originating From the Synergistic Effect of Graphene Modification and Carbon Coating," *Journal of Alloys and Compounds* 767 (2018): 528–537.

92. S. Wu, E. Luo, J. Ouyang, et al., "Tuning the Graphitization of the Carbon Coating Layer on $LiFePO_4$ Enables Superior Properties," *International Journal of Electrochemical Science* 19 (2024): 100450.

93. H. Zhang, J. Li, L. Luo, et al., "Hierarchically Porous Mxene Decorated Carbon Coated $LiFePO_4$ as Cathode Material for High-Performance Lithium-Ion Batteries," *Journal of Alloys and Compounds* 876 (2021): 160210.

94. S. Kwak and Y. J. Park, "Improving the Performance of $LiFePO_4$ Cathodes With a Sulfur-Modified Carbon Layer," *Batteries* 10 (2024): 348.

95. N. D. Trinh, M. Saulnier, D. Lepage, and S. B. Schougaard, "Conductive Polymer Film Supporting $LiFePO_4$ as Composite Cathode for Lithium Ion Batteries," *Journal of Power Sources* 221 (2013): 284–289.

96. P. Li, K. Sun, and J. Ouyang, "Stretchable and Conductive Polymer Films Prepared by Solution Blending," *ACS Applied Materials & Interfaces* 7 (2015): 18415–18423.

97. A. Popov, B. Brasiunas, L. Mikoliunaite, G. Bagdziunas, A. Ramanavicius, and A. Ramanaviciene, "Comparative Study of Polyaniline (PANI), Poly(3,4-ethylenedioxythiophene) (PEDOT) and PANI-PEDOT Films Electrochemically Deposited on Transparent Indium Thin Oxide Based Electrodes," *Polymer* 172 (2019): 133–141.

98. M. Srivastava, A. K. M. R., and K. Zaghib, "Binders for Li-Ion Battery Technologies and Beyond: A Comprehensive Review," *Batteries* 10 (2024): 268.

99. P. Raghavan, X. Zhao, C. Shin, et al., "Preparation and Electrochemical Characterization of Polymer Electrolytes Based on Electrospun Poly (Vinylidene Fluoride-Co-Hexafluoropropylene)/Polyacrylonitrile Blend/ Composite Membranes for Lithium Batteries," *Journal of Power Sources* 195 (2010): 6088–6094.

100. C.-H. Tsao, C.-H. Hsu, and P.-L. Kuo, "Ionic Conducting and Surface Active Binder of Poly (Ethylene Oxide)-Block-Poly(Acrylonitrile) for High Power Lithium-Ion Battery," *Electrochimica Acta* 196 (2016): 41–47.

101. I. Boyano, J. A. Blazquez, I. de Meatza, et al., "Preparation of C-$LiFePO_4$/Polypyrrole Lithium Rechargeable Cathode by Consecutive Potential Steps Electrodeposition," *Journal of Power Sources* 195 (2010): 5351–5359.

102. J. Xu and G. Chen, "Effects of Doping on the Electronic Properties of $LiFePO_4$: A First-Principles Investigation," *Physica B: Condensed Matter* 405 (2010): 803–807.

103. Q. Zhao, S. Zhang, C. Wang, et al., "Combined First-Principles and Experimental Studies of a V-Doped $LiFePO_4$/C Composite as a Cathode Material for Lithium-Ion Batteries," *International Journal of Electrochemical Science* 16 (2021): 21053.

104. Z. Lv, M. Li, H. Yang, et al., "The First-Principles Study on Electrochemical Performance, Mechanical Properties, and Lithium-Ion Migration of $LiFePO_4$ Modified by Doping With Co and Nb," *Journal of Solid State Electrochemistry* 28 (2024): 2873–2883.

105. Z. Chen, Z. Zhang, Q. Zhao, J. Duan, and H. Zhu, "Understanding the Impact of K-Doping on the Structure and Performance of $LiFePO_4$/C Cathode Materials," *Journal of Nanoscience and Nanotechnology* 19 (2019): 119–124.

106. A. R. Madram and M. Faraji, "Site-Dependent Electrochemical Performance of Na and K Co-Doped $LiFePO_4$/C Cathode Material for Lithium-Ion Batteries," *New Journal of Chemistry* 41 (2017): 12190–12197.

107. X. Hou and S. Hu, "First Principles Studies on the Electronics Structures of $(Li_{1-x}Me_x)FePO_4$ (Me = Na and Be)," *Chinese Science Bulletin* 55 (2010): 3222–3227.

108. A. R. Madram, R. Daneshtalab, and M. R. Sovizi, "Effect of Na^+ and K^+ Co-Doping on the Structure and Electrochemical Behaviors of $LiFePO_4$/C Cathode Material for Lithium-Ion Batteries," *RSC Advances* 6 (2016): 101477–101484.

109. L. Li, X. Li, Z. Wang, L. Wu, J. Zheng, and H. Guo, "Stable Cycle-Life Properties of Ti-Doped $LiFePO_4$ Compounds Synthesized by Co-Precipitation and Normal Temperature Reduction Method," *Journal of Physics and Chemistry of Solids* 70 (2009): 238–242.

110. T. Kang, Y. Meng, and X. Liu, "Optimizing Lithium-Ion Diffusion in $LiFePO_4$: The Impact of Ti^{4+} Doping on High-Rate Capability and Electrochemical Stability," *Ionics* 31 (2025): 2419–2428.

111. Y. Xiao, Z. Zhao, Q. Zhang, and R. Qiao, "Doping $LiFePO_4$ With Al^{3+}: Suppression of Anti-Site Defects and Implications for Battery Recycling," *ACS Omega* 10 (2025): 1293–1302.

112. Y. Wang, Z. Feng, J. Chen, C. Zhang, X. Jin, and J. Hu, "First Principles Study on Electronic Properties and Occupancy Sites of Molybdenum Doped Into $LiFePO_4$," *Solid State Communications* 152 (2012): 1577–1580.

113. J. Geng, Z. Zou, T. Wang, et al., "Synthesis and Electrochemical Behavior of K^+ and Mn^{2+} Co-Doped $LiFePO_4$/C as a Cathode Material for Lithium-Ion Batteries and the Mechanism of Modification," *Journal of Electroanalytical Chemistry* 933 (2023): 117275.

114. L. Gao, Z. Xu, and S. Zhang, "The Co-Doping Effects of Zr and Co on Structure and Electrochemical Properties of $LiFePO_4$ Cathode Materials," *Journal of Alloys and Compounds* 739 (2018): 529–535.

115. Z. Cui, X. Guo, J. Ren, et al., "Enhanced Electrochemical Performance and Storage Mechanism of $LiFePO_4$ Doped by Co, Mn and S Elements for Lithium-Ion Batteries," *Electrochimica Acta* 388 (2021): 138592.

116. H. Wang, A. Lai, D. Huang, et al., "Y–F Co-Doping Behavior of $LiFePO_4$/C Nanocomposites for High-Rate Lithium-Ion Batteries," *New Journal of Chemistry* 45 (2021): 5695–5703.

117. J. Liu, Z. Bao, Y. Cui, et al., "Pathways for Practical High-Energy Long-Cycling Lithium Metal Batteries," *Nature Energy* 4 (2019): 180–186.

118. J. Molenda, A. Kulka, A. Milewska, W. Zając, and K. Świerczek, "Structural, Transport and Electrochemical Properties of $LiFePO_4$ Substituted in Lithium and Iron Sublattices (Al, Zr, W, Mn, Co and Ni)," *Materials* 6 (2013): 1656–1687.

119. A. Kulka, A. Braun, T.-W. Huang, et al., "Evidence for Al Doping in Lithium Sublattice of $LiFePO_4$," *Solid State Ionics* 270 (2015): 33–38.

120. H. Zhang, Z. Zou, S. Zhang, J. Liu, and S. Zhong, "A Review of the Doping Modification of $LiFePO_4$ as a Cathode Material for Lithium Ion Batteries," *International Journal of Electrochemical Science* 15 (2020): 12041–12067.

121. D. Zhang, J. Wang, K. Dong, and A. Hao, "First Principles Investigation on the Elastic and Electronic Properties of Mn, Co, Nb, Mo Doped $LiFePO_4$," *Computational Materials Science* 155 (2018): 410–415.

122. W. Yiming, G. Giuli, A. Moretti, et al., "Synthesis and Characterization of Zn-Doped $LiFePO_4$ Cathode Materials for Li-Ion Battery," *Materials Chemistry and Physics* 155 (2015): 191–204.

123. B. Lama, A. L. Smirnova, and T. R. Paudel, "Enhanced Li-Ion Diffusivity of $LiFePO_4$ by Ru Doping: *Ab Initio* and Machine Learning Force Field Results," *ACS Applied Energy Materials* 6 (2023): 10424–10431.

124. H. Gao, L. Jiao, J. Yang, Z. Qi, Y. Wang, and H. Yuan, "High Rate Capability of Co-Doped $LiFePO_4$/C," *Electrochimica Acta* 97 (2013): 143–149.

125. H. Lin, Y. Wen, C. Zhang, et al., "A GGA+ U Study of Lithium Diffusion in Vanadium Doped $LiFePO_4$," *Solid State Communications* 152 (2012): 999–1003.

126. M. Chen, L.-L. Shao, H.-B. Yang, T.-Z. Ren, G. Du, and Z.-Y. Yuan, "Vanadium-Doping of $LiFePO_4$/Carbon Composite Cathode Materials Synthesized With Organophosphorus Source," *Electrochimica Acta* 167 (2015): 278–286.

127. C. Latif, A. Firdausi, N. Nihlatunnur, et al., "Synchrotron Crystal and Local Structures, Microstructure, and Electrical Characterization of Cu-Doped $LiFePO_4$/C via Dissolution Method With Ironstone as Fe Source," *Journal of Materials Science: Materials in Electronics* 33 (2022): 17722–17732.

128. L. Wen, Z. Guan, L. Wang, et al., "Synthesis and Electrochemical Properties of Molybdenum-Doped $LiMn_{0.6}Fe_{0.4}PO_4$ Cathode Materials," *Journal of Materials Engineering and Performance* 33 (2024): 12884–12890.

129. H. Park, J. Choi, S. Yang, et al., "Surface-Modified Spherical Activated Carbon for High Carbon Loading and Its Desalting Performance in Flow-Electrode Capacitive Deionization," *RSC Advances* 6 (2016): 69720–69727.

130. Y. Liu, Y.-J. Gu, G.-Y. Luo, et al., "Ni-Doped $LiFePO_4$/C as High-Performance Cathode Composites for Li-Ion Batteries," *Ceramics International* 46 (2020): 14857–14863.

131. H. Yang, Z. Pan, L. Wang, et al., "Enhancing Electrochemical Performance of Mn Doped $LiFePO_4$ Cathode Materials for Lithium-Ion Batteries," *International Journal of Electrochemical Science* 18 (2023): 100079.

132. X. Ren, Y. Li, Z. He, et al., "Preparation of $LiFe_{0.99}Mn_{0.01}PO_4$ Cathode Material With Lower Fe-Li Antisite via Wet-Lithiation Following by Tavorite-Olivine Phase Transition," *Journal of the Electrochemical Society* 170 (2023): 100526.

133. Y. Mi, C. Yang, Z. Zuo, et al., "Positive Effect of Minor Manganese Doping on the Electrochemical Performance of $LiFePO_4$/C Under Extreme Conditions," *Electrochimica Acta* 176 (2015): 642–648.

134. R. Gupta, S. Saha, M. Tomar, V. Sachdev, and V. Gupta, "Effect of Manganese Doping on Conduction in Olivine $LiFePO_4$," *Journal of Materials Science: Materials in Electronics* 28 (2017): 5192–5199.

135. Y. Lin, Y. Lin, B. Zeng, et al., "An Optimized Mn-Doped $LiFePO_4$/C Composite Synthesized by Carbonthermal Reduction Technique," *International Journal of Electrochemical Science* 6 (2011): 6653–6661.

136. H. Yang, X.-L. Wu, M.-H. Cao, and Y.-G. Guo, "Solvothermal Synthesis of $LiFePO_4$ Hierarchically Dumbbell-Like Microstructures by Nanoplate Self-Assembly and Their Application as a Cathode Material in Lithium-Ion Batteries," *Journal of Physical Chemistry C* 113 (2009): 3345–3351.

137. Y. Li, C. Hu, Z. Hou, C. Wei, and J.-G. Wang, "Green Phytic Acid-Assisted Synthesis of $LiMn_{1-x}Fe_xPO_4$/C Cathodes for High-Performance Lithium-Ion Batteries," *Nanomaterials* 14 (2024): 1360.

138. H. Yu, E. Zhang, J. Yu, et al., "Relaxing the Jahn–Teller Distortion of $LiMn_{0.6}Fe_{0.4}PO_4$ Cathodes via Mg/Ni Dual-Doping for High-Rate and Long-Life Li-Ion Batteries," *Journal of Materials Chemistry A* 12 (2024): 26076–26082.

139. L. Dai, Y. Wang, L. Sun, et al., "Jahn–Teller Distortion Induced Mn^{2+}-Rich Cathode Enables Optimal Flexible Aqueous High-Voltage Zn-Mn Batteries," *Advanced Science* 8 (2021): 2004995.

140. P. Vanaphuti and A. Manthiram, "Enhancing the Mn Redox Kinetics of $LiMn_{0.5}Fe_{0.5}PO_4$ Cathodes Through a Synergistic Co-Doping With Niobium and Magnesium for Lithium-Ion Batteries," *Small* 20 (2024): 2404878.

141. J. Ma, C. Li, Q. Ji, et al., "V-Induced Low-Spin State Mn^{3+} Suppresses Jahn–Teller Distortion for High-Performance Aqueous Zinc Ion Batteries," *Angewandte Chemie International Edition* 64 (2025): e202513148.

142. N. Zhao, Y. Li, X. Zhi, et al., "Effect of Ce^{3+} Doping on the Properties of $LiFePO_4$ Cathode Material," *Journal of Rare Earths* 34 (2016): 174–180.

143. D. G. Tong, F. L. Luo, W. Chu, Y. L. Li, and P. Wu, "Effect of Rhodium Substitution on the Electrochemical Performance of $LiFePO_4$/C," *Materials Chemistry and Physics* 124 (2010): 1–5.

144. X. Meng, B. Han, Y. Wang, and J. Nan, "Effects of Samarium Doping on the Electrochemical Performance of $LiFePO_4$/C Cathode Material for Lithium-Ion Batteries," *Ceramics International* 42 (2016): 2599–2604.

145. H. Yuan, X. Wang, Q. Wu, H. Shu, and X. Yang, "Effects of Ni and Mn Doping on Physicochemical and Electrochemical Performances of $LiFePO_4$/C," *Journal of Alloys and Compounds* 675 (2016): 187–194.

146. Y.-F. Long, J. Su, X.-R. Cui, X.-Y. Lv, and Y.-X. Wen, "Enhanced Rate Performance of $LiFePO_4$/C by Co-Doping Titanium and Vanadium," *Solid State Sciences* 48 (2015): 104–111.

147. Z. Wang, X. Kong, Z. Fan, S. Ding, Q. Rong, and Y. Su, "A First-Principles Study of Anion Doping in $LiFePO_4$ Cathode Materials for Li-Ion Batteries," *Chemphyschem* 25 (2024): e202300756.

148. C. S. Sun, Y. Zhang, X. J. Zhang, and Z. Zhou, "Structural and Electrochemical Properties of Cl-Doped $LiFePO_4$/C," *Journal of Power Sources* 195 (2010): 3680–3683.

149. G. Xu, K. Zhong, J.-M. Zhang, and Z. Huang, "First-Principles Study of Structural, Electronic and Li-Ion Diffusion Properties of N-Doped $LiFePO_4$ (010) Surface," *Solid State Ionics* 281 (2015): 1–5.

150. J.-W. Zhao, S.-X. Zhao, X. Wu, H.-M. Cheng, and C.-W. Nan, "Double Role of Silicon in Improving the Rate Performance of $LiFePO_4$ Cathode Materials," *Journal of Alloys and Compounds* 699 (2017): 849–855.

151. C. Gao, J. Zhou, G. Liu, and L. Wang, "Synthesis of F-Doped $LiFePO_4$/C Cathode Materials for High Performance Lithium-Ion Batteries Using Co-Precipitation Method With Hydrofluoric Acid Source," *Journal of Alloys and Compounds* 727 (2017): 501–513.

152. J. Wang, M. Wang, Y. Liang, et al., "Effects of S Doping and S/N Co-Doping on Electronic Structure and Iondiffusion of $LiFePO_4$," *Chemical Physics* 563 (2022): 111687.

153. L. Wang, R. Wei, H. Zhang, et al., "B-Mg Co-Doping Behavior of $LiFePO_4$ Cathode Material: Balance of Oxygen Vacancy and Enhancement of Electrochemical Performance," *Ionics* 28 (2022): 593–600.

154. C. Ban, W.-J. Yin, H. Tang, S.-H. Wei, Y. Yan, and A. C. Dillon, "A Novel Codoping Approach for Enhancing the Performance of $LiFePO_4$ Cathodes," *Advanced Energy Materials* 2 (2012): 1028–1032.

155. H. Liu, S. Luo, S. Yan, et al., "A Novel and Low-Cost Iron Source for Synthesizing Cl-Doped $LiFePO_4$/C Cathode Materials for Lithium-Ion Batteries," *Journal of Electroanalytical Chemistry* 850 (2019): 113434.

156. X. Yang, Z. Hu, and J. Liang, "Effects of Sodium and Vanadium Co-Doping on the Structure and Electrochemical Performance of $LiFePO_4$/C Cathode Material for Lithium-Ion Batteries," *Ceramics International* 41 (2015): 2863–2868.

157. Z. Tian, Z. Zhou, S. Liu, F. Ye, and S. Yao, "Enhanced Properties of Olivine $LiFePO_4$/Graphene Co-Doped With Nb^{5+} and Ti^{4+} by a Sol–Gel Method," *Solid State Ionics* 278 (2015): 186–191.

158. Z. Ji, Y. Sun, X. Guan, Y. Zhou, J. Qian, and F. Chen, "Revealing the Superior Rate Performance and Cycle Stability of the La and F Co-Doping $LiFePO_4$/C," *Vacuum* 227 (2024): 113452.

159. Y. Lv, B. Huang, J. Tan, S. Jiang, S. Zhang, and Y. Wen, "Enhanced Low Temperature Electrochemical Performances of $LiFePO_4$/C by V^{3+} and F^- Co-Doping," *Materials Letters* 229 (2018): 349–352.

160. Y. Liu, W. Qin, D. Zhang, L. Feng, and L. Wu, "Effect of Na^+ In Situ Doping on $LiFePO_4$/C Cathode Material for Lithium-Ion Batteries," *Progress in Natural Science: Materials International* 31 (2021): 14–18.

161. Y.-C. Chang, C.-T. Peng, and I. M. Hung, "Synthesis and Electrochemical Properties of $LiFe_{0.95}V_xNi_{0.05-x}PO_4$/C Cathode Material for Lithium-Ion Battery," *Ceramics International* 41 (2015): 5370–5379.

162. J. Tu, K. Wu, H. Tang, H. Zhou, and S. Jiao, "Mg–Ti Co-Doping Behavior of Porous $LiFePO_4$ Microspheres for High-Rate Lithium-Ion Batteries," *Journal of Materials Chemistry A* 5 (2017): 17021–17028.

163. T. Teng, L. Xiao, L. Shen, et al., "Effect of Nb Doping at Fe Site on the Cycling Stability and Rate Capability of $LiFePO_4$ for Lithium-Ion Batteries," *Vacuum* 203 (2022): 111306.

164. F. Zhang, J. Huang, F. Zong, et al., "Effect of Ti Content on Preparation of $LiFePO_4$ Cathode From $FeSO_4{\cdot}7H_2O$ Waste Residue," *Journal of Alloys and Compounds* 955 (2023): 170270.

165. S. Yaroslavtsev, S. Novikova, V. Rusakov, et al., "$LiFe_{1-x}Mg_xPO_4$/C as Cathode Materials for Lithium-Ion Batteries," *Solid State Ionics* 317 (2018): 149–155.

166. B. Zhang, S. Wang, L. Liu, J. Wang, W. Liu, and J. Yang, "Facile Synthesis of S-Doped $LiFePO_4$@N/S-Doped Carbon Core–Shell Structured Composites for Lithium-Ion Batteries," *Nanotechnology* 33 (2022): 405601.

167. A. V. Radhamani, "Magnetic Phase Investigations on Fluorine (F) Doped $LiFePO_4$," *Materials Research Express* 5 (2018): 035509.

168. Q. Zhang, J. Zhou, G. Zeng, and S. Ren, "Effect of Lanthanum and Yttrium Doped $LiFePO_4$ Cathodes on Electrochemical Performance of Lithium-Ion Battery," *Journal of Materials Science* 58 (2023): 8463–8477.

169. Y. Gao, K. Xiong, H. Zhang, and B. Zhu, "Effect of Ru Doping on the Properties of $LiFePO_4$/C Cathode Materials for Lithium-Ion Batteries," *ACS Omega* 6 (2021): 14122–14129.

170. B. Zhang, X. Ma, W. Hou, et al., "Revealing the Ultrahigh Rate Performance of the La and Ce Co-Doping $LiFePO_4$ Composite," *ACS Applied Energy Materials* 5 (2022): 14712–14719.

171. G. Zhou, P. Wang, Z. Li, Y. Li, and Y. Yao, "Revealing Electrochemical Performance of Ni Doping $LiFePO_4$ Composite," *Bulletin of Materials Science* 47 (2024): 251.

172. Q. Zhang, Y. Zhou, Y. Tong, et al., "Reduced Graphene Oxide Coating $LiFePO_4$ Composite Cathodes for Advanced Lithium-Ion Battery Applications," *International Journal of Molecular Sciences* 24 (2023): 17549.

173. X. Li, Z. Shao, K. Liu, Q. Zhao, G. Liu, and B. Xu, "Enhancement of Nb-Doping on the Properties of $LiFePO_4$/C Prepared via a High-Temperature Ball Milling–Based Method," *Journal of Solid State Electrochemistry* 23 (2019): 465–473.

174. Y. Liu, Y.-J. Gu, J.-L. Deng, et al., "Effect of Doped Mn on Improving the Electrochemical Performance of $LiFePO_4$," *Journal of Materials Science: Materials in Electronics* 31 (2020): 2887–2894.

175. X. Jiang, Y. Xin, B. He, F. Zhang, and H. Tian, "Effect of Heteroatom Doping on Electrochemical Properties of Olivine $LiFePO_4$ Cathodes for High-Performance Lithium-Ion Batteries," *Materials* 17 (2024): 1299.

176. M. Yang, Z. Rong, X. Li, B. Yuan, and W. Zhang, "Zwitterionic Polymer as Binder for $LiFePO_4$ Cathodes in Lithium-Ion Batteries," *Chemical Engineering Journal* 505 (2025): 159332.

177. L. He, J. Peng, X. Liu, et al., "The Reduced Graphene Oxide Conductive Additives With a Certain Defect Concentration Enabling Rate-Capability of Lithium-Ion Batteries," *Electrochimica Acta* 511 (2025): 145353.

178. R. Zhu, G. Liu, G. Qu, et al., "Enhancing Volumetric Energy Density of $LiFePO_4$ Battery Using Liquid Metal as Conductive Agent," *Advanced Functional Materials* 34 (2024): 2409230.

179. Y. Liu, C. Qi, D. Cai, et al., "TaC-Modified $LiFePO_4$/C Composite as Cathode Material for High-Performance Lithium-Ion Batteries," *Ionics* 29 (2023): 2191–2198.

180. A. Amri, Y. B. Hendri, Y. B. Sunarno, et al., "Novel $LiFePO_4$/Very-few-Layer-Graphene (LFP/VFLG) Composites to Improve Structural and Electrochemical Properties of Lithium-Ion Battery Cathode," *Ceramics International* 50 (2024): 19806–19813.

181. J. Liu, X. Hu, F. Ran, K. Wang, J. Dai, and X. Zhu, "Electrospinning-Assisted Construction of 3D $LiFePO_4$@rGO/Carbon Nanofibers as Flexible Cathode to Boost the Rate Capabilities of Lithium-Ion Batteries," *Ceramics International* 49 (2023): 1401–1408.

182. D. Y. Semerukhin, A. V. Kubarkov, E. V. Antipov, and V. G. Sergeyev, "Carbon Nanotubes and Carbon-Coated Current Collector Significantly Improve the Performance of Lithium-Ion Battery With PEDOT: PSS Binder," *Mendeleev Communications* 33 (2023): 206–208.

183. J. P. Zhou, J. P. Tu, L. J. Cheng, et al., "$LiFePO_4$/Polyacene Nanocomposite Synthesized From a Pretreatment of Iron Phosphate: In-Situ Polymerization With Phenolic-Formaldehyde Resin," *Journal of the Electrochemical Society* 158 (2011): A1237.

184. I. Mahmud, D.-S. Kim, and S.-C. Ur, "Electrochemical Performance of NiO-Doped $LiFePO_4$/C Cathode Materials Prepared From Amorphous $FePO_4{\cdot}xH_2O$," *Journal of the Korean Physical Society* 68 (2016): 1211–1214.

185. B. León, C. P. Vicente, J. Tirado, P. Biensan, and C. Tessier, "Optimized Chemical Stability and Electrochemical Performance of $LiFePO_4$ Composite Materials Obtained by ZnO Coating," *Journal of the Electrochemical Society* 155 (2008): A211.

186. Y. Hu, J. Yao, Z. Zhao, et al., "ZnO-Doped $LiFePO_4$ Cathode Material for Lithium-Ion Battery Fabricated by Hydrothermal Method," *Materials Chemistry and Physics* 141 (2013): 835–841.

187. F. Croce, A. d'Epifanio, J. Hassoun, A. Deptula, T. Olczac, and B. Scrosati, "A Novel Concept for the Synthesis of an Improved $LiFePO_4$ Lithium Battery Cathode," *Electrochemical and Solid-State Letters* 5 (2002): A47.

188. X. Cheng, J. Kim, M. Li, and J. Bae, "DNA-Directed Fabrication of $LiFePO_4$ Micro-Roses as High-Performance Electrodes for Lithium-Ion Batteries," *Nano Energy* 134 (2025): 110577.

189. A. Belgibayeva, A. Rakhmetova, M. Rakhatkyzy, et al., "Lithium-Ion Batteries for Low-Temperature Applications: Limiting Factors and Solutions," *Journal of Power Sources* 557 (2023): 232550.

190. F. Wang, J. Chen, Z. Tan, et al., "Low-Temperature Electrochemical Performances of $LiFePO_4$ Cathode Materials for Lithium Ion Batteries," *Journal of the Taiwan Institute of Chemical Engineers* 45 (2014): 1321–1330.

191. A. Gupta and A. Manthiram, "Designing Advanced Lithium-Based Batteries for Low-Temperature Conditions," *Advanced Energy Materials* 10 (2020): 2001972.

192. A. S. Alhammadi, H. J. Yun, and D. Choi, "Investigation of $LiFePO_4$/MWCNT Cathode-Based Half-Cell Lithium-Ion Batteries in Subzero Temperature Environments," *Ionics* 29 (2023): 2163–2174.

193. J. Liu, K. Liang, J. He, et al., "Functionalized Porous Conductive Carbon Layer Improves the Low-Temperature Performance of $LiFePO_4$ Cathode Material for Lithium-Ion Batteries," *Carbon* 229 (2024): 119483.

194. Y. Gao, K. Xiong, H. Xu, and B. Zhu, "Enhanced High-Rate and Low-Temperature Electrochemical Properties of $LiFePO_4$/Polypyrrole Cathode Materials for Lithium-Ion Batteries," *International Journal of Electrochemical Science* 14 (2019): 3408–3417.

195. L. Zeng, Q. Gong, X. Liao, L. He, Y. He, and Z. Ma, "Enhanced Low-Temperature Performance of Slight Mn-Substituted $LiFePO_4$/C Cathode for Lithium Ion Batteries," *Chinese Science Bulletin* 56 (2011): 1262–1266.

196. H. Zhang, Y. Xu, C. Zhao, X. Yang, and Q. Jiang, "Effects of Carbon Coating and Metal Ions Doping on Low Temperature Electrochemical Properties of $LiFePO_4$ Cathode Material," *Electrochimica Acta* 83 (2012): 341–347.

197. X.-X. Gu, S. Qiao, X.-L. Ren, et al., "Multi-Core–Shell-Structured $LiFePO_4$@$Na_3V_2(PO_4)_3$@C Composite for Enhanced Low-Temperature Performance of Lithium-Ion Batteries," *Rare Metals* 40 (2021): 828–836.

198. X. Cui, K. Tuo, Y. Xie, et al., "Investigation on Electrochemical Performance at the Low Temperature of LFP/CP Composite Based on Phosphorus Doping Carbon Network," *Ionics* 26 (2020): 3795–3808.

199. Y. Yin, X. Li, X. Mao, X. Ding, and S. Yang, "Solid State Reaction Preparation of $LiFePO_4$/(C+Cu) Cathode Material and Its Electrochemical Performance," *Journal of Materials Science & Technology* 29 (2013): 937–942.

200. G. Cai, R. Guo, L. Liu, et al., "Enhanced Low Temperature Electrochemical Performances of $LiFePO_4$/C by Surface Modification With Ti_3SiC_2," *Journal of Power Sources* 288 (2015): 136–144.

201. Z. Li, X. Ren, Y. Zheng, et al., "Effect of Ti Doping on $LiFePO_4$/C Cathode Material With Enhanced Low-Temperature Electrochemical Performance," *Ionics* 26 (2020): 1599–1609.

202. Y. Peng, L. Zeng, S. Dai, F. Liu, X. Rao, and Y. Zhang, "$LiFePO_4$/C Twin Microspheres as Cathode Materials With Enhanced Electrochemical Performance," *RSC Advances* 13 (2023): 6983–6992.

203. J. Xue, Z. Zhang, H. Guo, et al., "Primary Particles With Ultra-Thin Carbon Layer Combined With Loose Secondary Particles to Jointly Promote the Low-Temperature Performance of $LiFePO_4$," *Ionics* 28 (2022): 4229–4237.

204. G. Wu, N. Liu, X. Gao, et al., "A Hydrothermally Synthesized $LiFePO_4$/C Composite With Superior Low-Temperature Performance and Cycle Life," *Applied Surface Science* 435 (2018): 1329–1336.

205. Y. Zhou, C. D. Gu, J. P. Zhou, et al., "Effect of Carbon Coating on Low Temperature Electrochemical Performance of $LiFePO_4$/C by Using Polystyrene Sphere as Carbon Source," *Electrochimica Acta* 56 (2011): 5054–5059.

206. S. Li, X. Liu, G. Liu, Y. Wan, and H. Liu, "Highly Enhanced Low-Temperature Performances of $LiFePO_4$/C Cathode Materials Prepared by Polyol Route for Lithium-Ion Batteries," *Ionics* 23 (2017): 19–26.

207. S. Li, X. Liu, R. Mi, et al., "A Facile Route to Modify Ferrous Phosphate and Its Use as an Iron-Containing Resource for $LiFePO_4$ via a Polyol Process," *ACS Applied Materials & Interfaces* 6 (2014): 9449–9457.

208. A. Lai, Y. Chu, J. Jiang, et al., "Self-Restriction to Form In-Situ N, P Co-Doped Carbon-Coated $LiFePO_4$ Nanocomposites for High-Performance Lithium Ion Batteries," *Electrochimica Acta* 414 (2022): 140161.

209. H. Tang, L. Tan, and J. Xu, "Synthesis and Characterization of $LiFePO_4$ Coating With Aluminum Doped Zinc Oxide," *Transactions of Nonferrous Metals Society of China* 23 (2013): 451–455.

210. S. Liu, H. Yin, H. Wang, and J. He, "Electrochemical Performance of WO_2 Modified $LiFePO_4$/C Cathode Material for Lithium-Ion Batteries," *Journal of Alloys and Compounds* 561 (2013): 129–134.

211. J. Yao, F. Wu, X. Qiu, N. Li, and Y. Su, "Effect of CeO_2-Coating on the Electrochemical Performances of $LiFePO_4$/C Cathode Material," *Electrochimica Acta* 56 (2011): 5587–5592.

212. L. Chen, C. Lu, S. Yin, et al., "Effect of Nb^{5+} Doping on the Structure and Electrochemical Performances of $LiFePO_4$," *IOP Conference Series: Materials Science and Engineering* (IOP Publishing, 2019), 012045.

213. J. Liu, Z. Wang, G. Zhang, Y. Liu, and A. Yu, "Size-Controlled Synthesis of $LiFePO_4$/C Composites as Cathode Materials for Lithium Ion Batteries," *International Journal of Electrochemical Science* 8 (2013): 2378–2387.

214. X. Huang, K. Zhang, F. Liang, Y. Dai, and Y. Yao, "Optimized Solvothermal Synthesis of $LiFePO_4$ Cathode Material for Enhanced High-Rate and Low Temperature Electrochemical Performances," *Electrochimica Acta* 258 (2017): 1149–1159.

215. J. Fan, J. Chen, Y. Chen, et al., "Hierarchical Structure $LiFePO_4$@C Synthesized by Oleylamine-Mediated Method for Low Temperature Applications," *Journal of Materials Chemistry A: Materials for Energy and Sustainability* 2 (2014): 4870–4873.

216. Q. Fan, Y. Zhang, Q. Xu, et al., "Coral-Shaped Porous $LiFePO_4$/Graphene Hybrids for High Rate and All-Climate Battery Applications," *Energy Storage Materials* 21 (2019): 457–463.

217. Y. Qiao, Y. Liu, J. Zhu, et al., "Surfactant-Assisted Synthesis of Micro/Nano-Structured $LiFePO_4$ Electrode Materials With Improved Electrochemical Performance," *Materials* 15 (2022): 8953.

218. D. Xie, G. Cai, Z. Liu, et al., "The Low Temperature Electrochemical Performances of $LiFePO_4$/C/Graphene Nanofiber With 3D-bridge Network Structure," *Electrochimica Acta* 217 (2016): 62–72.

219. L. Zhang, Z. Zhang, Y. Song, et al., "In Situ Confined Synthesis of $LiFePO_4$/Ti_3C_2@C Composites With High-Rate and Low-Temperature Long Cycling Performance," *Ionics* 29 (2023): 33–41.

220. X. Ren, J. Guo, R. Liu, H. Guo, and G. Liang, "Are Fe-Li Antisite Defects Necessarily Detrimental to the Diffusion of Li^+ in $LiFePO_4$/C?," *Journal of the Electrochemical Society* 169 (2022): 120507.

221. C. Hou, Y. Ma, H. Zhang, W. Geng, and Q. Zhang, "Magnetic Activation of a $LiFePO_4$@ C Composite Cathode Material," *International Journal of Electrochemical Science* 12 (2017): 3221–3230.

222. R. Fong, U. Von Sacken, and J. R. Dahn, "Studies of Lithium Intercalation Into Carbons Using Nonaqueous Electrochemical Cells," *Journal of the Electrochemical Society* 137 (1990): 2009–2013.

223. Z. M. S. Elbarbary, P. A. Hoskeri, A. A. Javidparvar, M. M. Alammar, A. Rajakannu, and T. A. Manfo, "Machine Learning Approach to the Possible Synergy Between Co-Doped Elements in the Case of $LiFePO_4$/C," *Journal of Alloys and Compounds* 1034 (2025): 181316.

224. S.-Y. Li, C.-W. Wu, L.-T. Liu, et al., "Machine Learning-Assisted Investigation of the Impact of Lithium-Ion De-Embedding on the Thermal Conductivity of $LiFePO_4$," *Applied Physics Letters* 122 (2023): 262201.

225. G. Xie, S.-Y. Li, Q. Liu, Y.-J. Zeng, and W. Zhou, "Influence of Na-Substitution on Thermal Conductivity of Cathode Material $LiFePO_4$: A Machine Learning Interatomic Potential-Assisted Investigation," available at SSRN 4906176.

226. X.-Y. Lv, X.-R. Cui, Y.-F. Long, J. Su, and Y.-X. Wen, "Optimization of Titanium and Vanadium Co-Doping in $LiFePO_4$/C Using Response Surface Methodology," *Ionics* 21 (2015): 2447–2455.

227. B. Wu, S. Han, K. G. Shin, and W. Lu, "Application of Artificial Neural Networks in Design of Lithium-Ion Batteries," *Journal of Power Sources* 395 (2018): 128–136.

228. Z. J. Baum, R. E. Bird, X. Yu, and J. Ma, "Lithium-Ion Battery Recycling—Overview of Techniques and Trends," *ACS Publications* 7 (2022): 712–719.

229. W. Lv, Z. Wang, H. Cao, Y. Sun, Y. Zhang, and Z. Sun, "A Critical Review and Analysis on the Recycling of Spent Lithium-Ion Batteries," *ACS Sustainable Chemistry & Engineering* 6 (2018): 1504–1521.

230. G. Zhang, M. Shi, X. Hu, H. Yang, and X. Yan, "Comparison of Life Cycle Assessment of Different Recycling Methods for Decommissioned Lithium Iron Phosphate Batteries," *Sustainable Energy Technologies and Assessments* 68 (2024): 103871.

231. S. Li, Z. Wu, M. Zhang, et al., "Direct Recycling of Cathode Materials From Spent Lithium-Ion Batteries: Principles, Strategies, and Perspectives," *Chemistry—A European Journal* 31 (2025): e202404461.

232. J. Xiao, J. Li, and Z. Xu, "Challenges to Future Development of Spent Lithium Ion Batteries Recovery From Environmental and Technological Perspectives," *Environmental Science & Technology* 54 (2020): 9–25.

233. J. Li, G. Wang, and Z. Xu, "Generation and Detection of Metal Ions and Volatile Organic Compounds (VOCs) Emissions From the Pretreatment Processes for Recycling Spent Lithium-Ion Batteries," *Waste Management* 52 (2016): 221–227.

234. H. Bi, H. Zhu, L. Zu, S. He, Y. Gao, and J. Peng, "Combined Mechanical Process Recycling Technology for Recovering Copper and Aluminium Components of Spent Lithium-Iron Phosphate Batteries," *Waste Management & Research: The Journal of the International Solid Wastes and Public Cleansing Association, ISWA* 37 (2019): 767–780.

235. X. Zhu, C. Zhang, P. Feng, X. Yang, and X. Yang, "A Novel Pulsated Pneumatic Separation With Variable-Diameter Structure and Its Application in the Recycling Spent Lithium-Ion Batteries," *Waste Management* 131 (2021): 20–30.

236. S. M. Shin, N. H. Kim, J. S. Sohn, D. H. Yang, and Y. H. Kim, "Development of a Metal Recovery Process From Li-Ion Battery Wastes," *Hydrometallurgy* 79 (2005): 172–181.

237. G. Zhang, Y. He, H. Wang, Y. Feng, W. Xie, and X. Zhu, "Removal of Organics by Pyrolysis for Enhancing Liberation and Flotation Behavior of Electrode Materials Derived From Spent Lithium-Ion Batteries," *ACS Sustainable Chemistry & Engineering* 8 (2020): 2205–2214.

238. W. Liu, X. Zhong, J. Han, et al., "Kinetic Study and Pyrolysis Behaviors of Spent $LiFePO_4$ Batteries," *ACS Sustainable Chemistry & Engineering* 7 (2018): 1289–1299.

239. L. Li, J. Lu, L. Zhai, et al., "A Facile Recovery Process for Cathodes From Spent Lithium Iron Phosphate Batteries by Using Oxalic Acid," *CSEE Journal of Power and Energy Systems* 4 (2018): 219–225.

240. W. Wang and Y. Wu, "An Overview of Recycling and Treatment of Spent $LiFePO_4$ Batteries in China," *Resources, Conservation And Recycling* 127 (2017): 233–243.

241. L. Li, J. Lu, Y. Ren, et al., "Ascorbic-Acid-Assisted Recovery of Cobalt and Lithium From Spent Li-Ion Batteries," *Journal of Power Sources* 218 (2012): 21–27.

242. J. Kumar, R. R. Neiber, J. Park, et al., "Recent Progress in Sustainable Recycling of $LiFePO_4$-type Lithium-Ion Batteries: Strategies for Highly Selective Lithium Recovery," *Chemical Engineering Journal* 431 (2022): 133993.

243. H. Li, S. Xing, Y. Liu, F. Li, H. Guo, and G. Kuang, "Recovery of Lithium, Iron, and Phosphorus From Spent $LiFePO_4$ Batteries Using Stoichiometric Sulfuric Acid Leaching System," *ACS Sustainable Chemistry & Engineering* 5 (2017): 8017–8024.

244. Y. Dai, Z. Xu, D. Hua, H. Gu, and N. Wang, "Theoretical-Molar Fe^{3+} Recovering Lithium From Spent $LiFePO_4$ Batteries: An Acid-Free, Efficient, and Selective Process," *Journal of Hazardous Materials* 396 (2020): 122707.

245. H. Jin, J. Zhang, D. Wang, Q. Jing, Y. Chen, and C. Wang, "Facile and Efficient Recovery of Lithium From Spent $LiFePO_4$ Batteries via Air Oxidation–Water Leaching at Room Temperature," *Green Chemistry* 24 (2022): 152–162.

246. J. Zhang, J. Hu, Y. Liu, et al., "Sustainable and Facile Method for the Selective Recovery of Lithium From Cathode Scrap of Spent $LiFePO_4$ Batteries," *ACS Sustainable Chemistry & Engineering* 7 (2019): 5626–5631.

247. K. He, Z.-Y. Zhang, and F.-S. Zhang, "A Green Process for Phosphorus Recovery From Spent $LiFePO_4$ Batteries by Transformation of Delithiated $LiFePO_4$ Crystal Into $NaFeS_2$," *Journal of Hazardous Materials* 395 (2020): 122614.

248. L. Wu, F.-S. Zhang, Z.-Y. Zhang, and C.-C. Zhang, "An Environmentally Friendly Process for Selective Recovery of Lithium and Simultaneous Synthesis of $LiFe5O_8$ From Spent $LiFePO_4$ Battery by Mechanochemical," *Journal of Cleaner Production* 396 (2023): 136504.

249. K. Liu, Q. Tan, L. Liu, and J. Li, "Acid-Free and Selective Extraction of Lithium From Spent Lithium Iron Phosphate Batteries via a Mechanochemically Induced Isomorphic Substitution," *Environmental Science & Technology* 53 (2019): 9781–9788.

250. Z. Li, D. Liu, J. Xiong, L. He, Z. Zhao, and D. Wang, "Selective Recovery of Lithium and Iron Phosphate/Carbon From Spent Lithium Iron Phosphate Cathode Material by Anionic Membrane Slurry Electrolysis," *Waste Management* 107 (2020): 1–8.

251. K. Liu, S. Yang, F. Lai, et al., "Application of $H_4P_2O_7$ as Leaching Acid in One-Step Selective Recovery for Metals From Spent $LiFePO_4$ Batteries," *Ionics* 27 (2021): 5127–5135.

252. C. Yang, J. Zhang, Q. Jing, Y. Liu, Y. Chen, and C. Wang, "Recovery and Regeneration of $LiFePO_4$ From Spent Lithium-Ion Batteries via a Novel Pretreatment Process," *International Journal of Minerals, Metallurgy, and Materials* 28 (2021): 1478–1487.

253. Y. Yang, X. Zheng, H. Cao, et al., "A Closed-Loop Process for Selective Metal Recovery From Spent Lithium Iron Phosphate Batteries Through Mechanochemical Activation," *ACS Sustainable Chemistry & Engineering* 5 (2017): 9972–9980.

254. X. Lv, J. Lin, X. Sun, et al., "Direct Recycling of Spent $LiFePO_4$ Cathodes Through Photocatalytic Correction of Anti-Site Defects," *Advanced Materials* 37 (2025): 2503398.

255. D. Tang, G. Ji, J. Wang, et al., "A Multifunctional Amino Acid Enables Direct Recycling of Spent $LiFePO_4$ Cathode Material," *Advanced Materials* 36 (2024): 2309722.

256. J. Kumar, X. Shen, B. Li, H. Liu, and J. Zhao, "Selective Recovery of Li and $FePO_4$ From Spent $LiFePO_4$ Cathode Scraps by Organic Acids and the Properties of the Regenerated $LiFePO_4$," *Waste Management* 113 (2020): 32–40.

257. Y. Yang, X. Meng, H. Cao, et al., "Selective Recovery of Lithium From Spent Lithium Iron Phosphate Batteries: A Sustainable Process," *Green Chemistry* 20 (2018): 3121–3133.

258. H. Mahandra and A. Ghahreman, "A Sustainable Process for Selective Recovery of Lithium as Lithium Phosphate From Spent $LiFePO_4$ Batteries," *Resources, Conservation and Recycling* 175 (2021): 105883.

259. P. Yadav, C. J. Jie, S. Tan, and M. Srinivasan, "Recycling of Cathode From Spent Lithium Iron Phosphate Batteries," *Journal of Hazardous Materials* 399 (2020): 123068.

260. B. Li, C. Li, Y. Gao, et al., "Influence of Heat Treatment on Corrosion–Wear Behavior of Ni-Based Coating in Artificial Seawater," *Journal of Materials Engineering and Performance* 28 (2019): 7828–7834.

261. Z. Lai, J. Long, Y. Lu, et al., "Direct Recycling of Retired Lithium-Ion Batteries: Emerging Methods for Sustainable Reuse," *Advanced Energy Materials* 15 (2025): 2501009.

262. G. Ji, J. Wang, Z. Liang, et al., "Direct Regeneration of Degraded Lithium-Ion Battery Cathodes With a Multifunctional Organic Lithium Salt," *Nature Communications* 14 (2023): 584.

263. X. Qiu, C. Wang, L. Xie, L. Zhu, X. Cao, and X. Ji, "Challenges and Perspectives Towards Direct Regeneration of Spent $LiFePO_4$ Cathode," *Journal of Power Sources* 602 (2024): 234365.

264. J. Chen, Q. Li, J. Song, D. Song, L. Zhang, and X. Shi, "Environmentally Friendly Recycling and Effective Repairing of Cathode Powders From Spent $LiFePO_4$ Batteries," *Green Chemistry* 18 (2016): 2500–2506.

265. L. Wang, J. Li, H. Zhou, et al., "Regeneration Cathode Material Mixture From Spent Lithium Iron Phosphate Batteries," *Journal of Materials Science: Materials in Electronics* 29 (2018): 9283–9290.

266. C. Li, R. Gong, Y. Zhang, Q. Meng, and P. Dong, "Direct Regeneration of Degraded $LiFePO_4$ Cathode via Reductive Solution Relithiation Regeneration Process," *Molecules* 29 (2024): 3340.

267. Q. Jing, J. Zhang, Y. Liu, W. Zhang, Y. Chen, and C. Wang, "Direct Regeneration of Spent $LiFePO_4$ Cathode Material by a Green and Efficient One-Step Hydrothermal Method," *ACS Sustainable Chemistry & Engineering* 8 (2020): 17622–17628.

268. P. Xu, Q. Dai, H. Gao, et al., "Efficient Direct Recycling of Lithium-Ion Battery Cathodes by Targeted Healing," *Joule* 4 (2020): 2609–2626.

269. X. Li, J. Zhang, D. Song, J. Song, and L. Zhang, "Direct Regeneration of Recycled Cathode Material Mixture From Scrapped $LiFePO_4$ Batteries," *Journal of Power Sources* 345 (2017): 78–84.

270. F. Pei, Y. Wu, W. H. Zhang, X. Tian, and J. Yu, "Preparing $LiFePO_4$ Using Recovered Materials From Waste Li-Ion Battery," *Advanced Materials Research* 726–731 (2013): 2940–2944.

271. Q. Liang, H. Yue, S. Wang, S. Yang, K. Lam, and X. Hou, "Recycling and Crystal Regeneration of Commercial Used $LiFePO_4$ Cathode Materials," *Electrochimica Acta* 330 (2020): 135323.

272. K. Jia, J. Ma, J. Wang, et al., "Long-Life Regenerated $LiFePO_4$ From Spent Cathode by Elevating the d-Band Center of Fe," *Advanced Materials* 35 (2023): 2208034.

273. L. Song, C. Qi, S. Wang, et al., "Direct Regeneration of Waste $LiFePO_4$ Cathode Materials With a Solid-Phase Method Promoted by Activated CNTs," *Waste Management* 157 (2023): 141–148.

274. Q. Sun, X. Li, H. Zhang, et al., "Resynthesizing $LiFePO_4$/C Materials From the Recycled Cathode via a Green Full-Solid Route," *Journal of Alloys and Compounds* 818 (2020): 153292.

275. L. Sun and K. Qiu, "Vacuum Pyrolysis and Hydrometallurgical Process for the Recovery of Valuable Metals From Spent Lithium-Ion Batteries," *Journal of Hazardous Materials* 194 (2011): 378–384.

276. X. Liu, M. Wang, L. Deng, Y.-J. Cheng, J. Gao, and Y. Xia, "Direct Regeneration of Spent Lithium Iron Phosphate via a Low-Temperature Molten Salt Process Coupled With a Reductive Environment," *Industrial & Engineering Chemistry Research* 61 (2022): 3831–3839.

277. Y. Xu, B. Zhang, Z. Ge, et al., "Advances and Perspectives Towards Spent $LiFePO_4$ Battery Recycling," *Journal of Cleaner Production* 434 (2024): 140077.

278. A. Cornelio, A. Zanoletti, and E. Bontempi, "Recent Progress in Pyrometallurgy for the Recovery of Spent Lithium-Ion Batteries: A Review of State-of-The-Art Developments," *Current Opinion in Green and Sustainable Chemistry* 46 (2024): 100881.

279. W. Ding, S. Bao, Y. Zhang, et al., "Stepwise Recycling of Valuable Metals From Spent Lithium-Ion Batteries Based on In Situ Thermal Reduction and Ultrasonic-Assisted Water Leaching," *Green Chemistry* 25 (2023): 6652–6665.

280. X. Song, T. Hu, C. Liang, et al., "Direct Regeneration of Cathode Materials From Spent Lithium Iron Phosphate Batteries Using a Solid Phase Sintering Method," *RSC Advances* 7 (2017): 4783–4790.

281. C. Hanisch, T. Loellhoeffel, J. Diekmann, K. J. Markley, W. Haselrieder, and A. Kwade, "Recycling of Lithium-Ion Batteries: A Novel Method to Separate Coating and Foil of Electrodes," *Journal of Cleaner Production* 108 (2015): 301–311.

282. P. M. Tembo, C. Dyer, and V. Subramanian, "Lithium-Ion Battery Recycling—A Review of the Material Supply and Policy Infrastructure," *NPG Asia Materials* 16 (2024): 43.

283. R. Zheng, L. Zhao, W. Wang, et al., "Optimized Li and Fe Recovery From Spent Lithium-Ion Batteries via a Solution-Precipitation Method," *RSC Advances* 6 (2016): 43613–43625.

284. S. Tao, J. Li, L. Wang, L. Hu, and H. Zhou, "A Method for Recovering Li_3PO_4 From Spent Lithium Iron Phosphate Cathode Material Through High-Temperature Activation," *Ionics* 25 (2019): 5643–5653.

285. J.-f Zhang, W. Hu, J. Zou, et al., "Directional High-Value Regeneration of Lithium, Iron, and Phosphorus From Spent Lithium Iron Phosphate Batteries," *ACS Sustainable Chemistry & Engineering* 10 (2022): 13424–13434.

286. X. Li, Y. Qian, T. Liu, et al., "Enhanced Lithium and Electron Diffusion of $LiFePO_4$ Cathode With Two-Dimensional Ti_3C_2 MXene Nanosheets," *Journal of Materials Science* 53 (2018): 11078–11090.

287. T. Lotenberg, C. Samuel, D. Larcher, et al., "Porous $LiFePO_4$/PVDF Composites for Large Scale Redox Targeting Flow Battery," *Journal of Power Sources* 602 (2024): 234290.

288. K. Kwon, J. Kim, S. Han, et al., "Low-Resistance $LiFePO_4$ Thick Film Electrode Processed With Dry Electrode Technology for High-Energy-Density Lithium-Ion Batteries," *Small Science* 4 (2024): 2300302.

289. S. Han, H. Lee, S. Yang, et al., "High-Energy-Density Li-Ion Batteries Employing Gradient Porosity $LiFePO_4$ Electrode for Enhancing Li-Ion Kinetics and Electron Transfer," *Small Structures* 6 (2025): 70016.

290. Y.-J. Lv, Y.-F. Long, J. Su, X.-Y. Lv, and Y.-X. Wen, "Synthesis of Bowl-Like Mesoporous $LiFePO_4$/C Composites as Cathode Materials for Lithium Ion Batteries," *Electrochimica Acta* 119 (2014): 155–163.

291. R. Yin, W. Zhu, Z. Zhao, W. Xu, X. Liu, and L. He, "Lithium Recovery From Brine by PEG-Modified Porous $LiFePO_4$/$FePO_4$ Electrode System," *Separation and Purification Technology* 338 (2024): 126375.

292. Z. Chen and J. R. Dahn, "Reducing Carbon in $LiFePO_4$/C Composite Electrodes to Maximize Specific Energy, Volumetric Energy, and Tap Density," *Journal of the Electrochemical Society* 149 (2002): A1184.

293. Z.-R. Chang, H.-J. Lv, H.-W. Tang, H.-J. Li, X.-Z. Yuan, and H. Wang, "Synthesis and Characterization of High-Density $LiFePO_4$/C Composites as Cathode Materials for Lithium-Ion Batteries," *Electrochimica Acta* 54 (2009): 4595–4599.

294. Z. Liu, X. Zhang, and L. Hong, "Preparation and Electrochemical Properties of Spherical $LiFePO_4$ and $LiFe_{0.9}Mg_{0.1}PO_4$ Cathode Materials for Lithium Rechargeable Batteries," *Journal of Applied Electrochemistry* 39 (2009): 2433–2438.

295. T. Takeuchi, M. Tabuchi, A. Nakashima, et al., "Preparation of Dense $LiFePO_4$/C Composite Positive Electrodes Using Spark-Plasma-Sintering Process," *Journal of Power Sources* 146 (2005): 575–579.

296. M. E. Zhong and Z. T. Zhou, "Preparation of High Tap-Density $LiFePO_4$/C Composite Cathode Materials by Carbothermal Reduction Method Using Two Kinds of Fe^{3+} Precursors," *Materials Chemistry and Physics* 119 (2010): 428–431.

297. S. W. Oh, H. J. Bang, S.-T. Myung, Y. C. Bae, S.-M. Lee, and Y.-K. Sun, "The Effect of Morphological Properties on the Electrochemical Behavior of High Tap Density C–$LiFePO_4$ Prepared via Coprecipitation," *Journal of the Electrochemical Society* 155 (2008): A414.

298. S. W. Oh, S.-T. Myung, H. J. Bang, C. S. Yoon, K. Amine, and Y.-K. Sun, "Nanoporous Structured $LiFePO_4$ With Spherical Microscale Particles Having High Volumetric Capacity for Lithium Batteries," *Electrochemical and solid-state letters* 12 (2009): A181.

299. S. W. Oh, S. T. Myung, S. M. Oh, et al., "Double Carbon Coating of $LiFePO_4$ as High Rate Electrode for Rechargeable Lithium Batteries," *Advanced Materials* 22 (2010): 4842–4845.

300. S. W. Oh, S.-T. Myung, S.-M. Oh, C. S. Yoon, K. Amine, and Y.-K. Sun, "Polyvinylpyrrolidone-Assisted Synthesis of Microscale C-$LiFePO_4$ With High Tap Density as Positive Electrode Materials for Lithium Batteries," *Electrochimica Acta* 55 (2010): 1193–1199.

301. R. Tao, B. Steinhoff, X.-G. Sun, et al., "High-Throughput and High-Performance Lithium-Ion Batteries via Dry Processing," *Chemical Engineering Journal* 471 (2023): 144300.

302. R. Tao, B. Steinhoff, C. H. Sawicki, et al., "Unraveling the Impact of the Degree of Dry Mixing on Dry-Processed Lithium-Ion Battery Electrodes," *Journal of Power Sources* 580 (2023): 233379.

303. M. Ryu, Y.-K. Hong, S.-Y. Lee, and J. H. Park, "Ultrahigh Loading Dry-Process for Solvent-Free Lithium-Ion Battery Electrode Fabrication," *Nature Communications* 14 (2023): 1316.

304. Y. Peng, H. Wang, C. Jin, et al., "Thermal Runaway Induced Gas Hazard for Cell-To-Pack (CTP) Lithium-Ion Battery Pack," *Journal of Energy Storage* 72 (2023): 108324.

305. J. Gorsch, J. Schneiders, M. Frieges, et al., "Contrasting a BYD Blade Prismatic Cell and Tesla 4680 Cylindrical Cell With a Teardown Analysis of Design and Performance," *Cell Reports Physical Science* 6 (2025): 102453.

306. M. Ue, "Current Status and Trends of Automotive Lithium-Ion Batteries," *Electrochemistry* 93 (2025): 062002.

307. G. Wang, W. Gao, X. He, et al., "Numerical Investigation on Thermal Runaway Propagation and Prevention in Cell-to-Chassis Lithium-Ion Battery System," *Applied Thermal Engineering* 236 (2024): 121528.

308. S. Chen, G. Zhang, C. Wu, et al., "Multi-Objective Optimization Design for a Double-Direction Liquid Heating System-Based Cell-to-Chassis Battery Module," *International Journal of Heat and Mass Transfer* 183 (2022): 122184.

309. L. H. Saw, Y. Ye, and A. A. O. Tay, "Integration Issues of Lithium-Ion Battery Into Electric Vehicles Battery Pack," *Journal of Cleaner Production* 113 (2016): 1032–1045.

310. E. Pierri, V. Cirillo, T. Vietor, and M. Sorrentino, "Adopting a Conversion Design Approach to Maximize the Energy Density of Battery Packs in Electric Vehicles," *Energies* 14 (2021): 1939.

311. P. Saechan and I. Dhuchakallaya, "Numerical Investigation of Air Cooling System for a Densely Packed Battery to Enhance the Cooling Performance Through Cell Arrangement Strategy," *International Journal of Energy Research* 46 (2022): 20670–20684.

312. X. Liu, H. Zhang, F. Wang, et al., "Role of Phase Change Material in Improving the Thermal Management Performance of the Fast Charging Module," *Sustainable Energy Technologies and Assessments* 53 (2022): 102598.

313. B. E. Lebrouhi, B. Lamrani, M. Ouassaid, M. Abd-Lefdil, M. Maaroufi, and T. Kousksou, "Low-Cost Numerical Lumped

Modelling of Lithium-Ion Battery Pack With Phase Change Material and Liquid Cooling Thermal Management System," *Journal of Energy Storage* 54 (2022): 105293.

314. P. Cicconi and P. Kumar, "Design Approaches for Li-Ion Battery Packs: A Review," *Journal of Energy Storage* 73 (2023): 109197.

315. A. Kumar Thakur, R. Sathyamurthy, R. Velraj, et al., "A State-of-The Art Review on Advancing Battery Thermal Management Systems for Fast-Charging," *Applied Thermal Engineering* 226 (2023): 120303.

316. F. S. Hwang, T. Confrey, C. Reidy, et al., "Review of Battery Thermal Management Systems in Electric Vehicles," *Renewable and Sustainable Energy Reviews* 192 (2024): 114171.